

A FRAMEWORK FOR INDIVIDUAL-BASED SIMULATION OF
HETEROGENEOUS CELL POPULATIONS

by

Nezar Abdennur

A thesis submitted to the
Faculty of Graduate and Postdoctoral Studies
in partial fulfilment of the requirements for the degree of
Master of Science in Cellular and Molecular Medicine
with Specialization in Bioinformatics

Department of Cellular and Molecular Medicine
Faculty of Medicine
University of Ottawa

© Nezar Abdennur, Ottawa, Canada, 2012

Abstract

An object-oriented framework is presented for developing and simulating individual-based models of cell populations. The framework supplies classes to define objects called simulation channels that encapsulate the algorithms that make up a simulation model. These may govern state-updating events at the individual level, perform global state changes, or trigger cell division. Simulation engines control the scheduling and execution of collections of simulation channels, while a simulation manager coordinates the engines according to one of two scheduling protocols. When the ensemble of cells being simulated reaches a specified maximum size, a procedure is introduced whereby random cells are ejected from the simulation and replaced by newborn cells to keep the sample population size constant but representative in composition. The framework permits recording of population snapshot data and/or cell lineage histories. Use of the framework is demonstrated through validation benchmarks and two case studies based on experiments from the literature.

Acknowledgements

I would like to thank my supervisor, Dr. Mads Kaern, for his guidance and support, as well as my committee advisors, Dr. Theodore Perkins and Dr. André Longtin, for their feedback.

I would also like to thank current members of the Kaern lab—specifically, Daniel Charlebois, for helping to develop the replicative aging model and for proofreading the thesis, and Hilary Phenix, for generously providing flow cytometry data. But mostly, I would like to thank them both as well as lab members Alex Power, Daniel Jedrasiak and Sarah Voll, for providing a stimulating work environment and simply for being great colleagues and friends.

I am also grateful to Dr. Matthew Scott at the University of Waterloo for taking the time to offer me a one-on-one crash course on stochastic processes just prior to beginning my Master’s project. What I picked up in those few days laid the foundation for acquiring knowledge on many of the topics that now permeate the pages of this thesis.

I would also like to thank a few “real” computer scientists—Georg Summer, Martina Kutmon, and especially Andrei Anisenia—for valuable discussions which lead to great improvements in the design of the framework.

Finally, I would like to thank my family and friends outside the academic environment for their constant support and encouragement.

Contents

1	Introduction	1
1.1	Heterogeneity in isogenic cell populations	1
1.2	Seeing heterogeneity	2
1.3	Sources of heterogeneity	4
1.3.1	Nonlinear dynamics	4
1.3.2	Stochasticity	5
1.3.3	Division and inheritance	7
1.3.4	Reproductive dynamics	8
1.4	Overview of the thesis	8
2	Background	10
2.1	Modeling individual cells	11
2.1.1	Biochemical kinetics	11
2.1.2	The stochastic simulation algorithm	14
2.1.3	Division and cell physiology	17
2.2	Modeling structured cell populations	19
2.2.1	Population balance equations	19
2.2.2	Individual-based models	21
2.3	A framework for individual-based simulation	24

3 The Framework	26
3.1 Simulation events as generalized reactions	26
3.2 Object orientation and frameworks	29
3.3 Design	32
3.3.1 A simulation engine coordinates each individual	32
3.3.2 The simulation manager coordinates the engines	35
3.3.3 Execution patterns of simulation events	36
3.4 Simulation meta-algorithm	40
3.4.1 Simulation engine	40
3.4.2 Simulation manager	41
3.5 Implementation	50
4 Validation and Case Studies	54
4.1 Stochastic gene expression	54
4.1.1 Implementing an SSA simulation channel	55
4.1.2 Incorporating growth and division	58
4.1.3 Incorporating extrinsic sources of variability into the reaction kinetics	61
4.2 Differential reproduction and the constant-number method	66
4.2.1 Background	66
4.2.2 Model	66
4.2.3 Results and discussion	69
4.3 Size and replicative lifespan in budding yeast	73
4.3.1 Background	73
4.3.2 Model	75
4.3.3 Results and discussion	76
4.4 Epigenetic memory in the response to stress	78
4.4.1 Background	78
4.4.2 Model	81

4.4.3	Results and discussion	85
5	Conclusion	90
	References	96
	A Simulator implementation	109
A.1	Classes	109
A.2	Meta-algorithm implementations and performance	111
	B The birth-migration process	114

List of Figures

1.1	Two experimental methods, flow cytometry and time-lapse microscopy provide complementary perspectives of cellular dynamics.	3
2.1	Time series of protein concentrations generated from deterministic and stochastic simulations of the same gene expression model.	12
2.2	Population growth and balanced growth.	21
2.3	Cell chains, cell populations and the constant-number method.	23
3.1	Simulation event channels form the basic units of a simulation in the CPS framework.	27
3.2	Pseudocode describing the methods of local and global simulation channels.	34
3.3	Relationship between simulation engines and the simulation manager. . .	36
3.4	The First-Engine Method meta-algorithm.	44
3.5	The Asynchronous Method meta-algorithm.	48
3.6	Screenshot of a script that runs a simulation of a complete model. . . .	52
3.7	Screenshot of a class definition file for a simulation channel that performs cell division.	53
4.1	Validation of SSA simulation channel.	57
4.2	Joint density histograms of cellular volume and protein levels in the cases of symmetric and asymmetric division.	59
4.3	Lineage dynamics starting from a single cell in the cases of symmetric and asymmetric division.	60
4.4	Modified SSA algorithm for time-varying propensities.	63
4.5	Simulating gene expression with extrinsic sources of fluctuation. . . .	65
4.6	Model of bistable phenotype switching and reproduction.	67
4.7	Comparing the sizes of subpopulations in simulations with and without the constant-number size cap.	69
4.8	Simulating the bistable switching model using the constant-number method.	70
4.9	Assessing the N_{\max} -dependence of the constant-number method. . . .	72
4.10	Theory of the size-limited replicative aging of budding yeast.	74
4.11	Simulating size-dependent replicative aging in budding yeast.	77
4.12	Gene expression noise and epigenetic memory.	80
4.13	Experiments showing adaptive drift of $URA3^{GFP}$ -expressing yeast cell populations under prolonged exposure to stress.	82
4.14	The Ornstein-Uhlenbeck process.	83

4.15	Slower relaxation of fluctuations causes adaptive drift of the population expression distribution under stress and confers resistance.	86
4.16	Varying the position and steepness of the reproductive rate function. . .	88
4.17	Reversible adaptive drift of mean expression for different values of τ . . .	89
5.1	Possible extension of the framework.	93
A.1	UML diagram of main CPS framework classes in the MATLAB implementation.	110

List of Tables

3.1 Types of simulation channels having different execution patterns	38
--	----

List of Algorithms

2.1	SSA (Direct Method)	16
2.2	SSA (First-Reaction Method)	17
3.1	Simulation engine algorithm	40
3.2	Gap closure procedure	41
3.3	The First-Engine Method	43
3.4	The Asynchronous Method	47
4.1	<code>SSADirect</code> simulation channel	56
4.2	<code>RxnStep</code> channel	64
4.3	<code>BarrierStep</code> channel	64

Chapter 1

Introduction

1.1 Heterogeneity in isogenic cell populations

Much of the study of cellular systems hinges on the implicit assumption that the individual cells of a population are similar or functionally identical, at least on average. This is the basis for attaching meaning to macroscopic parameters like growth yield and respiratory rate, or to the results of biochemical assays that measure average or aggregate levels of analytes pooled from large numbers of cells [1]. However, such averaged or macroscopic analyses can often be misleading. Take, for instance, the classic example of the maturation of *Xenopus* frog oocytes, in which graded input of progesterone translates into a graded population-averaged measurement of phosphorylation of p42 MAP kinase, yet for individual cells, the maturation response is actually all-or-nothing [2]. In this case, as in countless others, it is necessary to consider the heterogeneity of the population to truly understand the underlying biological process.

Over the last few decades, a great deal of research has demonstrated that even genetically identical cells in the same environment will exhibit substantial heterogeneity in phenotype and physiology [3, 4, 5]. This applies not just to natural populations and

multicellular organisms, but even to clonal microbial cell cultures grown under axenic laboratory conditions [6, 7]. This variability reflects the underlying dynamic character of individual cells. It can have functionally important consequences, producing heterogeneous responses to perturbations such as drug treatments [8], or providing fitness advantages in fluctuating or uncertain environments in the absence of significant genetic variation [9, 10, 11].

1.2 Seeing heterogeneity

Advances in technology continue to offer ways of getting a closer look at the biological dynamics of cells. Two technologies in particular, flow cytometry and time-lapse microscopy, have gained wide popularity and exemplify two different conceptual levels of quantifying and analyzing cellular heterogeneity.

Flow cytometry is a high-throughput technique for the multiparametric analysis of the physical and/or chemical characteristics of large numbers of cells in a population [6, 12]. It involves passing individual cells through an illumination zone in a hydrodynamically focused stream of liquid and detecting optical scattering properties and/or the light emission of one or more fluorescent labels simultaneously. These readings are sorted electronically into bins, forming histograms of the distributions of cell parameters. One thus obtains physiological “snapshots” of the population composition at a given point in time at single-cell resolution (see Figure 1.1A). One can further sort a heterogeneous mixture of cells into two or more containers using a specialized method called fluorescence-activated cell sorting (FACS), whereby the fluid stream is charged as it exits the fluidics system and then passes through an electrostatic field to deflect cells to the appropriate container. While flow cytometry measurements can be taken from a population at multiple time points, the technique does not allow the same cell to be tracked over time.

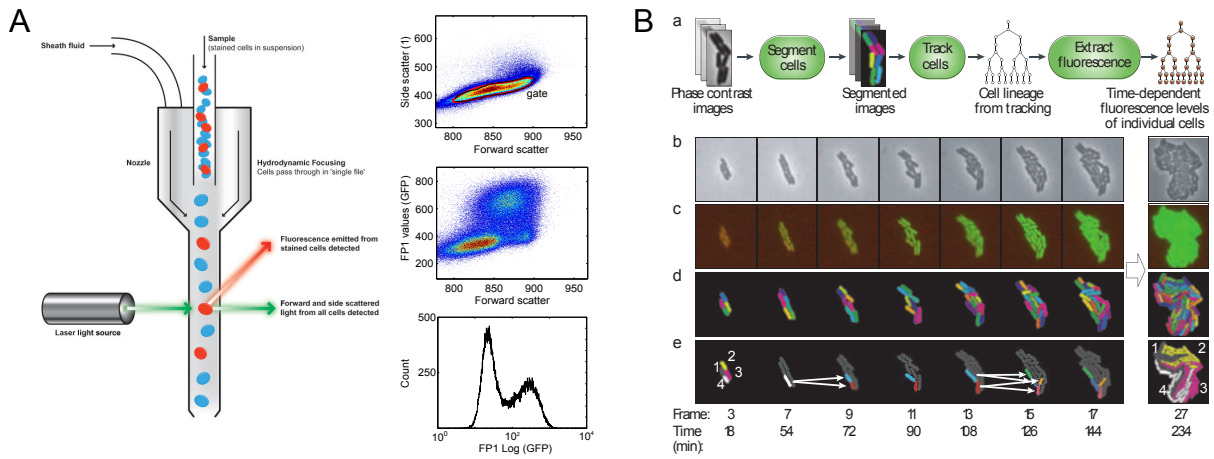


Figure 1.1: Two experimental methods, flow cytometry and time-lapse microscopy provide complementary perspectives of cellular dynamics. **(A)** Flow cytometry enables multi-variate analysis of single-cell light scattering properties and emission of fluorescent probes and stains. Shown are density plots and histograms from *S. cerevisiae* YPH499 cells expressing yeast-enhanced green fluorescent protein driven by the *RNR3* promoter, whose transcriptional activity is responsive to a DNA-methylating drug. Data courtesy of H. Phenix. **(B)** Analysis of time-lapse microscopy images involves algorithms for segmentation of cells, feature quantification, and lineage tracking. Shown is the input and output from image analysis of a microcolony of *E. coli*. Figure reproduced with permission from Locke *et al.* [13].

By contrast, time-lapse microscopy of live cells along with quantitative image analysis allows the dynamics of individual cells and genealogical lineages to be followed over time by photographing cells at regular time intervals over several hours (see Figure 1.1B). For example, cells can be engineered to express fluorescent reporters for key genes, enabling the characterization of the dynamics and physiological function of gene circuits as well as correlations and the heritability of states, all at the single-cell level. Such movies have provided many new insights into the behaviour of gene networks (for a review of recent work, see [13]). In contrast to the throughput of flow cytometry, time-lapse microscopy experiments are more time-consuming, large population statistics are harder to generate, and image analysis can be painstaking. However, advances in live-cell imaging and microfluidics technologies are constantly improving the throughput and precision of live cell microscopy experiments [14]. Furthermore, new molecular techniques are enabling even closer inspection capabilities, such as the development of single-molecule detection

to examine low-level gene expression in individual cells [15, 16, 17].

In summary, heterogeneity can be characterized with single-cell resolution in terms of the profile of characteristics of an ensemble (i.e., population snapshots) or through the variable temporal dynamics of individual cells and their progeny (i.e., cell lineages). The two perspectives are complementary, but by observing or explaining one it can be challenging to predict the other. Quantitative modeling can play an important role in bridging the relationship between single-cell dynamics and cell population dynamics.

1.3 Sources of heterogeneity

In the absence of spatiotemporal heterogeneity in the environment (e.g., microenvironments and niches), or self-organizing interactions or communication between cells, the population profile is a direct consequence of internal single-cell dynamics. Here, some of the properties of single-cell dynamics that give rise to the diversity seen at the population level are discussed.

1.3.1 Nonlinear dynamics

Cellular processes involve complex networks of biomolecules whose interaction kinetic rates exhibit saturations, thresholds, and other nonlinearities [18]. This gives rise to rich dynamical behaviour including oscillations and the existence of multiple stable states (multi-stability). Biochemical networks—genetic, metabolic and signalling—all involve regulatory loops and control structures, allowing cells to sense and respond to changing conditions. These networks are thought to be decomposable to some extent. For instance, small sets of recurring regulation patterns, called network motifs, have been found to occur in transcriptional and other biological networks and can carry out specific information-processing functions [19, 20]. Many biological networks have evolved

to be robust, in that they generate reliable output that is maintained in the face of internal perturbations or external variations [21]. Today, synthetic biologists seek to both uncover and exploit the design principles of biological circuitry through the genetic engineering of sensors, toggles, oscillators, pulse generators and more complex devices in cells [22, 23, 24].

Importantly, the existence of multiple stable gene expression programs and robust phenotypes conferred by biochemical networks gives rise to the type of differentiation process described by C. H. Waddington (1957) in his metaphor of the “epigenetic landscape” [25], where cells spontaneously adopt stable phenotypes in a manner akin to marbles rolling down hills towards “attracting” valleys. The shape of the landscape represents the phenotypic paths that cells can follow towards a stable cell type and the fate of a cell is determined by the constant modulation of the epigenetic landscape by internal and external signals. More recently, it has been suggested that this picture be extended to consider the effects of molecular noise as a source of “thermal fluctuations” that move cells around the landscape [26].

1.3.2 Stochasticity

The cellular milieu itself is a crowded, heterogeneous environment, with many macromolecular species present in very small copy numbers. This results in biochemical networks being subject to stochastic fluctuations or *noise*. Such effects have a critical role in processes including cytoskeletal dynamics, cell polarization, and neural activity [27]. However, stochasticity has received the most attention, and is particularly acute, in the case of gene expression [28].

It has become generally accepted that gene expression occurs in bursts, both of mRNA and protein [15, 16, 17, 29]. Fluctuations in gene products are also propagated through networks: they can be amplified or suppressed by regulation, or averaged away by slow

degradation of downstream elements [30, 31]. Gene expression noise is often described in terms of *intrinsic* and *extrinsic* components. This is based on a landmark study that quantified from image microscopy snapshots the variability or “noise”¹ from two identical copies of a promoter in *E. coli* driving the expression of different fluorescent reporters [33]. The term intrinsic was used to refer to the variation that affected each copy independently, while extrinsic referred to correlated variation in expression from the two promoters. Generally, intrinsic fluctuations are those associated with noise generation, while extrinsic fluctuations are attributed to noise propagation from other systems [30]. In the case of a single constitutive gene, the former would be due to bursting, while the latter would be caused by variations in factors such as housekeeping machinery (e.g., levels of RNAP, ribosomes, ATP, ribonucleases and proteases), upstream regulators and the cell cycle [5, 34].

Noise can be detrimental as it corrupts deterministic intra-cellular signals, but many studies have shown that noise also provides critical functions and can facilitate evolutionary adaptation and development. For example, stochasticity in gene expression is implicated in several examples of cells assuming different and heritable fates in the absence of genetic or environmental differences. Some documented examples of this phenomenon, known as cellular decision making [26] or probabilistic differentiation [27], include the decision of *B. subtilis* to initiate competence to take up DNA from the environment under starvation [35, 36], the random activation of the galactose uptake system in *S. cerevisiae* when exposed to a mixture of low glucose and high galactose [37], and the random photoreceptor patterning of the ~ 750 ommatidia of the compound eye of *D. melanogaster* [38]. In all these cases, cell fate was found to be driven by noisy molecular circuitry.

¹This use of the term noise is to refer to a measure of population variation, usually the coefficient of variation (standard deviation divided by the mean) [32]. The interchangeable use of the term is unfortunate, because it can misleadingly give the impression that measured heterogeneity only reflects spontaneous differences in the timing of biochemical reaction events.

1.3.3 Division and inheritance

Another source of variation in cell populations is the cell division cycle. Progression through the cell cycle involves the modulation of many enzymes, transcriptional regulators, and signalling cascades, increased gene copy number due to DNA replication and overall cell growth. A major contribution to population heterogeneity is that cells are typically *unsynchronized* in culture, unless specifically manipulated to be [39]. The same applies to other biological rhythms in the absence of mechanisms to entrain or synchronize cells by some external signal or cell communication.

Cell division entails the redistribution of cell volume, membrane surface area, organelles, macromolecules, metabolites, and other components between newborn cells. Asymmetry and noise in endowment can generate significant variation and often has important biological consequences. While some components, like DNA, are segregated evenly and in a highly ordered fashion, other organelles and macromolecules have been observed to follow independent or at least mildly disordered partitioning, which gives rise to some degree of stochastic partitioning error [40]. On the other hand, in many species, some cellular contents are distributed asymmetrically between daughter cells. Asymmetry in cell division can give rise to daughter cells with different fates. This can occur, for example, in stem cell differentiation and self-renewal [41, 42]. Asymmetry is also thought to be a key determinant of aging effects in some cell types. For example, even though *E. coli* grows as a rod and divides in a morphologically symmetric manner, fission produces one new cell pole per newborn per division event, resulting in age asymmetry in a cell's two poles. Stewart *et al.* [43] observed by time lapse microscopy that cells which inherited older cell poles exhibited slower growth and increased incidence of death.

1.3.4 Reproductive dynamics

One facet of population heterogeneity that is often underappreciated is heterogeneity in proliferation. If a population consists of cells of different types or metabolic states which possess different growth rates, then the population profile will be affected by the balance between the rates of reproduction, quiescence and death of cells with different phenotypes. For example, this is observed in the phenomenon of persistence in which bacteria switch stochastically into a “persister” state, characterized by slower growth under nutrient abundance but increased immunity to environmental stresses, such as antibiotic treatment [44]. The coexistence of the two subpopulations ensures survival of the population in the face of unpredictable changes in the environment, while the environmental conditions determine the relative sizes of the normal and persister subpopulations. Aging is also typically associated with slower growth [43, 45], and the different growth rates thus determine the age structure of the population.

1.4 Overview of the thesis

In a uniform environment that may be time-varying, the non-interactive sources of variability in an isogenic population of cells include the nonlinear and noisy dynamics of biomolecular networks, asynchrony in oscillatory and non-steady processes, the statistics and symmetry of endowment, and differential reproductive dynamics. Most cellular modeling and simulation methodologies in systems biology do not incorporate all of these sources, resorting either to detailed descriptions of idealized single cells (e.g., [34, 46]) or coarse-grained descriptions of cell populations (e.g., [47, 48]). However, to truly bridge the gap between the “snapshot” and “lineage” perspectives of cell heterogeneity requires the ability to simulate the dynamics of structured cell populations based on models of individual cells. The work here describes a computational framework to facilitate the

construction and execution of just such individual-based models. Chapter 2 provides the background and motivation for the approach from a modeling perspective, while Chapter 3 describes the object-oriented design of the simulation framework and a prototype implementation in MATLAB. Chapter 4 demonstrates the use of the framework through a set of validation benchmarks and two case study models. Finally, a general discussion about the framework is provided in Chapter 5.

Chapter 2

Background

The sheer complexity of cellular processes puts limits on what can be gleaned from qualitative reasoning based on static cartoons of molecular pathways, especially when it comes to understanding cell-cell variability. As more molecular details come to light, precise, quantitative descriptions—usually mathematical—are required to integrate the information to describe the time-dependent biochemical or electrophysiological properties of single cells or cell populations. Because rigorous mathematical analysis is usually only possible for relatively simple models, computer simulation becomes an indispensable tool for study as more complex dynamics are taken into account. Computational models provide the means for the construction, analysis and testing of biological hypotheses *in silico*, and for prediction and comparison with wet experiments. Section 2.1 describes some common modeling approaches for single cells, which provides the motivation for individual-based modeling of cell populations, discussed in Section 2.2.

2.1 Modeling individual cells

2.1.1 Biochemical kinetics

A goal of systems biology is to obtain predictive physicochemical models describing the biochemical transformations that determine cellular physiology. The biochemical networks that shape the physiological properties of single cells are usually classified as gene regulatory networks, signalling networks, and metabolic networks [49]. The most common approach for modeling biochemical networks is the continuous, deterministic formalism based on classical macroscopic chemical kinetics. The concentrations of each individual biomolecular species in the system are modeled as continuous variables, whose temporal dynamics are driven by a system of ordinary differential equations (ODEs). The terms of the ODEs represent rates of biochemical transformations including production, consumption, complex assembly, and movement between compartments. Usually, ODEs are formulated in terms of elementary reactions with mass action kinetics. However, other algebraic rate laws such as Michaelis-Menten or Hill-type transfer functions are often also used, either as phenomenological rate expressions, or as a simplification based on timescale differences in the model (e.g., equilibrium or quasi-steady state assumptions) [50]. Other algebraic equations typically serve as constraints on the system.

Most ODE models of biochemical networks are complex and nonlinear and cannot be solved analytically, so time trajectories are normally obtained by numerical solution given a set of initial conditions. Model analysis is also largely computational in nature, with several methodologies for sensitivity analysis (with close ties to engineering control theory [51]), robustness analysis, and parameter estimation [52]. Biochemical network models often involve many parameters to characterize the interactions between diverse components. Parameter estimation, or model calibration, is a challenging task because many rate parameters cannot be measured directly, but only constrained by experimental

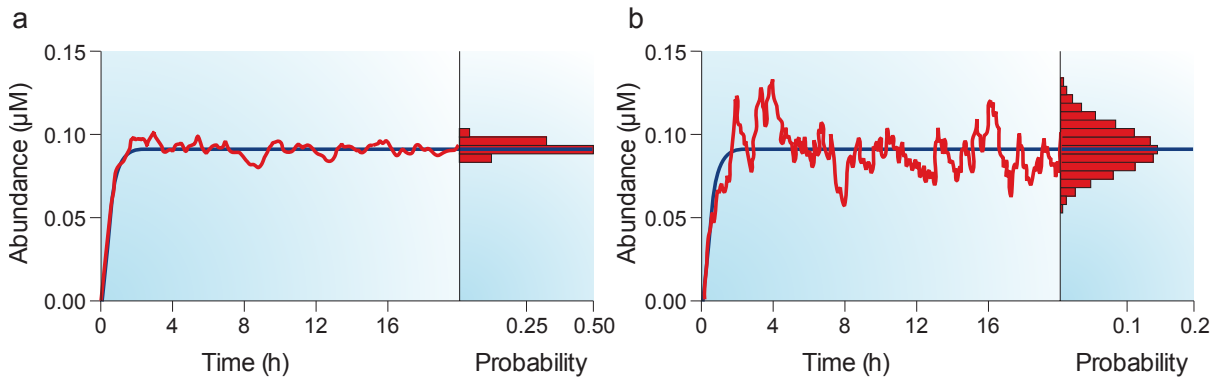


Figure 2.1: Time series of protein concentrations generated from deterministic and stochastic simulations of the same gene expression model (blue and red curves, respectively) with histograms in the right-hand panels. **(A)** Low-amplitude fluctuations occur with high numbers of mRNA and protein molecules ($\sim 3,000$ and $10,000$, respectively) and large cell volume ($200\mu\text{m}^3$). **(B)** Fluctuations increase in amplitude with a decrease in the number of mRNA and protein molecules (to roughly 30 and 100 , respectively) and smaller volume. Transcription rates were decreased and cell volume was decreased approximately 100-fold with compared with (A). Figure used with permission from Kaern et al. [28].

data and physical considerations [50, 52]. Because of the uncertainty in parameters and difficulty in assessing small quantitative changes experimentally, an important approach is to analyze the classes of qualitative behaviour a model can produce through bifurcation analysis [53]. This can indicate, for instance, whether the steady states of a model are stable or whether it can produce limit cycle oscillations.

The primary assumptions justifying use of the ODE formalism are that all compartments (e.g., cytoplasm, nucleus, etc.) remain well-mixed over the timescale of the reactions being modeled, and that transport between compartments is slow enough to be associated with an observable rate [50, 53]. If these assumptions are not satisfied, then it is necessary to model changes in species concentrations explicitly with respect to space (typically using partial differential equations). Another assumption is that species concentrations can accurately be approximated as a continuum. When molecule numbers are low, this is no longer valid and discrete stochastic fluctuations become significant [28] (see Figure 2.1).

The stochastic formulation of chemical kinetics takes into account the fact that at the molecular level, species levels change in discrete, integer amounts [54, 55]. Given a system of molecules of N chemical species $\{S_1, S_2, \dots, S_N\}$ interacting via M chemical reactions $\{R_1, R_2, \dots, R_M\}$, the fundamental hypothesis of the stochastic formulation of chemical kinetics supposes that there exists for each reaction R_j a stochastic reaction constant c_j such that $c_j dt$ is the average probability that a specific combination of R_j reactant molecules will react in the next infinitesimal time interval dt . It is argued that this assumption holds when the system is “well-mixed”, either through convective stirring, or simply if non-reactive molecular collisions are much more frequent than reactive ones [54]. When the number of possible R_j reactant combinations h_j is taken into account, we obtain a quantity $a_j = h_j c_j$ called the *propensity* of reaction R_j such that

$$a_j dt = \text{the average probability that a } R_j \text{ reaction will occur in the system in the next infinitesimal time interval } dt. \quad (2.1)$$

Thus a reaction’s propensity is a function of the state of the system. To illustrate, if we take the hypothetical dimerization reaction $A + A \rightarrow A_2$ with reaction constant c , and denote the current number of A molecules in the system n_A , then the number of distinct A reactant molecule pairs that could combine would be $n_A(n_A - 1)/2$. According to (2.1), the current propensity of the reaction would then be $c n_A(n_A - 1)/2$.

Let $X_i(t)$ denote the number of molecules of species S_i in the system at time t and $\boldsymbol{\nu}_j$ denote the stoichiometric state-change vector associated with reaction R_j , specifying how many molecules of each species is gained or lost by an R_j reaction event. The goal is then to estimate the state vector $\mathbf{X}(t) := (X_1(t), \dots, X_N(t))$, given that the system is in state $\mathbf{X}(t_0) = \mathbf{x}_0$ at some initial time t_0 . The time evolution of the probability $P(\mathbf{x}, t) := \Pr\{\mathbf{X}(t) = \mathbf{x} | \mathbf{X}(t_0) = \mathbf{x}_0\}$ is governed by a differential-difference equation called the chemical master equation (CME):

$$\frac{\partial P(\mathbf{x}, t)}{\partial t} = \sum_{j=1}^M [a_j(\mathbf{x} - \boldsymbol{\nu}_j)P(\mathbf{x} - \boldsymbol{\nu}_j, t) - a_j(\mathbf{x})P(\mathbf{x}, t)], \quad (2.2)$$

which considers all transitions into and out of state \mathbf{x} and can be derived from the initial premise (2.1). The CME describes the probability distribution associated with a continuous-time Markov process.¹ The CME is normally infinite-dimensional (it is a set of coupled ODEs, with one equation for every possible combination of reactant molecules); it can only be solved analytically in a few simple cases, and numerical solution is often prohibitively difficult [56]. However, it turns out that single realizations of the Markov process can easily be produced by numerical simulation, as described below. The statistics of the probability density of $\mathbf{X}(t)$ can then be calculated from the results of many realizations.

2.1.2 The stochastic simulation algorithm

Gillespie (1976 [54], 1977 [57]) first proposed the stochastic simulation algorithm (SSA)—also known as the Gillespie algorithm—as a Monte Carlo procedure to generate realizations of the Markov process underlying the CME. Its formulation is based on the same premise as the CME (2.1) and the algorithm is said to be *exact* in that it produces trajectories that are in exact statistical agreement with the time-dependent probability distribution governed by the CME. The development of the SSA is based on focusing on a quantity called the Reaction Probability Density, $P(\tau, \mu | \mathbf{x}, t)$ which describes the probability, given $\mathbf{X}(t) = \mathbf{x}$, that the very next reaction in the system will occur in the infinitesimal time interval $[t + \tau, t + \tau + dt]$ and will be an R_μ reaction. This was shown to be

$$P(\tau, \mu | \mathbf{x}, t) = a_\mu(\mathbf{x}) \exp\left(-\sum_{j=1}^M a_j(\mathbf{x})\tau\right), \quad (2.3)$$

¹Also called a continuous-time Markov chain or jump Markov process.

which is related to the fact that the putative waiting time τ_i for an R_i reaction to occur in the absence of other reaction channels is exponentially distributed according to $a_i(\mathbf{x}) \exp(-a_i(\mathbf{x})\tau_i)$.

Gillespie presented two versions of the SSA, the Direct Method and the First-Reaction Method, each of which samples distribution (2.3) in a different way to obtain values for the time until the next reaction occurrence τ and which of the reactions it will be μ . The system state is then updated by the stoichiometry of the reaction that fired and the time is advanced by τ . This process is repeated until the simulation stop time is reached. In the Direct Method (Alg. 2.1), two uniform random variates from the unit interval are used to separately calculate τ and μ at each step. By contrast, the First-Reaction Method (Alg. 2.2) uses M random variates to calculate each of the putative reaction times τ_j , $j = 1, \dots, M$. The reaction with the smallest reaction time, $\min(\tau_1, \dots, \tau_M)$, is then fired and all putative reaction times are recomputed. The First-Reaction Method is usually less efficient than the Direct Method because it uses more random numbers and because it wastefully resamples the putative reaction times from distributions that were not affected by the last reaction event.

Gibson and Bruck [58] later developed an improved version of the First-Reaction Method that makes clever use of data structures. Called the Next-Reaction Method, it makes use of a dependency graph to denote the dependencies between reactions, thus avoiding redundant reaction time recalculations. The search for the smallest reaction time is also improved by scheduling reactions in absolute time ($t + \tau_j$) rather than relative time and storing them in a self-sorting data structure called an indexed priority queue. Furthermore, the Next-Reaction Method is also able to “recycle” random variates so that only a single one need be generated per time step.

Other optimized variants of the exact Direct and First-Reaction Methods have been developed [59, 60, 61] as well as extensions to allow, for instance, the inclusion of delayed

Algorithm 2.1 SSA (Direct Method)

Require: System initialized at $t = t_0$ with state $\mathbf{x}(t_0) = \mathbf{x}_0$

while *termination condition* is not satisfied **do**

1. Evaluate and sum all propensities for the M reaction channels:

$$a_0(\mathbf{x}) = \sum_{j=1}^M a_j(\mathbf{x}).$$

2. Draw two unit-interval random numbers, r_1 and r_2 .

3. Calculate the time step to the next reaction event:

$$\tau = -\frac{1}{a_0(\mathbf{x})} \ln(r_1).$$

4. Determine identity of next reaction:

$$\mu = \text{the smallest integer satisfying } \sum_{j=1}^{\mu} a_j(\mathbf{x}) > r_2 a_0(\mathbf{x}).$$

5. Update the system state $\mathbf{x} \leftarrow \mathbf{x} + \boldsymbol{\nu}_{\mu}$ and time $t \leftarrow t + \tau$.

6. Record (\mathbf{x}, t) as desired.
-

reactions [62] and spatial considerations [63, 64]. Because exact methods simulate each reaction event explicitly, they become prohibitively slow as the total number of molecules in the system increases. Several approximation methods have been developed to sacrifice some accuracy for speed for large systems as well as for dynamically stiff systems. For instance, the tau-leaping method, first introduced by Gillespie in 2001 [65] and elaborated upon by numerous other [66], allows leaping in time steps τ that produce many different reaction events, but only if τ satisfies a certain criterion known as the “leap condition”: it must be small enough that no significant change occurs in any of the propensity values.

It can be shown that under conditions where the values of τ can be chosen so that each reaction produces on average a very large number of firings, one can further approximate the tau-leaping procedure by simulation of a continuous stochastic differential equation known as a Langevin equation [56, 65]. Further taking the large-number limit where the $a_j(\mathbf{x})\tau \rightarrow \infty$, the noise terms of the Langevin equation disappear, time evolution becomes smooth, and one obtains deterministic reaction rate ODEs. Thus, the deterministic formalism is recovered from stochastic chemical kinetics at the so-called thermodynamic

Algorithm 2.2 SSA (First-Reaction Method)

Require: System initialized at $t = t_0$ with state $\mathbf{x}(t_0) = \mathbf{x}_0$

while *termination condition* is not satisfied **do**

1. Evaluate the propensities for the M reaction channels: $a_j(\mathbf{x})$
2. Draw M random numbers r_1, \dots, r_M from the unit-interval and compute the putative firing time steps:

$$\tau_j = -\frac{1}{a_j(\mathbf{x})} \ln(r_j).$$

3. Determine the time step to the next reaction event:

$$\tau = \text{the smallest of the } \{\tau_j\}.$$

4. Determine the identity of the next reaction:

$$\mu = \text{the index of the smallest of the } \{\tau_j\}.$$

5. Update the system state $\mathbf{x} \leftarrow \mathbf{x} + \boldsymbol{\nu}_\mu$ and time $t \leftarrow t + \tau$.

6. Record (\mathbf{x}, t) as desired.
-

limit (scaling up the species numbers and volume at a given concentration).

2.1.3 Division and cell physiology

Single-cell models tend to ignore or idealize the effects of cell growth and division. In concentration-based ODE models, the dilution effect of cell growth is often lumped into effective first-order degradation terms, but this is technically only correct if it can be assumed that cell volume increases exponentially with time [67]. A similar trick is often used in discrete stochastic models in which the effect of partitioning at cell division and/or growth is approximated by having all components decay at a higher rate [68]. However, growth and cell division can have important effects that cannot be averaged away, and, in the worst case, their effects cannot be discriminated from those of intrinsic expression noise. For example, it was demonstrated theoretically by Huh and Paulsson [40] that fluctuations caused by segregation of gene products at cell division can propagate in a way that mimic the effects of gene expression noise.

When the interest is in population dynamics and mechanisms of inheritance, division and partitioning need to be handled explicitly. In the case of partitioning, when N individual molecules or components are assumed to segregate independently, partitioning can be simulated by drawing from a binomial distribution $B(N, p)$. Models of more disordered segregation (e.g., clustering due to packaging in vesicles) might be modeled as a multinomial process [40]. Determining the timing of cell division and its connection to other cellular processes varies with the scope of the model. In models that ignore size, division could simply be treated as a periodic or random process. One option for using a size-based threshold is the model of sloppy cell size control [69], which assumes individual cells grow according to some specified growth law and, after reaching a minimum size, divide with a probability that increases with increasing size.

On the other hand, simulations that explicitly account for cell division and inheritance can be valuable for investigating the coordination of growth physiology, cell signalling, size control and the cell cycle. Models may seek to explain how major transitions emerge from molecular mechanisms. For example, mathematical models of the cell cycle in yeasts yield DNA replication and nuclear division as an outcome of a dynamic signalling network controlled by a relatively well-understood core regulatory machinery [70]. Conversely, the kinetics of gene expression are known to be intimately coupled to the growth physiology of the cell. Even simple constitutive gene expression in exponentially growing bacteria was shown to be strongly tied to global parameters such as basal transcriptional and translational activity, gene dosage, and cell volume, all of which vary with growth rate [71]. Some empirical growth laws for bacteria have recently been proposed that integrate these observations but do not consider molecular details [72].

2.2 Modeling structured cell populations

2.2.1 Population balance equations

Population balance modelling is a name for a mathematical framework for describing particulate systems such as aerosols, colloidal dispersions, and polymerization. The behaviour of a population of particles is described in terms of the behaviour of single particles, taking into account birth and death processes (e.g., nucleation, fission, aggregation), using a set of integro-partial differential equations known as population balance equations (PBEs) [73]. These types of equations have been used to describe the time-evolving structure of populations of proliferating cells by mathematical biologists and bioprocess engineers since the middle of the twentieth century [74, 75].

Let $F(\mathbf{x}, t)$ represent the number or concentration of cells (number of cells per unit volume), where \mathbf{x} is a vector of extensive quantities representing the state of individual cells. Typically, a single property, age or mass, is used as an index of cell state, but other properties like chemical species and spatial coordinates could be included, giving a higher dimensional state space. A population balance equation is a special case of a general transport equation: an advection term takes into account the (deterministic) flow of cells in the state space, a source term accounts for the creation of two newborn cells, and a sink term accounts for the loss of mother cells that divide. In the simple one dimensional case, say cell mass x , with no nutrient limitation and no cell death, the PBE formulation of Fredrickson and co-workers [76] is as follows:

$$\underbrace{\frac{\partial F(x, t)}{\partial t}}_{\text{transient term}} + \underbrace{\frac{\partial}{\partial x} [r(x)F(x, t)]}_{\text{advection term}} = \underbrace{-\gamma(x)F(x, t) + 2 \int_x^{\infty} p(x, x')\gamma(x')F(x', t)dx'}_{\text{source and sink terms}}, \quad (2.4)$$

where $r(x)$ is called the growth rate function or velocity function of x , $\gamma(x)$ is the division rate function or fission intensity function that describes how the probability of a cell

dividing varies with x , and $p(x, x')$ is a partitioning function that describes the probability of a parent cell that divides with mass x to produce two newborn cells with masses x' and $x - x'$. A complete description thus requires formulations of $r(x)$, $\gamma(x)$, and $p(x, x')$, boundary conditions, and an initial distribution $F(x, 0)$.

A PBE is deterministic in that its time-evolution is uniquely determined by the initial distribution. Theoretically, the PBE can be derived at the limit of very large population size from a type of stochastic master equation describing the probability of the size and composition of a finite and discrete population, in a way analogous to how deterministic ODEs emerge from the chemical master equation at the thermodynamic limit [77]. In the absence of nutrient limitation, the cell concentration normally grows exponentially in time; however, the population distribution usually reaches a state where its shape becomes time-invariant. In that case, the cell *number density*

$$f(t, x) = \frac{F(t, x)}{\int_0^\infty F(t, x) dx} \quad (2.5)$$

reaches a steady state, with $\int_0^\infty f(t, x) dx = 1$. This is usually referred to as the state of “balanced growth” (see Figure 2.2) where all extensive properties of a cell culture accumulate with the same specific growth rate [78]. PBEs can be formulated in terms of the number density rather than the total number of cells [79].

PBE models are sometimes extended to include growth dependence on an external substrate concentration $S(t)$ [80]. One assumption in (2.4) is that all cells change state according to the same deterministic law $r(x)$. Incorporating more heterogeneity involves adding more complexity to the model. For example, a diffusion term can be added to the PBE to account for randomness in the evolution of the cells in state space (i.e., noise). Furthermore, modeling discrete morphological stages or phases of the cell cycle requires a set of coupled partial differential equations. Most PBEs cannot be solved analytically, but can be discretized and integrated numerically. Unfortunately, with greater structure

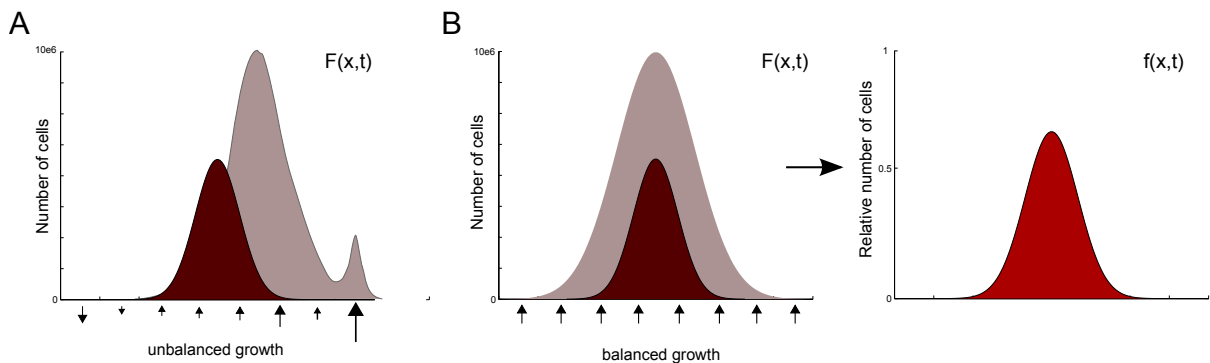


Figure 2.2: Population growth and balanced growth of an extensive property, such as cell mass. (A) Growth is unbalanced: Starting in one state (brown), the population changes in size and in composition to the grey histogram at a later time. (B) When growth is balanced the number of cells grows and the shape of the cell count histogram remains constant. Thus the histogram normalized to the total number of cells becomes stationary. PBEs describe continuous functions, $F(x, t)$ and $f(x, t)$, that represent the “expectation” distributions corresponding to such histograms.

and higher dimensionality, not only do the functional terms and boundary conditions of a PBE model become very complicated and difficult to formulate, but numerical integration quickly becomes computationally intractable [80].

2.2.2 Individual-based models

A more direct approach to obtaining the composition of a population based on single-cell descriptions is to simulate a sufficiently large ensemble of individual cells, which serve as a finite, representative sample of the “true” population. This puts the entire toolkit for single-cell simulation at our disposal without the difficulty of integrating complicated and heterogeneous single-cell behaviour into a broader mathematical framework. While most individual-based models are not amenable to mathematical analysis, their discrete and computational nature places virtually no constraints on the types of heterogeneous mechanisms that can be formulated and simulated.

In the case of simulating a population of non-dividing cells that do not interact locally, the individual-based approach is usually as simple as performing numerous realizations of

a single-cell model. On the other hand, if cells can divide, then, starting with an initial ensemble of cells, one might propose two possible approaches to obtain the long-term population distribution:

1. Simulate the time courses of single cells, randomly choosing one of the two newborns to follow when a cell divides. The result is a collection of cell chains (see Figure 2.3A).
2. Simulate the time courses of single cells, and continue to simulate all newborn cells produced.

One problem with using the random cell chain approach for simulating cell population dynamics is that it does not take into account the proliferative competition between cells in different physiological states, and so will fail to provide the correct joint distribution of cell properties except in the case where all of the cells divide at the same rate all the time. Hence, the second approach must be used when dealing with a model in which the growth rate of cells can vary with properties such as generational age, biochemical composition, or cell type. Another drawback of the cell chain approach is that it cannot be used to provide the temporal history of a complete genealogical cell lineage. However, the cell chain approach can be valuable for investigating the range of phenotypes individual cells can assume and how long they tend to reside in different states.

The problem with the second individual-based approach is that in simulations of rapidly proliferating cells, the size of the simulation ensemble can rapidly grow to the point of intractability. One way to get around this constraint is to use a Monte Carlo technique called the *constant-number method*. This was originally developed as one of a variety of so-called Monte Carlo methods to approximate the solution of population balance models of particulate processes through an individual-based approach rather than through numerical integration of the continuous PBE model [81]. The idea is that the number of particles being simulated is kept fixed but its composition still reflects the

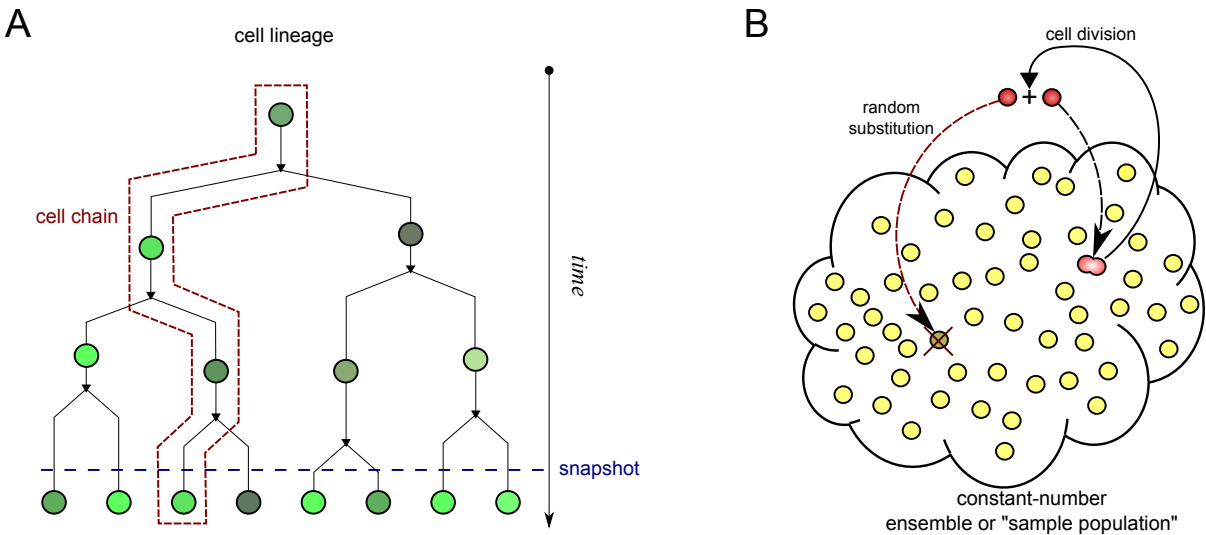


Figure 2.3: Cell chains, cell populations and the constant-number method.

number density of the true population. This is done by ejecting a randomly chosen individual each time a new one is introduced, and copying a randomly chosen individual to fill the vacancy produced when an individual is removed. By choosing the individual particles for substitution randomly, the statistical properties of the distribution remain intact. Hence, through these *resampling substitutions*, the constant-number method maintains statistical accuracy and can simulate growth over arbitrarily long times.

When simulating dividing cells, each time a cell divides, one can replace the parent cell with one of the newborns, but a second surplus newborn cell is left over. In this context, the constant-number method consists of substituting the surplus cell for one of the existing cells in the ensemble or “sample population”, where each cell has an equal probability of being replaced, as depicted in Figure 2.3B. The constant-number method has recently been applied to the simulation of heterogeneous populations. Specifically, Mantzaris used the method in conjunction with deterministic [79] and stochastic Langevin [82] models of single-cell dynamics, along with methods to determine the timing of cell divisions and partitioning of cell contents that agree with the population balance formalism. The constant-number method has also recently been incorporated into a parallel algorithm

for simulating stochastic gene expression using the Gillespie algorithm in growing and dividing cells [83].

2.3 A framework for individual-based simulation

Ultimately, the scope and granularity of a model depends on the nature of the biological problem being investigated. Based on what information is currently known about a system, its complexity, and hypotheses being tested, judicious assumptions must be made as to what processes can be ignored and to what degree one should inject into the model detailed mechanisms vs. lumped descriptions and phenomenology. However as more complexity is considered, it is not only the number of components but the multi-scale nature of their interactions which makes both mathematical and computational analysis of biological systems challenging. For instance, as the need grows to integrate cell signalling, metabolism, and gross physiology with division mechanisms and population dynamics, hybrid simulation methods are required to handle the multiple temporal and spatial scales involved [66]. Hybrid simulation implies the amalgamation of different algorithms, and from a programming perspective seamless interaction between algorithms requires the use of abstract programming interfaces and modular design. Object orientation is one paradigm provides both the abstraction and extensibility to support the building of these kinds of simulation models [84].

The work presented here is a general, object-oriented, computational framework for developing and conducting individual-based simulations of cell populations. The framework design is based on defining a set of software objects that serve as algorithmic primitives of a simulation. There are primitives that drive the time evolution of the states of individuals and others that execute global state changes. Correct scheduling and execution of the primitives is coordinated by the framework meta-algorithm, allowing the combination of simulation algorithms that execute continuous and discrete events with

different time-advancing mechanisms. The framework further supports single-cell, cell chain and cell population dynamics simulations. In population dynamics simulations, the framework regulates the production of newborn cells, allowing a simulation to begin with as few as one cell and proceed until a pre-specified maximum population size is reached, at which point resampling substitution (i.e., the constant-number method) is introduced to keep a fixed sample population size with the appropriate composition. Furthermore, the recording of either cell lineages, population snapshots, or other simulation data, is easily implemented via the algorithmic primitives.

Chapter 3

The Framework

This chapter describes the design of a framework for simulating individual-based models of cell populations called the cell population simulation (CPS) framework. Its purpose is to provide a general means to manage the time evolution of the single cell models and coordinate resampling substitution events and global events. Sections 3.1 and 3.2 provide the motivation behind the framework design, and sections 3.3 and 3.4 describe the design and general algorithm. An implementation of the framework in MATLAB is described in section 3.5.

3.1 Simulation events as generalized reactions

The conceptual basis for the simulation framework is essentially a generalization of the notion of reaction channel in the stochastic simulation algorithm for chemical kinetics. Recall that in a chemical reaction network, the system state is defined by a vector of N species amounts $\mathbf{x} = (x_1, x_2, \dots, x_N)$ in some state space S , which are modified by a set of M reactions or reaction “channels”, labelled R_1, R_2, \dots, R_M , where each R_j is associated with a propensity function $a_j(\mathbf{x}) : S \rightarrow \mathbb{R}$ and a state-change vector $\boldsymbol{\nu}_j$. When an R_j reaction event occurs (or we can say, reaction channel R_j “fires”) after a time τ , it

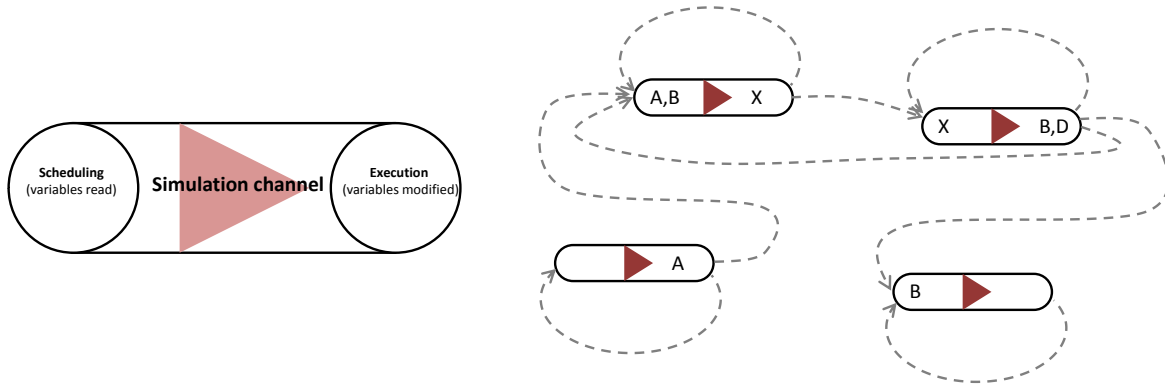


Figure 3.1: Simulation event channels form the basic atomic units of a simulation in the CPS framework. A scheduling dependency graph is illustrated by the dashed arrows.

carries the system from one discrete state to another via the transformation $t' = t + \tau$, $\mathbf{x}(t') = \mathbf{x}(t) + \boldsymbol{\nu}_j$.

It was shown by Gillespie that the firing of a reaction channel has an exponentially distributed waiting time in isolation and that the expected value of that waiting time is the inverse of the reaction's propensity. So, at a given moment while the system is in state $\mathbf{x}(t)$, we can think of the firing time of each reaction channel as being *scheduled* by a random sampling from its waiting time distribution. The earliest of these times would correspond to the next event, so we may leap forward to that time and *execute* or fire the reaction event. This interpretation is made explicit in the variant of the Gillespie algorithm known as the First-Reaction Method (see Alg. 2.2). Since the system state is modified after a reaction occurs, we may need to reschedule any reaction channels whose propensity values have been modified before jumping to the next firing time. The First-Reaction Method is naive in this regard and reschedules *all* reaction channels after each event. Optimized methods, like the Next-Reaction Method and others, make use of the dependencies between the products and reactants of reactions so that only necessary channels are rescheduled.

In general, we are interested in simulating not only the stochastic kinetics of small numbers of reactant species, but arbitrary processes that may include cell growth, division, metabolic fluxes, etc. and perhaps several processes occurring concomitantly. Arbitrary dynamic processes affect one or more *state variables* of a cell—variables which define the physiological state of the cell and may evolve deterministically or stochastically, continuously or discretely. From a computational perspective, these processes translate into simulation algorithms that perform a sequence of *simulation events*, and the goal is to combine different algorithms with different stepping and updating rules, potentially acting on the same data. The approach chosen here is to define simulation events in an analogous way to the transition events of a reaction network Markov process.

As long as the putative time steps for state updates can be calculated from the system state (i.e., simulation events can be scheduled) and the procedure for performing the state updates can be specified (i.e., simulation events can be executed) in a well-defined manner, then we can speak of generalized ***simulation event channels*** or simply, simulation channels. Simulation channels possess all the information required to schedule and perform a particular simulation event when provided with the collection of state variables defining the cell. They form the basic atomic units of a simulation in the CPS framework. They perform two operations: *scheduling*, whereby the putative time of a simulation event is determined; and *execution*, whereby the simulation event is performed. When simulation channels are combined, they are related through a *scheduling dependency graph* (see Figure 3.1). The dependency graph establishes the relationship that a simulation channel that uses a variable for scheduling requires rescheduling when another simulation channel modifies that variable. Simulation channels must also be rescheduled after they execute an event.

3.2 Object orientation and frameworks

Using the notion of simulation channels, a model of phenotypic or physiological evolution of a cell would therefore consist of 1) defining of the state variables of a cell and 2) defining the set of simulation channels that operate on the state variables. This would serve as a flexible format for encoding models computationally. To conduct actual simulation runs, one can envision a simulation engine driving the simulation clock forward and directing the scheduling and execution of the sequence of events through some type of higher-level algorithm (here termed the simulation *meta-algorithm*) that uses the simulation channels supplied to it without the need to “know” the details of the model it is simulating. Similarly, the definitions of the simulation channels do not have to depend on the implementation details of the engine, so that the development and maintenance of the two components is not strongly interdependent. Having a decoupled design is valuable because it allows simulation channels to serve as pluggable, reusable modules and confines their logic to the domain of the model they are being used to realize and not to the underlying meta-algorithm used to execute them.

The type of system just described is well suited to an object-oriented approach. Today, object-oriented programming (OOP) is a mainstream paradigm in software development, but to the unfamiliarized, the terminology can be varied and confusing (especially since everyday words are often used to denote specific programming features). Some of the major concepts of OOP are briefly described in the following paragraphs. Obviously, it does not do justice to the topic; it serves primarily to clarify the use of terms. For more information, the unfamiliar reader may consult any popular textbook on OOP, such as [85, 86].

OOP deals with data structures referred to as *objects* that possess both data and behaviour (i.e., operations that act on data). The data fields of an object are often referred to as fields, member variables, properties or *attributes* while the procedures or operations

possessed by an object are usually called member functions or *methods*. Objects are the actors of a program and interact by passing messages (i.e., calling methods). Constructs called *classes* provide the blueprints to create objects of a particular type. Objects may also be called class instances (object creation is also referred to as instantiation). While in procedural programming, applications are designed primarily in terms of data flow and data processing, in OOP design is focused on the conceptual entities that objects represent and how they interact.

In OOP there is an important distinction between a class's *interface*, normally consisting of method declarations and describing what an object does, and the *implementation* of those methods, which describes how the object does what it does. OOP supports data *encapsulation* because classes provide well-defined *public* interfaces, consisting of the fields and methods of an object accessible to its clients, while hiding and restricting access to other members (e.g., *private* fields and methods are only accessible internally by the object). Objects are usually assigned a responsibility, and classes are designed around that responsibility and the data to be shared. Good object-oriented design should focus on defining classes with a cohesive set of responsibilities and a low degree of mutual interdependence. Encapsulation supports such a design.

In addition, classes can be extended through a feature called *inheritance*, whereby new classes, known as derived classes or subclasses, inherit the attributes and behaviour of pre-existing classes, known as base classes or superclasses. The inheritance relationship gives rise to an inheritance hierarchy of types, which facilitates compartmentalization and code reuse. Classes that provide one or more method interfaces without any implementation can be defined; such *abstract* classes cannot be instantiated themselves, but through inheritance different concrete classes with commonalities can be derived from an abstract class. One use is to wrap different implementations of some input-output behaviour beneath a common class interface to allow communication and integration with other classes. Furthermore, subclasses can override the implementations of methods inherited

from a superclass, so that objects belonging to different classes respond to method calls of the same name with different type-specific behaviour. This ability of subclass objects to be used in place of objects resulting in different behaviour is referred to as *polymorphism*.

An important use of OOP is in the creation of software *frameworks*. These normally refer to sets of libraries or classes that provide generic functionality which can be selectively overridden or specialized by user code to provide specific functionality. While users can extend a framework, they cannot modify its internal code. In this chapter, the conceptual design of a simulation framework for simulating individual-based models of cells is presented along with a working implementation of that design. The CPS framework provides classes that serve as a standard interface for simulation event channels, which a user may extend by defining his or her own channels that perform the simulation events specific to a biological model. The internal framework components, however, handle the simulation meta-algorithm. The former level of abstraction, dealing with the simulation algorithms of a specific model, could be called the *model layer*, while the latter dealing with the general meta-algorithm could be called the *framework layer*. OOP is a natural paradigm for such a layered design. In a similar vein, a naive end-user may not be concerned with the details about how simulation events are performed algorithmically, but he or she may want to simulate a fully formed model with specified set of model parameters and initial conditions through an interface that hides the technical details (such as a graphical user interface). This last “user interface layer” is concerned with specific application development and is not dealt with in this work.

3.3 Design

3.3.1 A simulation engine coordinates each individual

The conceptual design of the CPS framework is described in this section. In the framework, each cell is simulated as a separate individual. A simulation may also comprise one or more global state variables that impact the entire collectivity or a subset of cells; these variables are aggregated, giving rise to one additional “individual”. The most basic types of objects used to perform a simulation at the individual level are described below.

Simulation entities are objects that encapsulate the *state variables* of an individual. They expose their data to simulation event channels. The set of state variables that an entity possesses are model-dependent. One entity class, `Cell`, represents individual biological cells, and the state variables that cell entities encapsulate will be referred to as *local* state variables. The other entity class, `GlobalData`, is used to encapsulate state variables that may represent common environmental conditions or external resources (e.g., temperature, drug concentrations), which will be called *global* state variables.

Simulation event channels, or simply, simulation channels, represent simulation processes or algorithms that access and modify state variables, in analogy to the way reaction channels modify species quantities in chemical network models. Simulation channels can be of two subtypes, *local* or *global*, based on which type of entity they are associated with. Simulation channel objects possess an attribute called `eventTime`, which specifies the putative time of the next occurrence of a simulation event. Simulation channel objects have two public methods: 1) `schedule`, which takes the current time and a variable referencing the entity and as two of its input parameters and calculates the value of `eventTime`, and 2) `execute`, which also takes a variable referencing the entity as input and carries out a simulation event by performing some operation on the state variables of the entity.

Because it is often the case that a local simulation channel requires information about some global state variable in order to schedule a local simulation event, a reference pointing to the global data entity is supplied to the `schedule` method as an additional input parameter; however, access to the global variables should be read-only so as to enforce the rule that simulation channels only modify their associated entity. Similarly, an array referencing all of the cell entities individually (i.e., the ensemble) is supplied to the `schedule` method of global simulation channels because the scheduling of global simulation events may require querying the states of individual cells. Thus, the method signatures of local and global simulation channel classes will resemble the pseudocode in Figure 3.2.

The scheduling and execution of simulation events invoked upon each entity is managed by a **simulation engine** that drives simulation forward. Each existing entity in the simulation is paired with a unique simulation engine, which manages that entity's collection of simulation channels and its associated simulation clock. Because two types of simulation entity were defined, we also define two subtypes of simulation engine. Keeping the same naming pattern as for state variables and channels, those that handle cell entities are called *local* simulation engines, while the single engine that handles the global data entity is called the *global* simulation engine. Engines have the responsibility to keep all simulation channels properly scheduled and to trigger the execution of the channel corresponding to the earliest event time when instructed to do so. The simplest way to keep the simulation channels properly scheduled would be to reschedule all simulation channels after any given channel executes; however, that would be wasteful because generally not all simulation channels are affected by a given simulation event. Therefore, a graph of *channel scheduling dependencies* is used by the engine so that the previous channel that fired and those that depend on it are the only channels that get rescheduled (see Figure 3.1).

A simulation engine thus possesses the entity, its associated simulation channels, the

```

class LocalSimulationChannel

public SCHEDULE(cell-entity†, global-data†, time)
...
    set the event time

public EXECUTE(cell-entity, global-data†, time, buffer)
...
    return boolean specifying whether cell-entity was modified

```

```

class GlobalSimulationChannel

public SCHEDULE(global-data†, Set⟨cell-entity†⟩, time)
...
    set the event time

public EXECUTE(global-data, Set⟨cell-entity†⟩, time)
...
    return boolean specifying whether global-data was modified

```

Figure 3.2: Pseudocode describing the methods of local and global simulation channels. Methods receive as input the current time and references pointing to entity objects. A variable referencing a buffer for storing newborn cells is passed to the `execute` method of local simulation channels. Objects that should not be modified within a method (this can be enforced in some languages) are labelled with †.

scheduling dependencies of the channels, and the clock as attributes. Other attributes of the engine class include `nextEventTime` and `nextChannel`, which respectively specify when the next simulation channel will fire, and which of the channels it will be—semantically, the equivalents of the parameters τ and μ of the Gillespie algorithm.

To simulate division (or, more correctly, cytokinesis), a cell entity object possesses a method to allow a copy of itself to be made, which may be invoked within the `execute` method of a simulation channel. The state variables of the two resulting cell entities may then be modified or adjusted to simulate the partitioning of cellular contents resulting in

two newborn daughter cells. On return of `execute`, the first newborn cell is just the same entity as the parent cell and takes its place, remaining actively associated with the engine (i.e., the *active* cell entity). The second newborn cell entity is set aside temporarily by placing it in a buffer; the buffer is held by the engine, which records the time of birth.

3.3.2 The simulation manager coordinates the engines

To some extent, each entity can be simulated independently of the others. However, the complications that arise are 1) the division of cells, which results in the creation of a new cell entity and potentially the random substitution of an existing cell entity with the newly created one; and 2) the modification of global state variables, which may alter the simulation of as many as all of the individual cells simultaneously. Therefore, a new type of object is introduced whose job is to orchestrate the overall simulation. A single **simulation manager** object is responsible for handling newly produced daughter cell entities and for directing the execution of the individual simulation engines. When some termination condition is satisfied, the simulation manager ceases execution of the engines and ends the simulation.

The relationship between the two types of simulation engine and the simulation manager are depicted in Figure 3.3. The simulation manager is responsible for directing and synchronizing the execution of the local simulation engines and the global simulation engine. The manager also gathers any newborn cell entities set aside by the local engines and handles them appropriately. If the maximum number of local engines has not been reached, the manager assigns the newborns to new local simulation engines; otherwise, the manager performs substitution on existing local engines. The manager is also responsible for providing local engines with a reference pointing to the global data entity and providing the global engine with references pointing to the cell entities to be used for scheduling as described in 3.3.1. Moreover, when a global simulation channel fires, the

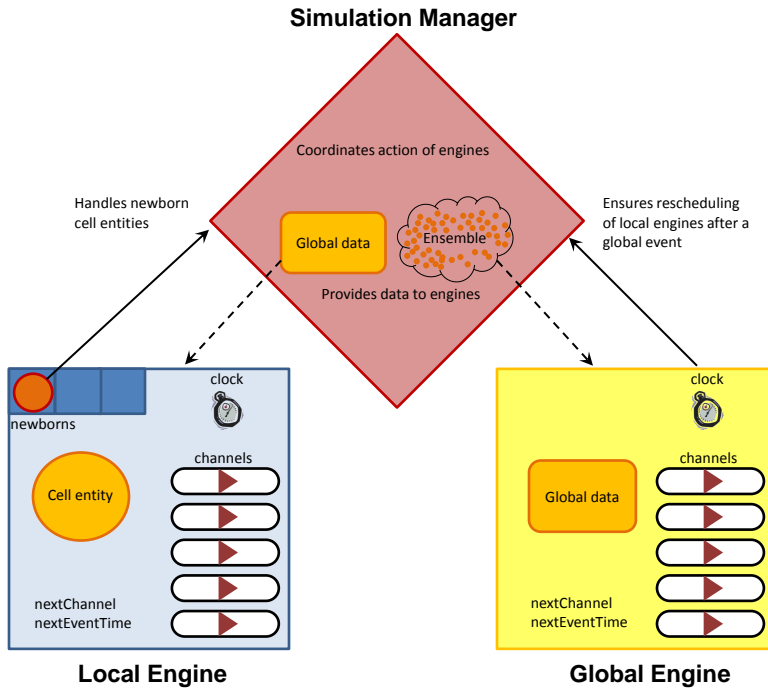


Figure 3.3: Relationship between simulation engines and the simulation manager.

global engine will notify the manager about whether any global state variables have been modified. If that is the case, the manager will instruct the local engines to reschedule *all* of their simulation channels¹.

3.3.3 Execution patterns of simulation events

It is important to note that the term “simulation event” used here does not always correspond to a discrete event at the conceptual level of the model of a physical system. Strictly speaking, a simulation event is an increment in the simulation clock potentially coupled with a change of one or more state variables. The former kind of events will be called “model events” so as to distinguish them from purely algorithmic simulation events.

¹Alternatively, some form of map of the dependencies between global channels and local channels, or between global state variables and local channels, could be introduced to optimize this rescheduling procedure. This has not been attempted.

In the simulation literature, the pattern with which simulation events are executed is usually divided into two categories: *time-driven* and *event-driven* [87].

In event-driven algorithms, simulation events are driven by a stream of time-stamped model events; the simulation jumps from the time of one state change to the next, skipping the dead time in between because the physical process being modeled does not affect the variables between those time points. Examples include the simulation of queuing models, continuous time Markov chains (e.g., the Gillespie algorithm), and other discrete event processes. In these cases, the exact time of the next state change can be predicted in advance. By contrast, a time-driven or time-stepping execution pattern involves advancing the simulation clock with predefined time increments. There are at least two cases when this pattern is necessary. The first is when one is simulating a continuously changing variable by numerical approximation, such as a variable governed by a differential equation in which appropriate time steps are required for numerical accuracy and stability. The other case is when the timing of a discrete physical event cannot be predicted in advance, but it depends on some conditional expression (such as a variable crossing a threshold value) in order for it to be “triggered”. In such scenarios, execution must step in small enough increments to capture the model event accurately. Time steps can be fixed or adaptive, and state information could be used to adjust the pace. Therefore rather than discrete and exact updating, time-driven algorithms approximate the continuous monitoring or continuous updating of state variables.

Simulation engines can support a combination of simulation channels that follow different execution patterns. The execution pattern of a simulation channel can be classified according to the mode of action of the `schedule` and `execute` methods. In the case of an event-driven simulation channel, the `schedule` method assesses the current state of its input entity and schedules the putative next state change, while the `execute` method carries out the state change. For a time-driven simulation channel, the `schedule` method would set the event time to be the current time t plus a time increment Δt , while the

Table 3.1: Types of simulation channels having different execution patterns

Type of process	Execution pattern	State change
discrete-event	event-driven	always
continuous	time-driven	always
triggered	time-driven	conditional
null	either	never

`execute` method may or may not carry out a state change depending on whether the model event has been triggered. If not, this is signalled to the simulation engine so that it need not invoke any rescheduling dependencies (see Figure 3.2). Simulation channels can further be categorized according to the type of physical process they are realizing and whether or not state variables are always modified upon execution (see Table 3.1). The examples of channels already described above are denoted as discrete-event, continuous and triggered, respectively. Additionally, a simulation channel may be defined simply to record data at certain points in time: such a “null” channel never causes a change in any state variable.

A few subtle remarks regarding scheduling dependencies are appropriate. Firstly, note that a simulation channel must always be rescheduled after executing—channels are always self-dependent. However, a channel could also be rescheduled as a result of other channels executing, and this would affect its *scheduling* pattern. For instance, suppose that a simulation channel handling cell division has a `schedule` method that sets division to occur immediately if the cell is deemed ready to divide, and further suppose that this division channel is dependent on other simulation channels so that whenever they are executed, the scheduling method of the division channel subsequently gets invoked. Then the result is that the *scheduling* of the division channel is slaved to, or contingent on, the *execution* pattern of the other channels. This, in turn, could make the actual execution pattern of the division channel depend on what other kinds of channels it is associated with. So, while the processes listed in Table 3.1 have well-defined execution patterns in

isolation, the execution pattern of a simulation channel may sometimes be determined by context, that is, by the channels its scheduling depends on.

Secondly, it is often the case with hybrid simulation algorithms that the existence of a relatively small time step creates an efficiency bottleneck [88]. Sometimes, fine-grained time stepping is unavoidable due to large differences in the time scale of the physical events being modeled by different channels. Other times, fine-grained time stepping of a time-driven simulation channel can be used as a kind of trick that allows one to eliminate the need for channel dependencies: if a channel triggers its own rescheduling frequently enough, it does not need to be reminded every time some other channel modifies a state variable by a small amount.

Applying a coarse-grained time step to a time-driven channel can improve efficiency, but care must be taken when the simulation clock approaches a final time point or reaches a time barrier where the simulation engine must stop. An event-driven channel does not need to be executed once its next event time exceeds the time barrier because it is not supposed to produce an effect during the intervening period leading up to the barrier. On the other hand, a time-driven channel represents a continuous process. If a time-driven simulation channel is scheduled to fire at a time beyond the barrier, then in order to ensure that all state variables are properly updated, it ought to be made to fire exactly at the time barrier before simulation terminates. Once again, if the channel's time step is sufficiently small, the error associated with the ignored *time gap* can be neglected. Otherwise, a terminal simulation step needs to be enforced by the simulation engine. Channels that require such a forced terminal step will be called *gap channels*.

3.4 Simulation meta-algorithm

3.4.1 Simulation engine

A simulation engine is equipped with a simulation entity and a collection of simulation channels. Its clock is a measure of time elapsed in the model (i.e., *model time*, as opposed to wallclock time or runtime). To instruct a simulation engine occupying a given point in model time to conduct simulation over an interval of model time, it is provided with a limit or time barrier at which to stop execution. The basic engine meta-algorithm then follows a scheme analogous to the Next-Reaction or First-Reaction variants of the Gillespie algorithm (Alg. 3.1).

If the user labels any of the simulation channels as being gap channels, then the engine will perform a final step whereby the gap channels have their event times forcibly set to the barrier time; they are then executed and the final rescheduling dependencies are invoked (Alg. 3.2).

Algorithm 3.1 Simulation engine algorithm

Require: All simulation channels C_1, C_2, \dots, C_n of entity e are scheduled.

```

while clock does not exceed time barrier do
    Find simulation channel with earliest time stamp:  $C_i$ .
    Execute  $C_i$  event. Advance clock.
    Reschedule  $C_i$ .
    Reschedule dependent channels  $\subseteq \{C_j \mid j \neq i\}$ 
        (select all if dependencies are not provided).

```

Algorithm 3.2 Gap closure procedure

```

if there are any gap channels then
    for each gap channel  $G$  do
        if eventTime  $\leq$  time barrier then
            Set eventTime to time barrier
            Execute  $G$  event. Advance clock.
            Reschedule  $G$  and dependent channels.

```

3.4.2 Simulation manager

The individual simulation engines cannot run autonomously due to the occurrence of global events and the substitution of cells; both entail some form of indirect “communication” between engines. Because of these restrictions, the entire collection of simulation engines needs to advance jointly in model time to some extent. Here, two different versions of the meta-algorithm for coordinating the execution of the simulation engines are presented. Both have advantages and disadvantages but produce the same final result. Which one performs better ultimately depends on the nature of the model being simulated and the data structures used to perform search operations.

The First-Engine Method

The simplest way for the simulation manager to coordinate the engines is to use the fact that each engine “sees” the time of its next pending simulation event (the `nextEventTime` attribute). The manager can simply take the earliest of these times and instruct the corresponding simulation engine to execute the corresponding channel and invoke the required scheduling dependencies. The result is that at each step the entire system is *synchronized* in model time, with one minor exception. If any of the other engines possess gap channels, then the engines are not truly synchronized until the time gaps are closed. Fortunately, gap closure does not need to be performed at every step, but only just

before a global simulation event is executed. In addition, after a global simulation event is executed, the simulation manager must instruct the local engines to reschedule their channels. The pseudocode for the simulation meta-algorithm just described, called the First-Engine Method, is given in Alg. 3.3.

The First-Engine Method is illustrated in Figure 3.4. Evidently, in the First-Engine Method, global simulation events are the most costly since in every local simulation engine they can trigger 1) the gap closure procedure prior to their execution and 2) channel rescheduling following their execution.

The Asynchronous Method

In this section, an alternative meta-algorithm is presented that permits some degree of *concurrency* or logical parallelism between the simulation engines. This would make it possible to use parallel programming to improve the performance of simulation. However, the meta-algorithm is valid regardless of whether the engines perform their computations concurrently or in succession of one another. It is based on the parallel algorithm described by Charlebois *et al.* [83].

Note that the simulation engines do not need to have their clocks synchronized in model time at every step, as was the case in the first engine method. However, one can see that if a local engine were permitted to execute a local simulation event with a time stamp that surpassed that of a global simulation event *before* that same global event had been executed, the causality rules of the model might be violated, thus producing invalid results. The processing of events out of time stamp order is a frequent problem in parallel and distributed simulation, and if it is allowed to happen, it can only be remedied by devising methods that, whenever a conflict is detected, retract and reverse bad events after they are executed or roll the system back to an earlier state [87].

To avoid dealing with such complications, we will attempt to stick to what is called a

Algorithm 3.3 The First-Engine Method

Require: Local simulation engines $\mathbf{L}_1, \mathbf{L}_2, \dots, \mathbf{L}_N$, global simulation engine \mathbf{G}

```

INITIALIZATION:
1: Initialize entities
2: for each simulation engine  $\mathbf{E}$  do
3:    $\mathbf{E}$ : Schedule all simulation channels
4:    $\mathbf{E}$ : Find simulation channel with earliest time stamp

MAIN LOOP:
5: while termination condition is not satisfied do
6:   Find the engine  $\mathbf{E}_{\text{next}}$  with the earliest nextEventTime
7:   if  $\mathbf{E}_{\text{next}} \in \{\mathbf{L}_1, \mathbf{L}_2, \dots, \mathbf{L}_N\}$  then
8:      $\mathbf{E}_{\text{next}}$ : Execute the event associated with the corresponding nextChannel
9:      $\mathbf{E}_{\text{next}}$ : Advance clock
10:     $\mathbf{E}_{\text{next}}$ : Reschedule nextChannel and dependent channels
11:     $\mathbf{E}_{\text{next}}$ : Perform gap closure procedure (Alg. 3.2)
12:   else if  $\mathbf{E}_{\text{next}} == \mathbf{G}$  then
13:     for each local engine  $\mathbf{L}$  do
14:        $\mathbf{L}$ : Perform gap closure procedure (Alg. 3.2)
15:        $\mathbf{E}_{\text{next}}$ : Execute the event associated with the corresponding nextChannel
16:        $\mathbf{E}_{\text{next}}$ : Advance clock
17:        $\mathbf{E}_{\text{next}}$ : Reschedule nextChannel and dependent channels
18:        $\mathbf{E}_{\text{next}}$ : Perform gap closure procedure (Alg. 3.2)
19:     for each local engine  $\mathbf{L}$  do
20:        $\mathbf{L}$ : Reschedule all simulation channels
21:   if any cell divided then
22:     Collect newborn cell entity, birth time, and copied channels
23:     if  $N < N_{\max}$  then
24:       Send to new local engine  $\mathbf{L}_{N+1}$ 
25:        $\mathbf{L}_{N+1}$ : Schedule all simulation channels
26:        $N \leftarrow N + 1$ 
27:     else
28:       Generate random index  $r \in \{1, \dots, N\}$ 
29:       Perform substitution on local engine  $\mathbf{L}_r$ 
30:        $\mathbf{L}_r$ : Schedule all simulation channels

```

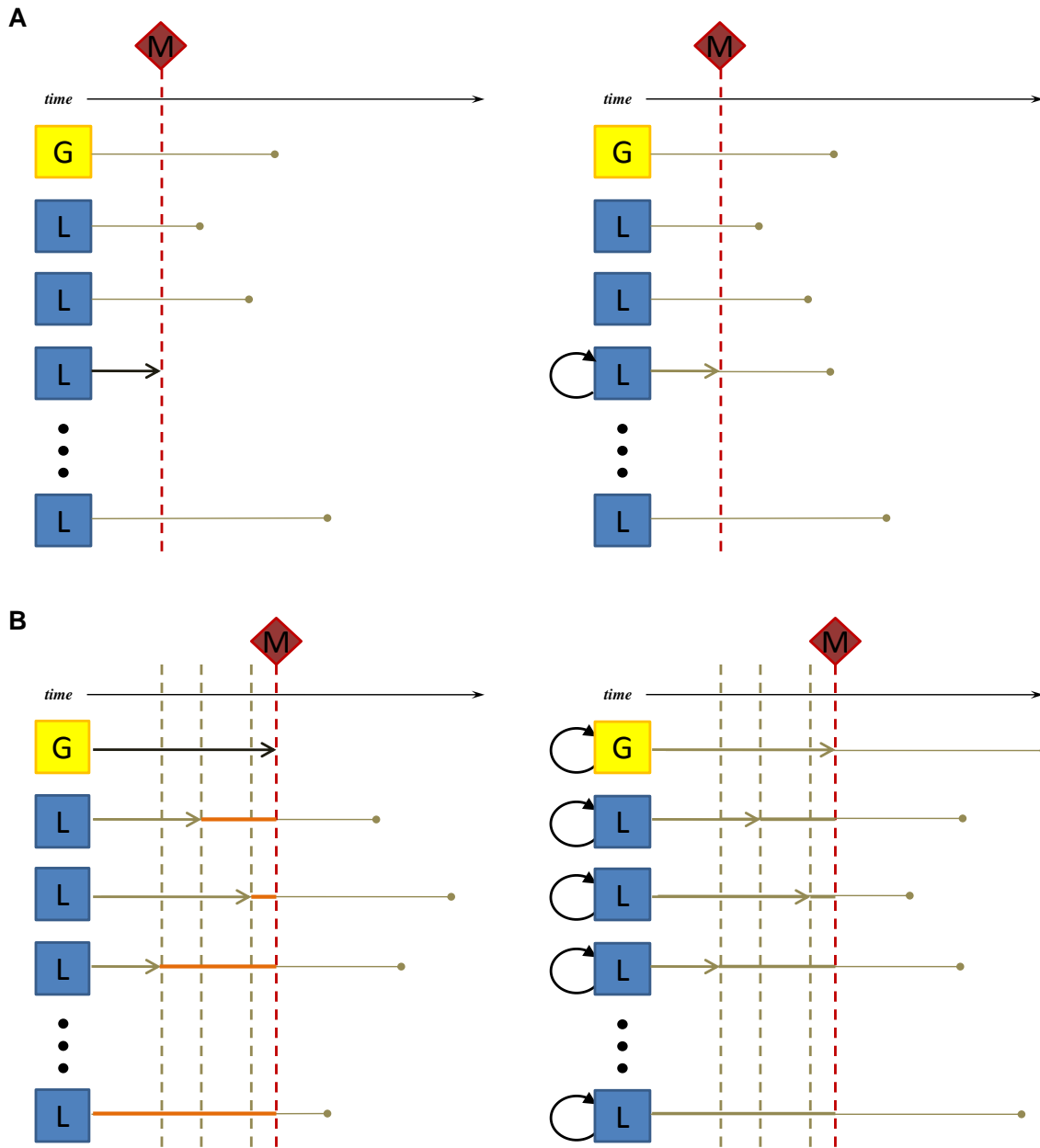


Figure 3.4: The First-Engine Method. The simulation manager selects the engine with the earliest `nextEventTime` (circles) to fire. (A) When the first engine is a local engine, its `nextChannel` is executed (left) and then dependent channels are rescheduled (right). (B) When the first engine is a global engine, all local engines invoke gap closure (depicted as orange lines) prior to the event (left), and rescheduling after the event (right).

conservative synchronization protocol [87], in which restrictions are put in place to prevent the processing of events out of time stamp order. The goal, then, is for the simulation manager to find the maximum “lookahead” for safe event execution and to use that time as a synchronization barrier for the engines. The `nextEventTime` of the global simulation engine serves as that barrier because none of the local simulation engines should surpass that time point until the global simulation event is executed. Therefore, the simulation manager establishes the synchronization barrier as the time of the next global event and “releases” the local engines, which may proceed asynchronously until they reach it, racing toward the finish line; once all have reached the barrier the global event can be executed.

However, a complication arises because cells may *divide* while the engines are en route between barriers. The handling of division is not trivial because the simulation manager performs resampling substitutions once the population reaches a size limit. There are two cases:

1. Cell division is invoked by a global simulation channel.²
2. Cell division is invoked by a local simulation channel.

In Case 1, all newborn cells are produced when the population is already synchronized; therefore, all of the substitutions occur in time stamp order. In Case 2, newborn cells are produced in between synchronizations. This complicates things because the order in which cells are created in wallclock time does not necessarily coincide with the time stamp order of the model, but the random substitutions need to be performed in the correct time stamp order.

Recall that when a cell entity divides, one of the resulting newborn cells takes the place of the parent, while the other newborn cell is set aside, frozen at the time of its birth. In order to handle Case 2, the solution is to proceed simulating the active

²Although, strictly speaking, this is prohibited in the current design as global channels are not supposed to modify cell entities, the same effect can be achieved if a global channel notifies a local channel to perform cell division through a change in a global state variable.

newborn cell entity until the synchronization barrier is reached. For generality, more than one division is allowed to occur over the interval between barriers, and the extra newborn cells produced are additionally stored. Once all the local engines reach the synchronization barrier, a processing stage is reached. Here, the simulation manager gathers all the pending newborn cell entities from the engines and sorts them by their division time stamp so that they can be substituted back into the population (sent to other local engines) in time stamp order (see Figure 3.5B). After that is done, because the newly substituted cell entities were blocked at the time they were born, they too must be advanced to the synchronization barrier by releasing their local engines. These cells may also divide; hence, the procedure may be repeated if necessary until all the cell entities are synchronized at the time barrier and no pending newborn entities remain. Then the global event is executed and the next one is scheduled, providing a new synchronization barrier. The pseudocode for the asynchronous method is listed in Alg. 3.4.

Case 1 is an option when cell division is event-driven, i.e., the exact time of cell division can easily be calculated in advance (rarely the case). On the other hand, if the division events for all cells were implemented using time-driven global simulation channels, the granularity of the time stepping required to accurately capture all division events would lead to very frequent synchronizations. If the goal is to exploit concurrency, then one would want to reduce the number of synchronizations by implementing division events using local simulation channels.

Unfortunately, Case 2 creates a different trade-off because it breaks the conservative synchronization protocol. The first problem is that, at each barrier, whenever a newborn cell entity replaces a random cell entity in the population, the destination engine's clock is wound back to the time of the new cell's birth and the old cell is discarded, meaning that the output of simulating the old cell from the substitution time to the barrier time is of no consequence (see Figure 3.5B). This superfluous simulation effort would not occur using a fully conservative algorithm like the first engine method. To minimize this performance

Algorithm 3.4 The Asynchronous Method

Require: Local simulation engines $\mathbf{L}_1, \mathbf{L}_2, \dots, \mathbf{L}_N$, global simulation engine \mathbf{G}

INITIALIZATION:

- 1: Initialize entities
- 2: **for each** simulation engine \mathbf{E} **do**
- 3: \mathbf{E} : Schedule all simulation channels
- 4: \mathbf{E} : Find simulation channel with earliest time stamp

MAIN LOOP

- 5: **while** *termination condition* is not satisfied **do**
- SET THE NEXT TIME BARRIER:
- 6: $t_{sync} \leftarrow \text{nextEventTime}$ of \mathbf{G}
- RELEASE THE LOCAL ENGINES:
- 7: **for each** local engine \mathbf{L} **do**
- 8: \mathbf{L} : Apply Alg. 3.1 and Alg. 3.2 with time barrier t_{sync}
- PROCESS NEWBORNS:
- 9: **while** there are any stored newborn cell entities **do**
- 10: Collect newborn entities c_1, \dots, c_j , times of birth, indices of engines of origin e_1, \dots, e_j , and copied channels.
- 11: Sort entities and engine indices by birth time stamp order $(c_{\sigma_1}, c_{\sigma_2}, \dots, c_{\sigma_j})$, $(e_{\sigma_1}, e_{\sigma_2}, \dots, e_{\sigma_j})$.
- 12: **for** $i \leftarrow 1$ **to** j **do**
- 13: **if** $N < N_{max}$ **then**
- 14: Send newborn c_{σ_i} to new local engine \mathbf{L}_{N+1}
- 15: $N \leftarrow N + 1$
- 16: **else**
- 17: **if** Engine of origin $\mathbf{L}_{e_{\sigma_i}}$ has already received a newborn **then**
- 18: c_{σ_i} is surplus. Discard.
- 19: **else**
- 20: Generate random index r of destination engine.
- 21: Perform substitution on \mathbf{L}_r . Reset engine clock.
- 22: Release affected local engines to time barrier t_{sync}
- SYNCHRONIZE:
- 23: \mathbf{G} : Execute next global simulation event
- 24: \mathbf{G} : Reschedule dependent global channels
- 25: **for each** local engine \mathbf{L} **do**
- 26: \mathbf{L} : Reschedule all simulation channels

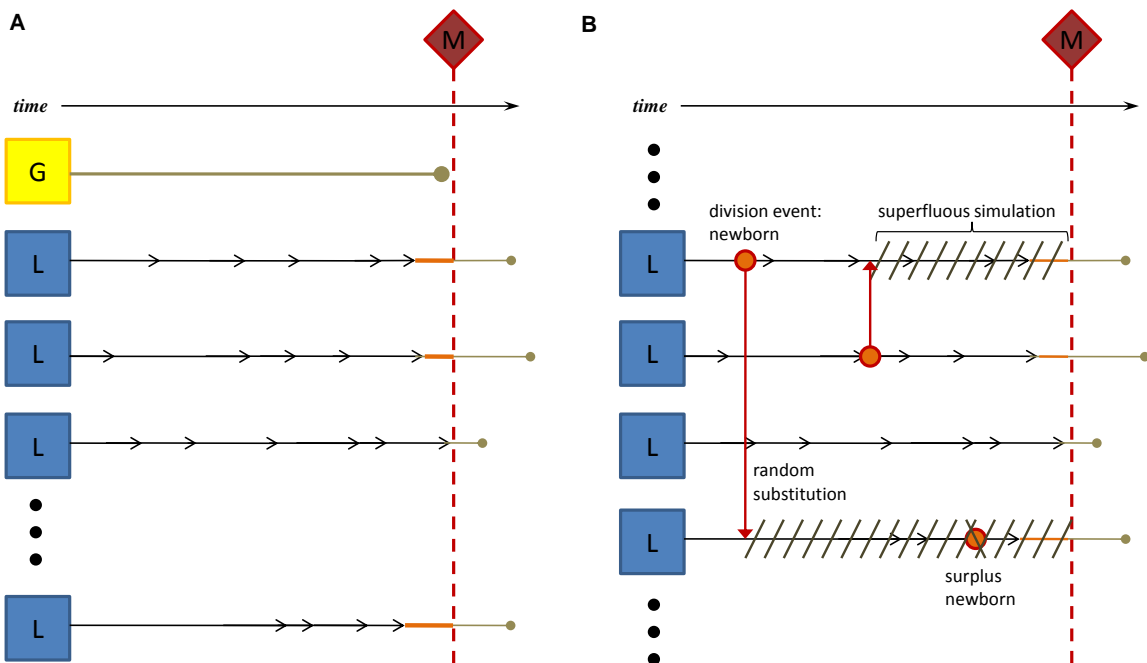


Figure 3.5: The Asynchronous Method. **(A)** The simulation manager selects the next global simulation event as the synchronization barrier. The local engines then proceed independently (asynchronously) until reaching it. **(B)** Any newborns produced between synchronizations must be handled by the manager. Substitutions can result in superfluous simulation and surplus newborns that get discarded.

penalty, the simulation manager would have to pace the synchronization frequency to the rate of cell proliferation in the population, balancing the performance gain through parallel execution with the performance loss due to superfluous simulation. Imposing arbitrary synchronizations can be done by using global null simulation channels, which perform no state modifications (see Section 3.3.3). Then the lengths of the inter-barrier intervals of model time could be tuned manually by the user or adjusted adaptively during the simulation run, for instance, by assessing cell reproduction rates through the null channel’s `schedule` method. In practice, the periodic recording of data using a global simulation channel often provides sufficient synchronizations.

The second problem with Case 2 is that it is possible for a newborn cell entity with a certain birth-time stamp to be sent to a local engine whose cell entity divided at a later time stamp. The newborn cell produced from this latter division event would never have been produced by a fully conservative algorithm and needs to be discarded. Therefore, during the newborn processing stage, such surplus newborns need to be detected and filtered out before substitution (Figure 3.5B).

Parallelization

The principal motivation for the asynchronous method was to use parallel computing to speed up single simulation runs. While the asynchronous method was developed conceptually by treating engines as being fully concurrent, any actual implementation of the asynchronous method is by no means restricted to this configuration. In one case, each local simulation engine could each indeed behave as a separate computational thread or process, all of which run simultaneously, or virtually so. Alternatively, the local simulation engines could be distributed among a set of simultaneously running computer processors, but on each processor they are “released” sequentially over each inter-barrier interval of model time. In the limit of many processors (e.g., on a large grid), every

engine would be assigned to a single processor and we again obtain a fully concurrent configuration. In the limit of a single processor, the result would be fully serial execution. The meta-algorithm described in 3.4 is general because it does not specify how the local engines should be “released”. The drawback of the asynchronous method is that it must be carefully used to provide a performance benefit.

3.5 Implementation

An implementation of the CPS framework was developed in MATLAB, version 7.11 (R2010b). It implements both the First Engine Method (Alg. 3.3) and the Asynchronous Method (Alg. 3.4) and uses the native Parallel Toolbox for parallelization. The Asynchronous Method supports three different modes of execution, one in a fully sequential manner which does not make use of the parallel toolbox, and two parallel modes which make use of different language constructs from the toolbox. All versions of the meta-algorithm were found to give consistent results. The main framework classes are stored in a package called `cps`. The user extends the classes `LocalChannel` and `GlobalChannel` to create custom simulation channels. Details about the implementation and a diagram of the classes used are given in Appendix A.

A simulation run is performed directly by passing named input arguments to the main simulation function, `CpsSimulate`. The inputs required to perform a simulation are: an instance of each type of simulation channel to be used, along with the maximum number of local engines (N_{\max}), the number of cell entities to start with (N_{init}), strings specifying the names of local and global state variables, and a handle to a user-defined initialization function (`InitFcn`) that sets the initial values of all the state variables. The local and global channel dependency graphs are provided as adjacency matrices (matrices of 0’s and 1’s that specify the connectivity of nodes). If none are provided, a complete graph is assumed. Screenshots of a script running a simulation and an example of a custom

simulation channel class definition are given in Figures 3.6 and 3.7.

The primary application of interest is to simulate isogenic cell populations, which typically implies that each cell entity be governed by an identical collection of local simulation channels. Hence, the user need only provide a single collection of local simulation channel objects which will be copied for each of the active cell entities. However, it would not be difficult to extend the current implementation to handle simulations of cells that have dissimilar collections of local simulation channels.

The main function requires that a global simulation channel of class **Recorder** (or a class derived from it) be provided. A recorder simulation channel is used to record snapshots of the synchronized system at specified sampling times. It uses another object of a class called **SimData** to determine how to record data. This simulation data object is returned by the main function when a run is completed. A simulation data object possesses a method called **snapshot** that receives references pointing to the cell entities and the global data from the recorder and is responsible for saving the state data of interest. The simulation data object also stores simulation run information. Although the **snapshot** method of the base class **SimData** performs no actual operation, two general purpose simulation data classes are derived: one that stores all state variables in memory, and one that saves all data to disk. If a user wishes to select exactly which variables to record, this can be done by writing a custom subclass of **SimData** and overriding the **snapshot** method. In order to record lineage data, one can use a local simulation channel that copies data whenever a cell divides, as will be shown in Section 4.1.

```

function sd = example
    %--- Simulate a model of stochastic gene expression with growth and division ---

    %Model parameters
    %-rate constants
    p.kR = 0.8;
    p.kP = 0.05;
    p.gR = 0.1;
    p.gP = 0.002;
    %-stoichiometry matrix
    p.S = [ 1  0;
            -1 0;
            0 1;
            0 -1 ];
    %-growth rate
    p.kV = log(2)/1800; %30min doubling time

    %Construct simulation channels
    %Each type of channel has a class definition
    gch1 = cps.Recorder('RecordingTimes',[0 100 200 300 400 500], 'SimData', cps.SimDataToMem());
    lch1 = SSADirect('StoichMatrix', p.S, 'PropensityFcn', @propFcn);
    lch2 = Growth('tstep',30);
    lch3 = Division('binomProb',0.5);

    %Dependency graph adjacency matrices (diagonal 0 elements are ignored)
    globDG = 1;
    locDG = [1 0 0; %ssa
              0 1 0; %growth
              1 1 1];%div

    %Run simulation. (returns simulation data)
    sd = CpsSimulate('MaxNumCells', 2000, ...
                      'InitNumCells', 10, ...
                      'LocalChannels', {lch1,lch2,lch3}, ...
                      'LocalDG', locDG, ...
                      'LocalGapChannelIdx', 2,... %growth is set as a gap channel
                      'GlobalChannels', {gch1}, ...
                      'GlobalDG', globDG, ...
                      'LocalVars', {'X', 'V', 'Vthresh','tLast','root_id','node_id'}, ...
                      'GlobalVars', {'kR','kP','gR','gP','kV'}, ...
                      'InitFcn', @initFcn, ...
                      'UserData', p,... %gets passed to initFcn
                      'Method', 'Async',...
                      'Mode', 'Serial');

end

function initFcn(cells, gdata, p)
    %set the initial global data
    gdata.State.kR = p.kR;
    gdata.State.kP = p.kP;
    gdata.State.gR = p.gR;
    gdata.State.gP = p.gP;
    gdata.State.kV = p.kV;

    %set the initial states of the cells
    for i = 1:10
        cells(i).State.X = zeros(1,2);
        cells(i).State.V = exp(rand*log(2));
        cells(i).State.Vthresh = 2 + 0.05*randn;
        cells(i).State.tLast = zeros(1,1);
        cells(i).State.root_id = i;
        cells(i).State.node_id = 1;
    end
end

```

Figure 3.6: Screenshot of a script that runs a simulation of a complete model.

```

classdef Division < cps.LocalChannel
%Class defining a simulation channel that performs cell division
%inherits getEventTime and setEventTime from base class cps.SimChannel

properties %attributes defined by the Division class
    binomProb
end

methods (Access = public)
    %Constructor
    function channel = Division(varargin)
        % Set properties by passing property-value pairs
        if nargin > 0
            for k = 1:2:length(varargin)
                channel.(varargin{k}) = varargin{k+1};
            end
        end
    end

    function schedule(self, cell, gdata, time)
        %determine the time until volume threshold is crossed
        tdiv = log(cell.State.Vthresh/cell.State.V)/gdata.State.kV;

        %set the event time
        self.setEventTime(time + tdiv);
    end

    function tf = execute(self, cell, gdata, time, nbuffer)
        %cell division --- clone parent cell
        new_cell = cell.copy();

        %modify cell and new_cell to their post-division states
        xprev = cell.State.X;
        xpart = binornd(xprev,self.binomProb); %binomial partitioning
        cell.State.X = xpart;
        new_cell.State.X = xprev - xpart;
        %..., etc... %

        %store new_cell in nbuffer
        nbuffer.insert(new_cell);

        %signal that cell entities were modified
        tf = true;
    end
end
end %classdef

```

Figure 3.7: Screenshot of a class definition file for a simulation channel that performs cell division.

Chapter 4

Validation and Case Studies

This chapter presents a set of simulation studies used to validate the implementation of the CPS framework and demonstrate realistic use cases related to experimental studies in the literature. In Section 4.1, algorithms are implemented to simulate stochastic gene expression and to incorporate the effects of division and partitioning. Section 4.2 validates the built-in use of the constant-number method in a simple model of dynamic subpopulations having different growth rates. Section 4.3 involves a model of aging and senescence in budding yeast, while a model involving the interplay of environmental stress and gene expression is presented in Section 4.4.

4.1 Stochastic gene expression

To validate the implementation of the CPS framework, a simulation channel was created to conduct simulations of a well-characterized model of stochastic gene expression without division. The results obtained are compared with previously derived analytical solutions. Division and asymmetric endowment are then incorporated using additional channels to demonstrate the framework’s ability to handle dynamics at the level of a single cell lineage as well as at the level of the aggregate distribution of cellular properties. Finally,

to demonstrate the versatility of the simulation channel formalism, an algorithm for incorporating extrinsic variability into models of noisy gene expression was implemented and tested.

4.1.1 Implementing an SSA simulation channel

First, we validate that the framework can reproduce the expected ensemble statistics of a simple gene expression model in the absence of reproductive dynamics. The model chosen is a “two-stage model” of expression of a single gene. It is a simplification of a three-stage gene expression model that excludes the kinetics of promoter states. This can be justified in the case of a constitutively expressed gene or the in case where the promoter kinetics are fast relative to the rate of transcription so that they get averaged away [89, 90]. The model assumes zero-order kinetics of transcription, first-order translation of mRNAs into protein, and first-order degradation of the gene products. It is given by the following elementary reactions:



where R is mRNA and P is protein. In 2002, Ozbudak *et al.* [91] used the two-state model to explain the results of flow cytometry experiments using strains of *B. subtilis* in which the transcriptional and translational rates of a fluorescent reporter gene were tuned through modulation of an inducible promoter and targeted mutations to the ribosome-binding site. In a more recent paper, Shahrezaei and Swain [92] derive closed analytical solution to the master equation of the two-stage model. Under the assumption that

$\gamma_R/\gamma_P \gg 1$, which is realistic for most stable proteins, the steady state probability distribution of protein level was shown to follow a negative binomial distribution

$$P(n) = \frac{\Gamma(a+n)}{\Gamma(n+1)\Gamma(a)} \left(\frac{b}{1+b}\right)^n \left(1 - \frac{b}{1+b}\right)^a, \quad (4.5)$$

where n is the number of protein molecules, $a = k_R/\gamma_P$, $b = k_P/\gamma_R$, and Γ is the Gamma function.

One way to realize this model in the CPS framework would be to create a separate simulation channel for each individual reaction channel, so that the framework naturally reproduces a variation of the Next-Reaction version of the SSA. A different approach was followed instead: a single simulation channel was created to implement the simulation of the entire reaction network as a whole. The simulation channel implements the Direct Method version of the SSA, and hence is named **SSADirect**. The class is designed to be generic, so that by supplying it with a handle to a function that computes the required propensities and with a matrix of reaction stoichiometries, it can simulate any reaction network model. The responsibilities of the **schedule** and **execute** methods are divided up as described in Alg. 4.1.

Algorithm 4.1 SSADirect simulation channel

- ▷ \mathbf{x} is a state variable of the cell entity
- ▷ τ , μ , the propensity functions a_i and the ν_j are properties of the channel

```

public SCHEDULE(cell-entity, global-data, t)
    Compute propensities  $a_i(\mathbf{x})$ .
    Calculate  $\tau$  and  $\mu$  as in Alg. 2.1.
    eventTime  $\leftarrow t + \tau$ 

public EXECUTE(cell-entity, global-data, t, buffer)
     $\mathbf{x} \leftarrow \mathbf{x} + \nu_\mu$ 
    return True
                                ▷ cell-entity was modified

```

A global simulation channel was also used to record snapshots of data at specified times. The pair of channels produced the results shown in Figure 4.1. Each simulation

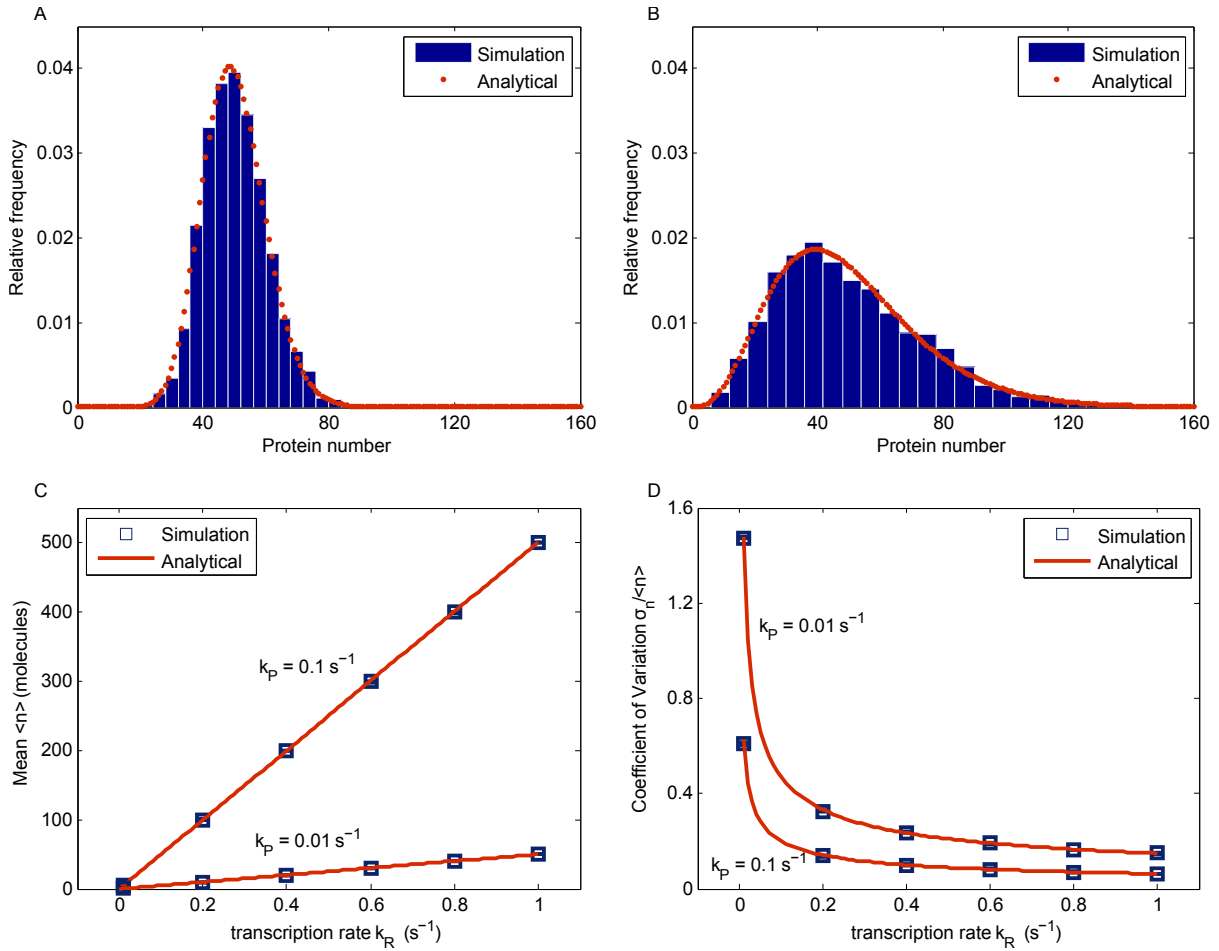


Figure 4.1: Validation of SSA simulation channel. (A,B) Steady-state distributions of protein in the two-stage model with (A) $k_R = 0.1\text{s}^{-1}$, $k_P = 0.1\text{s}^{-1}$ and (B) $k_R = 0.01\text{s}^{-1}$, $k_P = 1\text{s}^{-1}$. In both cases, $\gamma_R = 0.1\text{s}^{-1}$ and $\gamma_P = 0.002\text{s}^{-1}$. (C) Mean expression and (D) coefficient of variation as a function of transcription rate for two values of translation rate.

used $N_{\text{init}} = N_{\text{max}} = 5000$ cells. The top panels show the steady state distribution of protein with the same mean but obtained with different values of k_R and k_P . The bottom panels map the relationship of mean protein expression $\langle n \rangle$ and the coefficient of variation $\sigma_n/\langle n \rangle$ with the transcription and translation rate parameters. They are in excellent agreement with analytical results. Note that the distribution in 4.1B has a significantly greater spread than that in 4.1A. The greater variance is due to expression occurring in infrequent translational bursts. The ratio k_P/γ_R , measures the average burst size, that is, the average number of transcripts produced from a single mRNA molecule

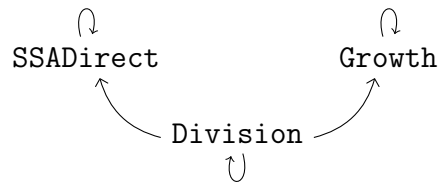
during its lifetime.

4.1.2 Incorporating growth and division

Next, cell division and the partitioning of gene product molecules is incorporated into the model by introducing two new local simulation channels: one to update the cell volume (**Growth**) and one to handle cell division (**Division**). Volume growth is assumed to be uncoupled from the reaction kinetics. It follows a deterministic exponential law

$$V(t) = V_0 e^{k_V t}, \quad (4.6)$$

where V_0 is the initial volume and k_V is the growth rate. The cell divides when it reaches a threshold volume V_{th} . The threshold is sloppy, sampled from a normal distribution with a mean value of \bar{V}_{th} at each division. Upon division, the parental volume is apportioned among the two newborn cells according to a fixed ratio f . The mRNA and protein contents are distributed binomially with parameter p —this amounts to “flipping a coin” for each molecule to determine to which cell it belongs. Two cases are considered: 1) symmetric division, in which contents are split 1:1 (i.e., $p = f = 0.5$), and 2) asymmetric division, in which contents are split 4:1 (i.e., $p = f = 0.2$). Because growth and reaction kinetics are not coupled, only **Division** triggers the rescheduling of other channels. The dependency graph looks like:



First, the two cases are simulated with $N_{\text{init}} = N_{\text{max}} = 2,000$ using a global simulation channel to record population snapshots. The cells are initialized at a random point in the division cycle and with zero mRNA and protein. The joint density distributions of

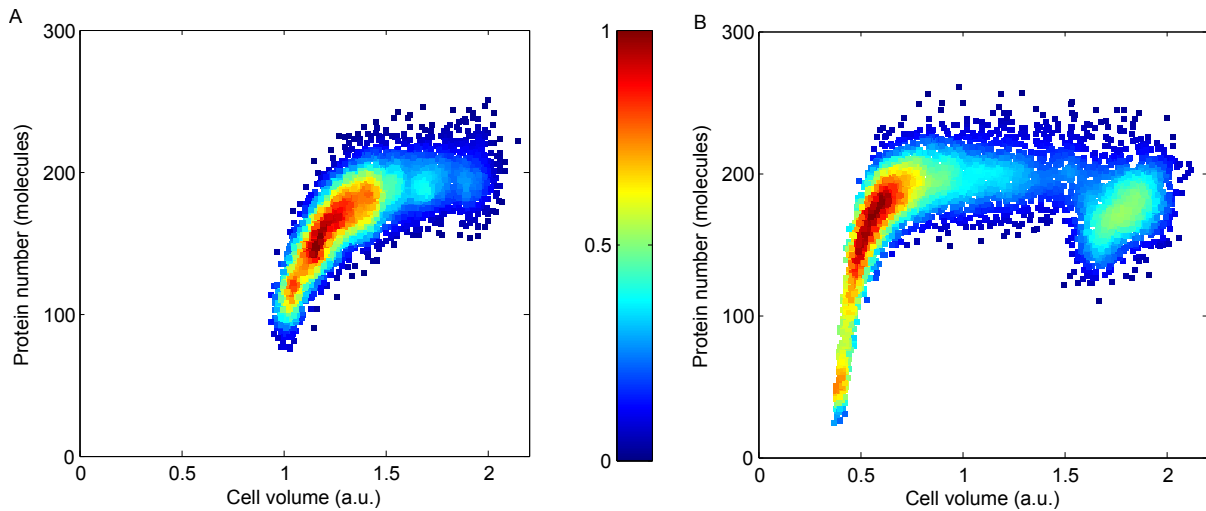


Figure 4.2: Joint density histograms of cellular volume and protein levels in the case of (A) symmetric division (1:1) and (B) asymmetric division (4:1). Asymmetry produces three discernible density peaks.

protein content and volume at steady state are shown in Figure 4.2. Note that symmetric division (4.2A) does not have a qualitative effect on the shape of the steady state protein distribution as compared to Figure 4.1, while strong asymmetry in division (4.2B) produces a profile that is bimodal with respect to each of protein and volume.

Next, modified versions of the simulation channels described were used to produce the full time courses of entire cell lineages instead of only population snapshot data. Instead of holding single values, the state variables of the cells are made to be arrays that store the time stamped event history of a cell during its life-cycle. To record lineage data, just before a cell divides the modified `Division` channel saves the event history of the cell to memory and resets the arrays for the daughter cells. The results of simulating cell lineages starting with a single cell entity is shown in Figure 4.3, with the case of symmetric division on the left and asymmetric division on the right.

Figure 4.3A/B and 4.3C/D show time traces of protein expression and cell volume, respectively, of the individual cells superposed in grey. The time trace of a single random cell chain is highlighted in each plot. The graphs displayed in 4.3E/F are lineage den-

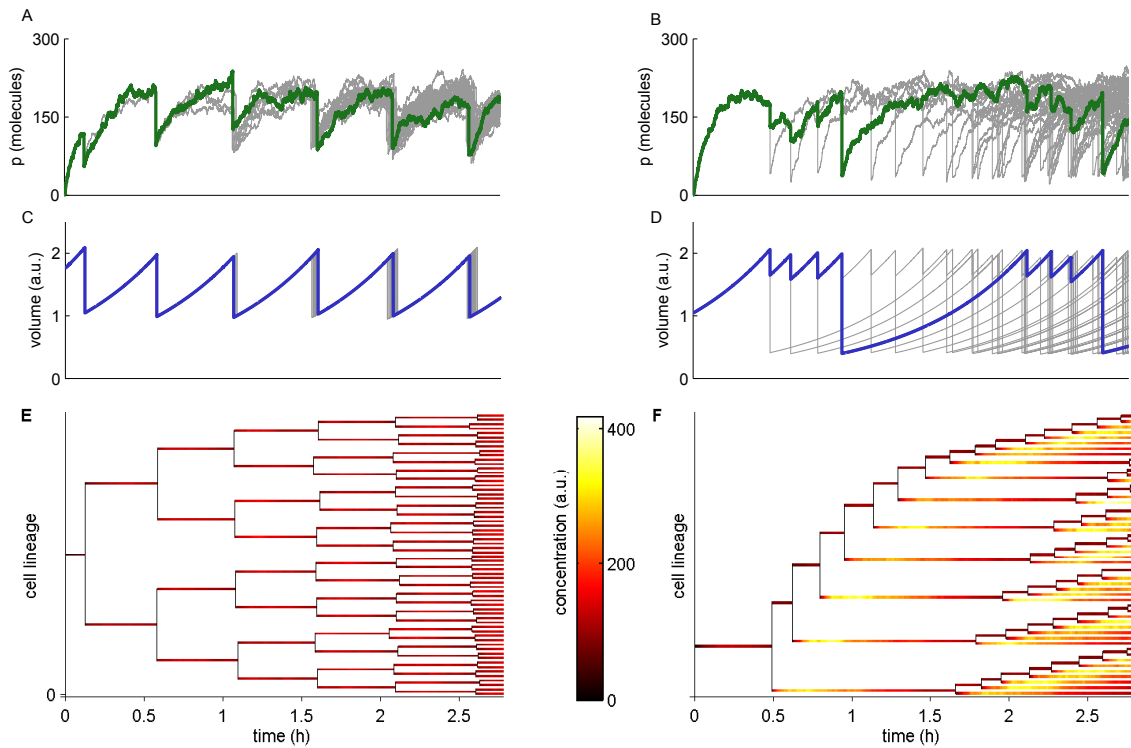


Figure 4.3: Lineage dynamics starting from a single cell in the case of symmetric division (A,C,E) and asymmetric division (B,D,F). **(A,B)** Superposition of time traces of protein expression. The time trace of a random cell chain is in green. **(C,D)** Superposition of time traces of cell volume with a random cell chain in blue. **(E,F)** Lineage dendograms coloured according to protein concentration.

drograms that display the temporal and genealogical relationship between the cells. The lines are coloured according to the protein concentration in order to provide a glimpse of the internal dynamics of the individual cells over time.

The data shows a gradual desynchronization of the single-cell dynamics per generation in the symmetric case due to noise in gene expression and sloppiness in the division cycle. In the asymmetric case, division produces a large cell that divides sooner (reaches the threshold volume rapidly) and a small daughter cell that divides much later, so that the dendrogram is unbalanced. Note that in the case of symmetric division, both protein number and volume drift continuously over the cell division cycle, while the protein concentration does not change considerably. However, in the asymmetric case, early after partitioning in the smaller daughter cells, protein levels rise proportionally more rapidly than volume, producing a transient spike in concentration.

4.1.3 Incorporating extrinsic sources of variability into the reaction kinetics

Much of the literature on stochastic gene expression has dealt with the problem of distinguishing noise origins from noise propagation in gene regulatory networks [27]. However, stochastic models of gene networks usually consist of a simplified set of elementary reactions whose kinetic rates involve only the copy numbers of the components of the network, that is, they only include sources of variability that are intrinsic to the system being considered. They ignore sources of variability extrinsic to the components being studied, such as variation of the elements of the transcriptional or translational machinery of the cell, the changing cell volume, or the levels of upstream regulators. The overall contribution of outside variables is thus tacitly “absorbed” into the rate constants of the model reactions and assumed not to change. Part of the problem is that the exact sources of extrinsic variability in gene networks are largely unknown and likely depend on the

system being studied, and it is not clear how to model them. However, they do tend to affect several components of the system of interest and the fluctuations they produce tend to have long time scales [5].

Incorporating the variation of extrinsic sources leads to rate “constants” that are *time-dependent* [32], which are not handled by the standard Gillespie algorithm. The problem with fluctuating rate parameters stems from the fact that when the propensity $a_j(t)$ of a reaction channel is time-dependent, the probability of its tentative reaction time step τ_j is

$$P(\tau_j) = a_j(\tau_j) \exp\left(\int_t^{t+\tau_j} a_j(t) dt\right), \quad (4.7)$$

and sampling τ_j from this distribution from a uniform random variate r_j between 0 and 1 then involves the formula

$$\int_t^{t+\tau_j} a_j(t) dt = -\ln(r_j). \quad (4.8)$$

An exact updating formula can be recovered only in special cases where the integral can be solved. For instance, this has been developed for the case of propensities that depend on an exponentially growing cell volume [93]. Otherwise τ_j needs to be found implicitly by computing the above integral numerically at each update, which can lead to unacceptably long run times, or an approximate method must be used.

The most basic approximate approach is to use the standard Gillespie algorithm and simply update the rate parameters before each scheduling step, but this is only accurate if the rate parameters change slowly relative to the frequency of reaction firings. A modestly efficient approach that maintains good accuracy was proposed by Shahrezaei and Swain [32]. It involves approximating the time-dependent propensities $a_j(t)$ as piecewise linear functions over sufficiently short time intervals. Their method is depicted in Figure 4.4. The method involves setting a series of time barriers at a fixed distance apart to

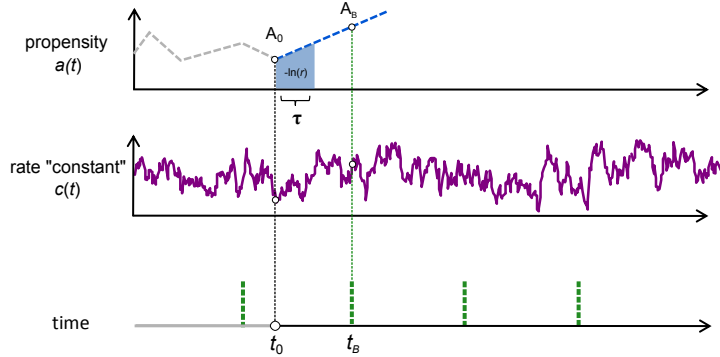


Figure 4.4: Modified SSA algorithm for time-varying propensities. Each time-dependent propensity function is approximated by a piecewise linear function. See text for details.

serve as an upper bound on the size of the piecewise linear intervals. Assume the system is at time t_0 with state $\mathbf{x}(t_0)$ and that the next barrier is at time t_B . For simplicity, assume only one reaction channel R_k is time-dependent with rate constant $c_k(t)$. Then to calculate τ_k , the values of the rate constant at the two time points $C_0 = c_k(t_0)$ and $C_B = c_k(t_B)$ are used along with the current state of the system $\mathbf{x}(t_0)$ to calculate $a_k(t_0)$ (call it A_0) and to estimate $a_k(t_B)$ (call it A_B). One can then approximate $a_k(t)$ locally by the straight line joining A_0 and A_B . The area under the approximated $a_k(t)$ curve is then a trapezoid and an explicit formula can be given to compute τ_k from a random variate r_k

$$\tau_k = \frac{A_0}{\alpha} \left(-1 + \sqrt{1 - \frac{2\alpha}{A_0^2} \ln(r_k)} \right), \text{ where } \alpha = \frac{A_B - A_0}{t_B - t_0}. \quad (4.9)$$

If $\alpha = 0$, then $a_k(t)$ is constant and the standard updating formula, $\tau_k = -\ln(r_k)/A_0$, is used instead. The value of the next time step τ is then obtained as in the First-Reaction method (Alg. 2.2). If $t_0 + \tau < t_B$, the next reaction channel is fired. If instead $t_0 + \tau \geq t_B$, the system is advanced to time t_B , no reaction is fired, and the next barrier is set at $t_B + T$. The reactions are then rescheduled.

The procedure described in [32] was implemented in a novel way by using two simulation channels: one to handle the reaction firing steps `RxnStep` and one to handle stepping to the time barrier `BarrierStep` (pseudocode in Alg. 4.2, 4.3). In terms of

Algorithm 4.2 RxnStep channel

```

public SCHEDULE(cell-entity, g-data, t)
    Calculate  $A_0$  and  $A_B$  from  $C_0$  and  $C_B$ 
    Calculate  $\tau_j$ 's
    Find  $\tau$  and  $\mu$ 
    eventTime  $\leftarrow t + \tau$ 

public EXECUTE(cell-entity, g-data, t, b)
     $C_0 \leftarrow c_k(\text{eventTime})$ 
     $x \leftarrow x + \nu_\mu$ 
    return True

```

Algorithm 4.3 BarrierStep channel

```

public SCHEDULE(cell-entity, g-data, t)
    eventTime  $\leftarrow t_B$ 

public EXECUTE(cell-entity, g-data, t, b)
     $C_0 \leftarrow C_B$ 
     $C_B \leftarrow c_k(t_B + T)$ 
     $t_B \leftarrow t_B + T$ 
    return True

```

scheduling dependencies, the execution of `BarrierStep` triggers scheduling of `RxnStep`, but the reverse dependence is not required.

To test the implementation, we simulate extrinsic fluctuations in a three-stage gene expression model, as in [32], where a continuous stochastic process drives the promoter activation rate k_{ON} . To observe the effect of extrinsic noise, one usually measures the output on two functionally identical “copies” of a system subject to the same extrinsic fluctuations. This is shown in Figure 4.5, which plots the joint histogram of expression data from two identical promoters collected at regular time points. The simulation on the left involves only intrinsic noise; the joint distribution is spread quite evenly because the sources of fluctuations are independent. On the right, a common source of extrinsic fluctuations induce correlations which cause the distribution to become skewed along the diagonal. The shapes of the distributions obtained agree with those in [32].

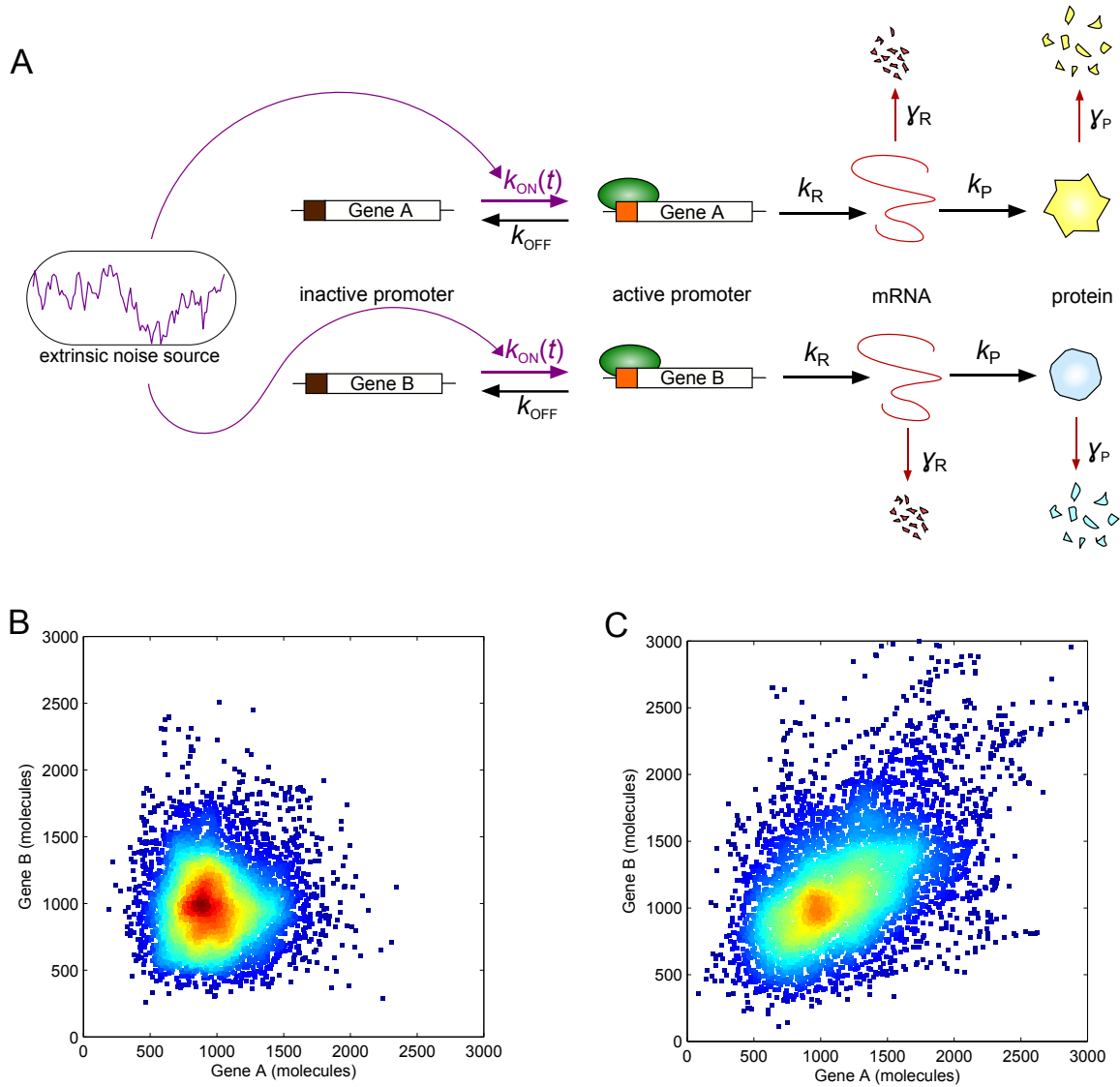


Figure 4.5: Simulating gene expression with extrinsic sources of fluctuation. **(A)** Three-stage gene expression model including promoter kinetics. A common extrinsic noise source drives the promoter activation rates of the two reporter genes, $k_{ON}(t) = k_0\xi(t)$, where $\xi(t)$ is a continuous stochastic process with a long autocorrelation time, as in [32]. **(B,C)** Joint distribution of two time courses of gene expression in the **(B)** absence and **(C)** presence of a time-varying promoter activation rate parameter $k_{ON}(t)$.

4.2 Differential reproduction and the constant-number method

4.2.1 Background

It has been demonstrated that the CPS framework can handle combinations of state updating algorithms along with cell division and partitioning, and can produce lineage structures. In this section, it is demonstrated that using the resampling substitution technique—the so-called constant-number method (see Section 2)—the framework can deal with cells reproducing at different rates in a large ensemble. The competitive growth in a population of differentially replicating cells is approximated in the constant-number method by a “selection-like” process of random substitution. Although the size of the simulated population no longer changes, the composition of the cell ensemble is meant to be a finite-number sample of the “true” population. Rather than consider a model where cells can exhibit a continuum of phenotypes, we restrict our analysis to a simple model of two discrete phenotypes. This is primarily because the model chosen has an analytic solution which can be used to compare and assess the performance of the simulation results.

4.2.2 Model

Discrete phenotype models have been used in the theoretical analysis of bistable or multi-stable gene expression states [9, 47]. Actual well-characterized genetic systems that exhibit bistable behaviour include the galactose utilization network in *S. cerevisiae*, the sporulation decision pathway in *B. subtilis*, and the lysis-lysogeny decision of bacteriophage lambda. In the model of bistability presented here (see Figure 4.6), cells can interchangeably assume an *OFF* or 0-state or an *ON* or 1-state, but the molecular details

of what drives the transitions is not made explicit. Rather, the telegraphic transitions are stochastic. Furthermore, the reproductive rates of cells in the *OFF* and *ON* states are λ_0 and λ_1 , respectively (division events are also modeled as a stochastic process). In addition, when a cell divides we include the possibility that the division process itself may induce a switch in the newborn to the other phenotypic state with a certain probability: each newborn is either assigned the state of its mother with probability σ_i or the opposite state with probability $1 - \sigma_i$, $i = 0, 1$.

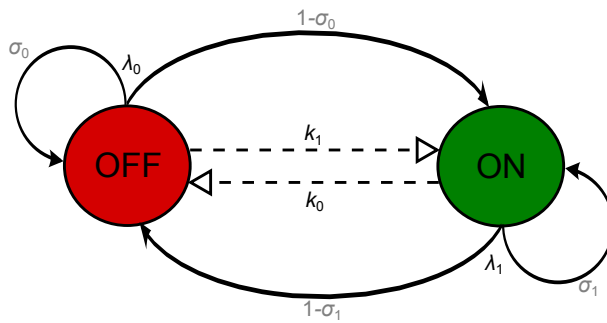


Figure 4.6: Model of bistable phenotype switching and reproduction. Cells in the two i subpopulations ($i = 0, 1$) can switch phenotypes (migrate between compartments, dashed arrows) with rates k_i . Cells also reproduce (solid arrows) with rates λ_i . Each newborn has a probability σ_i of inheriting the parental phenotype.

Finally, we impose the Markov property: that all the stochastic transition processes (i.e., birth and switching) have constant exponentially distributed inter-occurrence times in the absence of other processes. This implies that the transition processes are “memoryless”, which is a reasonable assumption in the case of state switching transitions, but it is not very realistic for cell division because it implies that the timing of division events is independent of the age of the cell since its birth! Despite this, the Markov property is imposed because it can be shown that the resulting model is equivalent to a special type of continuous-time Markov chain called a birth-migration (BM) process (see Appendix B), which is amenable to analysis. BM models, or more generally, birth-death-migration models, are often used in population ecology to model the movement of animal species between spatial compartments, ecological niches, mutation states, or

life-cycle stages [94, 95]. They are also mathematically the same kind of process as stochastic chemical reaction models (think of compartments as equivalent to chemical reactant species).

The equivalent BM formulation of the binary phenotype model has two compartments representing the two subpopulations of cells—i.e., two stochastic variables $X_0(t)$ and $X_1(t)$. In the individual-based formulation of the model, these variables correspond to the numbers of cell entities exhibiting the *OFF*-state and the *ON*-state, respectively, at a given time. Because of the fact that all of the transition rates in the BM model happen to be linear in the variables $X_0(t)$ and $X_1(t)$, we can derive a closed set of ordinary differential equations (see Appendix B) for the expected values $x_0 = \langle X_0(t) \rangle$ and $x_1 = \langle X_1(t) \rangle$:

$$\frac{dx_0}{dt} = k_0x_1 - k_1x_0 + (2\sigma_0 - 1)\lambda_0x_0 + 2(1 - \sigma_1)\lambda_1x_1, \quad (4.10)$$

$$\frac{dx_1}{dt} = k_1x_0 - k_0x_1 + (2\sigma_1 - 1)\lambda_1x_1 + 2(1 - \sigma_0)\lambda_0x_0. \quad (4.11)$$

These are also known as the first moments of $X_0(t)$ and $X_1(t)$ and describe the average trajectory of a large number of realizations of the BM process. They also describe the deterministic trajectory obtained at the limit of very large population size.

Since the total population grows indefinitely, it never reaches a steady state and simulating the BM process will slow down significantly over time. However, what is of interest is not the absolute numbers of individuals but the relative composition of the population, which does reach a steady state. The quantities of interest are therefore the *fraction* of cells in each subpopulation, denoted $F_0(t)$ and $F_1(t)$. Fortunately, the first moment equations $f_0 = \langle F_0(t) \rangle$ and $f_1 = \langle F_1(t) \rangle$ can also be derived (see Appendix B):

$$f_0(t) = 1 - f_1(t). \quad (4.12)$$

$$\begin{aligned} \frac{df_1}{dt} = & (\lambda_0 - \lambda_1)f_1(t)^2 + [\lambda_0(2\sigma_0 - 3) + \lambda_1(2\sigma_1 - 1) - k_0 - k_1] f_1(t) \\ & + k_1 - 2\lambda_0(\sigma_0 - 1), \end{aligned} \quad (4.13)$$

Because the constant-number method produces estimates of $F_0(t)$ and $F_1(t)$ (i.e., $\hat{F}_i = N_i/N_{\max}$, where N_i is the current number of cell entities in state i in the simulation), the solution to (4.12) and (4.13) provides a theoretical average trajectory for comparison. The individual-based version of the model is implemented in CPS using two event-driven simulation channel classes: one to handle state switching, and another to handle cell division, with the switching channel dependent on the division channel.

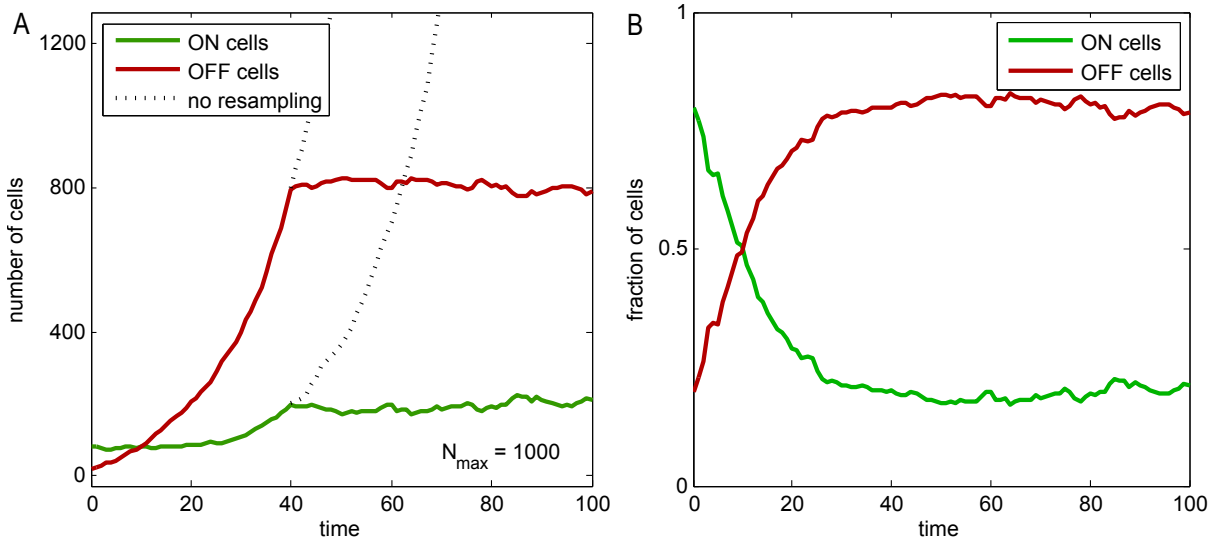


Figure 4.7: Comparing the sizes of subpopulations in simulations with and without the constant-number size cap. (A) The numbers of *ON*- and *OFF*-cells in a run of a population growing without bound (dotted) and, superposed, an identical run using a constant-number size cap. (B) The fractions of *ON*- and *OFF*-cells from the simulation in (A).

4.2.3 Results and discussion

Figure 4.7 shows a time course of the *number* of cell entities in each phenotype state over time with the population growing exponentially without bound. Superposed is an identical simulation run except that the population size was capped at $N_{\max} = 1,000$.

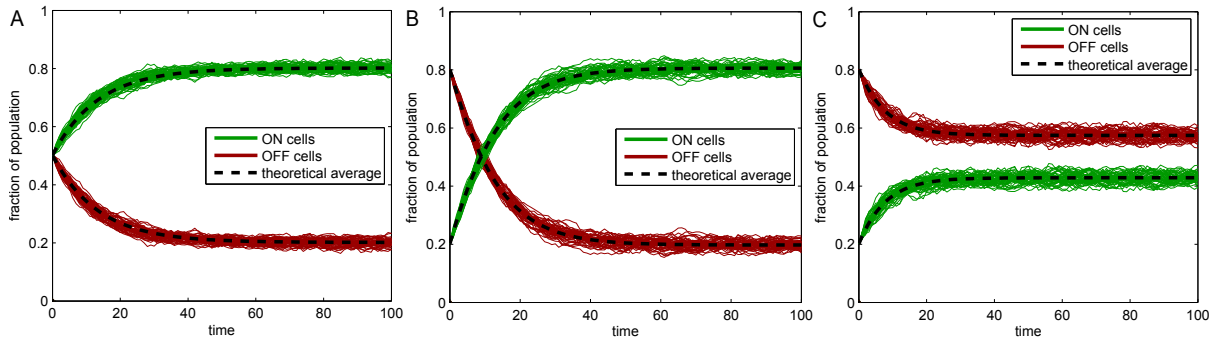


Figure 4.8: Simulating the bistable switching model using the constant-number method. Ensembles of time traces of subpopulation fractions from simulation runs in the case of (A) equal division rates in the two subpopulations ($\lambda_0 = \lambda_1 = 0.01$, $k_0 = 0.015$, $k_1 = 0.06$, $\sigma_0 = \sigma_1 = 1$), (B) unequal division rates ($\lambda_0 = 0.03$, $\lambda_1 = 0.07$, $k_0 = 0.02$, $k_1 = 0.05$, $\sigma_0 = \sigma_1 = 1$) and (C) division-induced state switching (same parameters as (B), except $\sigma_1 = 0.5$).

Notice that when resampling substitution kicked in, the relative abundance of *OFF*-cells and *ON*-cells had already reached a steady state, meaning that the population has achieved balanced growth.

Figure 4.8A-C plots the fraction of cell entities of each type (*OFF*-cells in red, *ON*-cells in green) from 50 simulation runs with $N_{\text{init}} = N_{\text{max}} = 1,000$. The time course in 4.8A starts with an initial distribution of 500 *ON*-cells and 500 *OFF*-cells, while that in 4.8B starts 200 *ON*-cells and 800 *OFF*-cells. In both cases, the *ON*-cells eventually dominate in a similar steady state proportion. In 4.8A the growth rates of both cell types are identical ($\lambda_0 = \lambda_1$) with no division-induced switching ($\sigma_0 = \sigma_1 = 1$), so the transient dynamics are solely due to difference in the phenotype switching rates ($k_1 > k_0$). In 4.8B both $k_1 > k_0$ and $\lambda_1 > \lambda_0$ with $\sigma_0 = \sigma_1 = 1$. Not surprisingly, the cell type with the faster growth rate dominates the population. Interestingly, the reverse tends to be true when cell division can induce some degree of switching into the other state. This is shown in Figure 4.8C, which uses the same parameters as 4.8B except that $\sigma_1 = 0.5$, meaning that on average half of the progeny of *ON*-cells are born as *OFF*-cells. Almost counterintuitively, a faster reproductive rate of the *ON*-subpopulation tips the balance in favour of the *OFF* subpopulation. All the simulation curves agree well with the curves

of the expectations, $f_0(t)$ and $f_1(t)$, given in black, indicating that constant-number method does reproduce an accurate demographic composition of a temporally changing population with replicative competition.

Next, we investigate how the variability in the phenotype distributions obtained by simulation scale with N_{\max} . Starting with the same initial conditions, the random substitutions of the constant-number method contribute to the variability between realizations; however, if the sample population is sufficiently big, its composition—averaged over realizations—should match the theoretical composition that corresponds to an infinitely large population (in this case, $f_0(t), f_1(t)$). Figure 4.9 shows the fraction of ON -cells in the simulation over time for A) $N_{\max} = 100$, B) $N_{\max} = 1000$, and C) $N_{\max} = 5000$, each with $N_{\text{init}} = N_{\max}$. Plotted is the ensemble-average trajectory of 20 runs with a 1-standard deviation envelope. Clearly, as the size of the constant-number sample population increases, the variance diminishes and the composition converges to the theoretical value. Figure 4.9D shows that the root mean square error of \hat{F}_1 at balanced growth scales as $1/\sqrt{N_{\max}}$, which is the same way fluctuations in the X_i would scale with the total number of cells N when not using the constant-number method [55]. For a given N_{\max} , the variance stays roughly constant and the average simulation trajectory does not appear to diverge over time from the theoretical average trajectory, suggesting that, in this model, the resampling substitutions do not produce any error propagation over time.

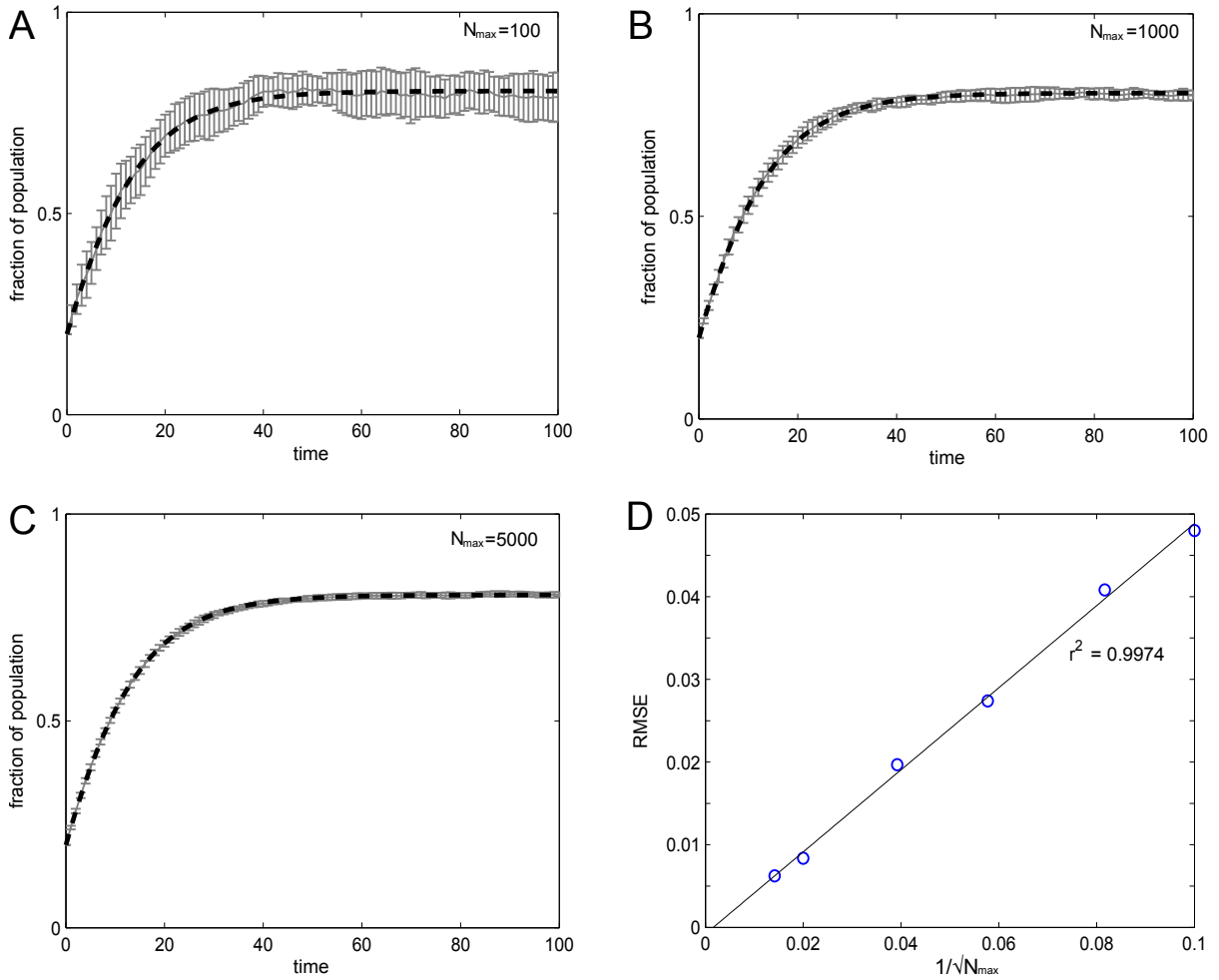


Figure 4.9: Assessing the N_{\max} -dependence of the constant-number method. In all simulations, $\lambda_0 = 0.03$, $\lambda_1 = 0.07$, $k_0 = 0.02$, $k_1 = 0.05$, $\sigma_0 = \sigma_1 = 1$, the initial fraction of *ON*-cells is 0.2, and $N_{\text{init}} = N_{\max}$. Variance reduction is observed when the bistable switching model is simulated with increasing N_{\max} of (A) 100, (B) 1000, (C) 5,000. The grey curves are average trajectories of 20 runs recorded at intervals of 1 time unit; error bars represent one standard deviation. The theoretical expected trajectory is given in black. (D) Root mean square deviation of simulated $\hat{F}_1(t)$ data from the theoretical expected value $f_1(t)$ over the time interval [50, 100] for different values of N_{\max} .

4.3 Size and replicative lifespan in budding yeast

4.3.1 Background

The existence of a limit of the number of cellular divisions, referred to as replicative aging, is common to somatic metazoan cells and yeast cells. In non-immortalized mammalian cell cultures, cells eventually reach a maximum number of divisions called the Hayflick limit, and the whole population eventually dies [96]. By contrast, in the budding yeast *Saccharomyces cerevisiae*, mother cells eventually cease to replicate while virgin daughter cells are constantly produced, so the whole population is immortal. Currently, a number of theories explaining the *replicative lifespan*—the number of cell divisions a cell achieves during its lifetime—of budding yeast have been proposed.

Unlike other eukaryotes, *S. cerevisiae* cells divide by budding, where a smaller daughter cell emerges from the mother cell as an independent compartment at the beginning of S-phase and pinches off at the end of the cell cycle. The asymmetry in this replication mechanism is thought to underlie the finite life span of individual yeast cells. An early theory held that division capacity was limited due to the formation of bud scars over the surface of the mother cell, but this was later dismissed by the observation that growth more than compensates for the loss of surface area due to scarring [45]. The most popular theory today postulates that some diffusible cytoplasmic “senescence factor” that is asymmetrically inherited by mother and daughter cell is responsible for aging. Though it has not yet been identified, some candidates include self-replicating extra-chromosomal ribosomal DNA circles that accumulate in the mother cell during the budding process, oxidized proteins, and damaged mitochondria [97].

One recent study on growth and aging in isogenic populations of budding yeast cells suggested that the replicative lifespan of yeast is limited by the progressive increase in volume due to asymmetric cell division [98]. The authors used three popular standard

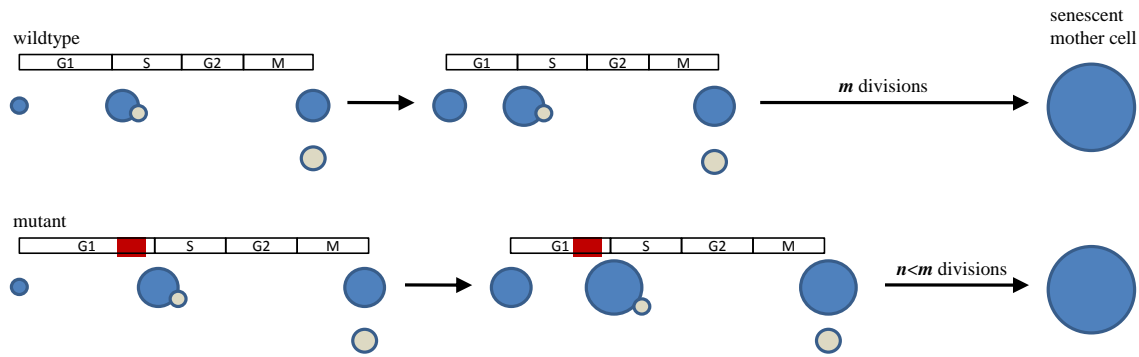


Figure 4.10: Theory of the size-limited replicative aging of budding yeast. A cell begins growing in G1 phase. Entry into S-phase is accompanied by bud formation. During S-phase growth primarily occurs in the bud, which separates after mitosis. Progressive increase in the size of the mother continues until reaching a critical size at which it cannot re-enter the cell cycle and becomes senescent. A hypothesized delay at the G1-S checkpoint that does not halt volume growth is depicted in red. Based on figure in Zadrag-Tecza *et al.* [98].

laboratory strains and mutant variants of those strains with various defects in antioxidant enzymes. Each pair of wild-type and mutant strains demonstrated a cessation of budding after reaching the same final volume, but had different replicative lifespans. Based on this and a previous study that used mating pheromone to inhibit budding but not volume growth [99], the authors propose that a genetically determined critical cell volume may be the main factor limiting the ability of mother yeast cells to accomplish a successful cell cycle. They explain that progressive growth of cell volume with each cycle is an unavoidable consequence of the mechanism of reproduction, because the mother cell experiences incremental growth during each G1 phase, before a new bud has even formed (see Figure 4.10). In the mutant cells, oxidative stress leading to DNA damage, would presumably cause delays at cell cycle checkpoints without hampering volume growth, so that mutants attain the limiting cell volume after a smaller number of cell divisions.

A more recent study [100] supports the above findings. The authors looked at a series of small-size, large-size and “longevity” mutant strains of yeast and observed the

same relationship between cell size and replicative lifespan. They found that cells that underwent fewer replications accrued more volume per generation and vice versa, reaching senescence at a similar maximal volume.

4.3.2 Model

Because the exact relationship between cell volume and the timing of S-phase entry and bud emergence, as well as the rates of volume growth of the unbudded mother and the bud at different stages of the cell cycle are poorly understood, we stick to a phenomenological model of growth that reproduces two observations:

1. The mother cell increases in volume after each division cycle [45],
2. The buds of older mothers tend to be larger [101].

While the studies described suggest that mother cell volume increases steadily with each generation, little is known about how fast volume accumulates over chronological time, so we make an arbitrary assumption. Gross (non-compartmentalized) cell volume growth was assumed to be linear at a given age (generation) and was modelled using $V(t) = V(t - 1) + \delta v$, where δv was obtained (for fixed time step $\delta t = 1$) using

$$\delta v = \frac{kg}{1 + \left(\frac{g}{k}\right)^2} \delta t, \quad (4.14)$$

where k is the maximal growth rate and g is the generation (number of buds produced). Thus, the growth rate is non-monotonic with age, increasing when the cell is younger, and tending to slow at old age. Cells divide asymmetrically, producing an “older” mother and a “virgin” daughter from the bud ($g = 0$). At each division, the daughter receives a fixed fraction (β) of the gross parental cell volume, while the mother receives the remaining fraction ($1 - \beta$). Division was set to occur every time a pre-specified (strain specific) volume *increment* ΔV was reached. When a critical volume is achieved after

cell division (V_{crit}), a cell is flagged as senescent and ceases to proliferate (i.e., it can not re-enter the cell cycle).

4.3.3 Results and discussion

Figure 4.11A shows the history of a single mother cell’s volume increasing over time. The periodic decrements are due to the budding off of daughter cells, which gradually get successively larger as well. When the mother cell volume crosses V_{crit} after division, it ceases to grow. Figure 4.11B presents a plot of gross cell volume as a function of generation. Different values of k and ΔV were chosen to produce results that mirrored the experimental results of Zadrag-Tecza *et al.* [98]. For the wild-type BY4741 strain $k = 4.6$ and $\Delta V = 12\mu\text{m}^3$, and for the Δprx antioxidant defective mutant strain $k = 1.15$ and $\Delta V = 42.3\mu\text{m}^3$. Both strains have a similar initial volume at age $g = 0$, but the mutant strain accrues volume at a faster rate. Because cells of both strains attain the same maximal volume, the mutant strain displays a shorter life-span. The data fits well to a linear trend as did the experimental results.

Figures 4.11 C and D are used to demonstrate an important result about simulating populations versus simulating ensembles of random cell chains. Figure 4.11C is the steady state gross cell volume distribution obtained from a simulation of 10,000 random cell chains. Simulating random cell chains in CPS is achieved simply by not producing or storing the extra newborn cell when a cell divides. A random cell chain means that at every division, there is a 50:50 chance of following the mother or the daughter cell. Figure 4.11D is the same distribution from a population simulation using resampling substitution with $N_{\text{init}} = N_{\text{max}} = 10,000$. Notice that the distributions are similar except for a second peak in 4.11C. This extra peak is an artifact that emerges as a result of slowly growing old cells and post-mitotic senescent cells that do not get out-competed by younger cells as they would in a population simulation, as can be seen in the age distributions

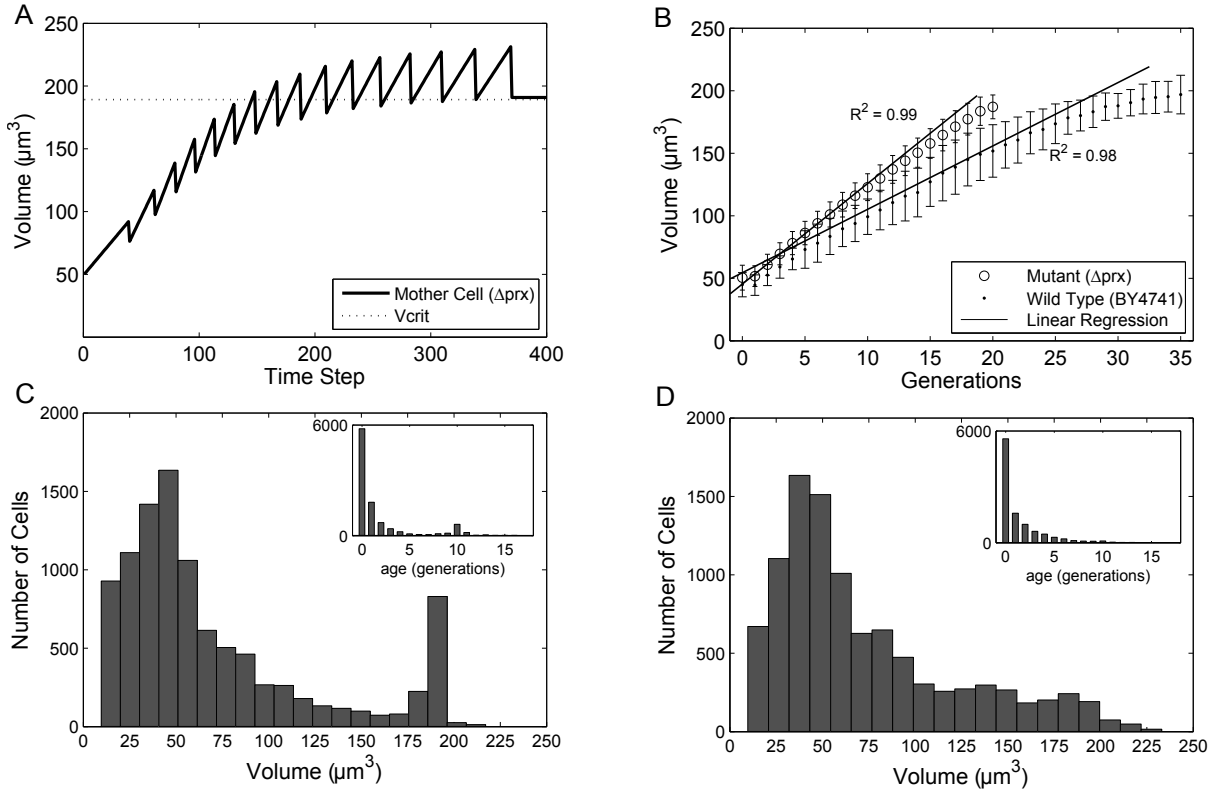


Figure 4.11: Simulating size-dependent replicative aging in budding yeast. **(A)** Time course of the gross volume of a single mother cell undergoing successive divisions until senescence. **(B)** Cell volume as a function of age in population simulations of wild-type and shorter-living mutant strains. **(C,D)** Steady state cell volume distributions from (C) ensemble simulation of cell chains and (D) population simulation using the constant-number method. Age distributions are inset.

(inset). The distributions obtained by a random cell chain approach are biased towards states of slower growth because cell chains remain in them for long periods without competition from fast replicators; senescence is an extreme case of an “absorbing” state because once entered, the cell ceases to change or divide. This highlights the importance of using the appropriate simulation methodology.

4.4 Epigenetic memory in the response to stress

4.4.1 Background

Organisms need to cope with a wide variety of environmental changes over a wide range of time scales. At the cellular level, gene expression patterns and programs have evolved to prepare for unknown challenges and respond to stress conditions. For example, cells maintain a fine balance between stress-related and growth-related gene expression programs, which are regulated by different signalling pathways and tend to have antagonistic physiological functions [102].

The fact that transcriptional dynamics can be tuned via hard-wired DNA regulatory elements suggests that expression noise is an evolvable trait [11], and much investigation has been conducted on how gene expression noise could be exploited to generate adaptive population variation to deal with environmental stress. This implies the use of gambling or bet-hedging strategies as a less costly alternative to investing in more precise sense-response mechanisms [9]. In support of this idea, promoters of stress-related genes tend to contain a TATA-box, an element which imparts not only faster transcription upon induction, but noisier expression [103, 104].

One group [105] tested the effect of noise on stress by introducing targeted promoter mutations to modulate transcriptional bursting in the expression of ZeoR, a protein conferring resistance to the antibiotic Zeocin. They compared the fitness of two strains with

low and high cell-cell variation in expression but similar mean level, as evinced by flow cytometry distributions. It was found that the strain with greater heterogeneity provided a selective advantage at high stress levels, while the less heterogeneous strain had greater fitness under low levels of stress. Theoretical models were used to explain the results by imagining different stress thresholds on the reproductive fitness of the population [11, 105], where cells expressing below the threshold perish and those expressing above the threshold are unaffected (see Figure 4.12A). When the stress level is low, a greater fraction of the low-noise strain can survive and reproduce (represented by the shaded areas), whereas when the stress level is high, the high-noise strain emerges as the more fit.

However, this conclusion suffers from the implicit assumption that the expression levels in the cells (and any offspring produced) are static over the time scale of stress exposure; it ignores the temporal variability in single cells. Fluctuations in gene expression can occur over a wide range of timescales—while intrinsic transcriptional bursting may occur on the order of milliseconds to minutes, extrinsic sources of variation can lead to long range fluctuations with timescales on the order of the cell cycle [107, 108]. The notion of a fluctuation *timescale* in gene expression is sometimes referred to as *epigenetic memory* in the physics literature. Note that this definition differs from the more common use of the term by geneticists and molecular biologists. Memory in the sense defined here can be quantified as the autocorrelation in an expression time series; thus another term for memory is “coloured” noise to contrast it with “white” noise in which fluctuations produce no temporal correlations. Figure 4.12 illustrates how the expression memory of a single gene in individual cells is hidden when observing the population snapshot. Expression could be varying rapidly in which cells visit the full range of phenotypes available to them over the experimental timescale, or it may be fluctuating slowly, in which each cell has a stable individuality (high degree of memory), which may be heritable. The conclusion of the model in 4.12A, which does not take memory into account, is only valid

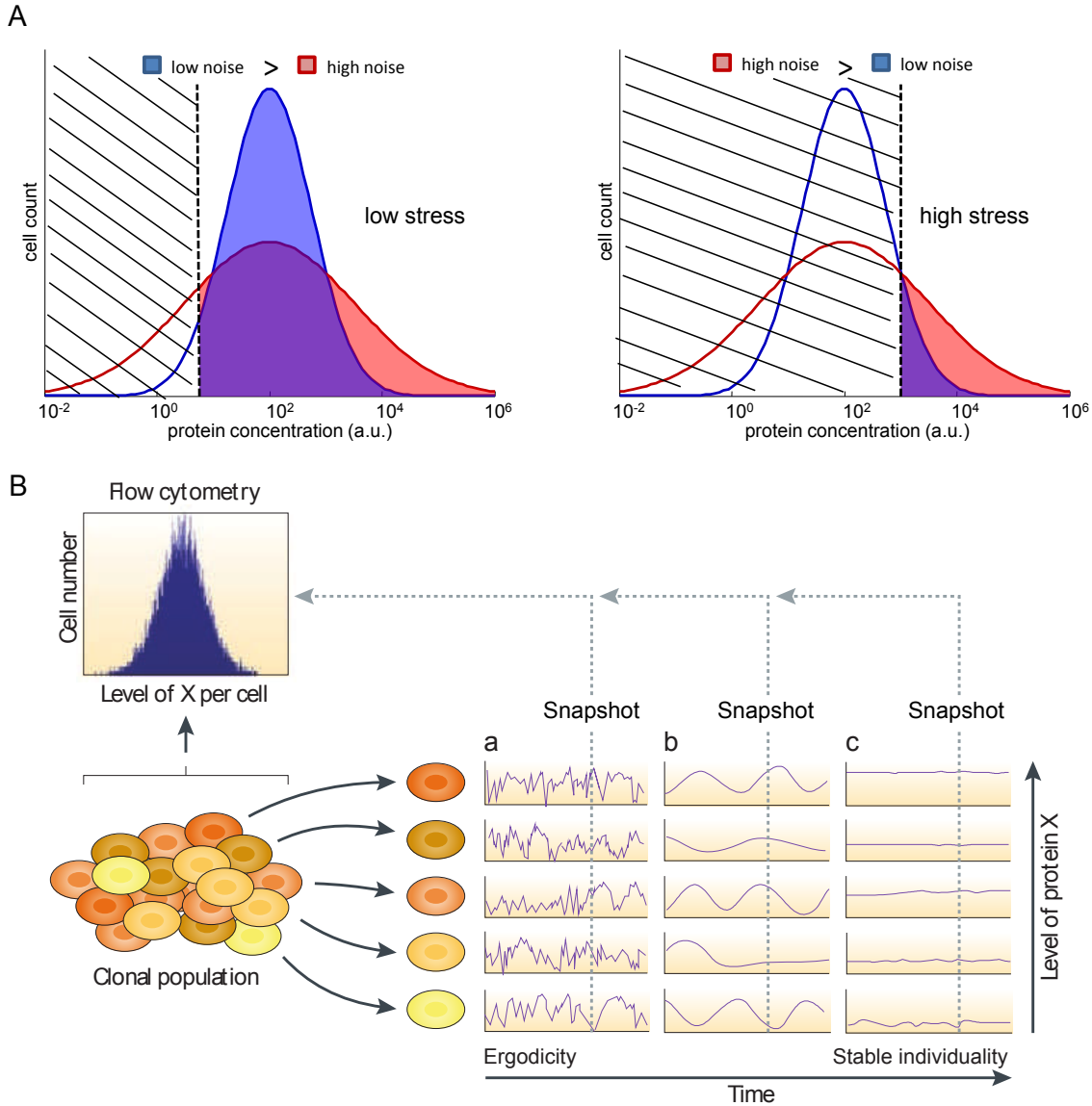


Figure 4.12: Gene expression noise and epigenetic memory. **(A)** Static model used to interpret the results of experiments by Blake *et al.* [105] that neglects expression dynamics. **(B)** The timescale of gene expression in individual cells is often hidden beneath the steady state population distribution, and can range from fast fluctuations (ergodicity) to stable individuality. Figure reproduced with permission from Brock *et al.* [106].

at the limit of severe and acute stress (where the unfit cells are instantaneously killed), or at the limit of infinite memory (where cells do not change expression).

A recent study in *S. cerevisiae* used a tunable synthetic gene network to produce populations with different distributions of a *URA3*-reporter fusion protein [109]. In the presence of the drug 5-fluoroorotic acid (FOA), the Ura3p enzyme produces a toxic metabolite¹. Under prolonged exposure to FOA, in some cases the protein distribution was observed to shift in the direction of lower toxicity, as shown in Figure 4.13. The “adaptive drift” was reversible, returning to pre-treatment levels upon removal of FOA. It was hypothesized that epigenetic memory could have been responsible for the observed dynamic response to imposed stress. Moreover, a similar role for epigenetic memory has been hypothesized to contribute to the emergence of drug resistance in cancer cell populations [106].

In this section, a model of coloured gene expression is developed to assess the adaptive effect of different expression timescales under long-term stress exposure.

4.4.2 Model

We use a continuous stochastic process called an Ornstein-Uhlenbeck (OU) process as a phenomenological model of stochastic expression of a single gene product with a tunable memory parameter. An OU process $x(t)$ is a continuous, mean-reverting stochastic process that can be represented using the stochastic differential equation:

$$x(t + dt) = x(t) - \frac{1}{\tau}(\mu - x(t))dt + \sqrt{c} dW(t), \quad (4.15)$$

where μ is the mean level, and $dW(t)$ is a temporally uncorrelated normal random variable with mean 0 and variance dt called a Wiener process. The OU process can also be

¹Hence, in contrast to the previous experiment that dealt with a drug-resistance gene, here lower gene expression is beneficial

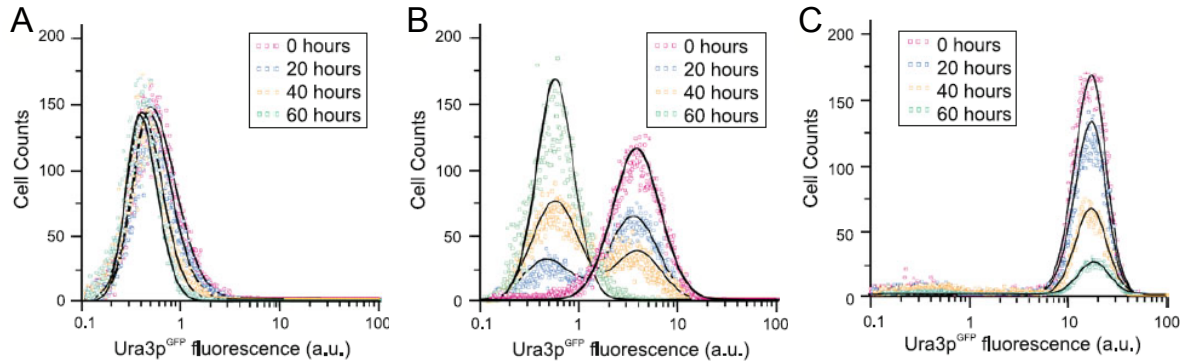


Figure 4.13: Adaptive drift of $URA3^{GFP}$ -expressing yeast cell populations under prolonged exposure to stress. The strain expresses $URA3^{GFP}$ driven by an *rtTA*-responsive promoter. *rtTA* is driven by a P_{gal} promoter so that its expression is modulated using galactose, while its activity is modulated using doxycycline, allowing the steady-state expression Ura3p^{GFP} distribution to be tuned. The flow cytometry distributions show the counts of viable cells at different times following the exposure to FOA. **(A)** A low-expressing population incurs a slight drift to lower expression levels, with most cells remaining viable. **(B)** A population with moderate expression experiences a dramatic change, undergoing a bimodal transition in which the high expression peak diminishes and a low-expressing subpopulation emerges. **(C)** A high-expressing population is subjected to high levels of stress and the population declines over time. Figure used with permission from Zhuravel *et al.* [109].

expressed using the Langevin form more familiar to physicists and engineers:

$$\frac{dx(t)}{dt} = \frac{1}{\tau}(\mu - x(t)) + \sqrt{c} \xi(t), \quad (4.16)$$

where $\xi(t)$ is Gaussian white noise ($\langle \xi(t) \rangle = 0$, $\langle \xi(t)\xi(t') \rangle = \delta(t)$). The parameter τ is called the relaxation time, and c is called the diffusion constant [110]. The diffusion constant determines the strength of random fluctuations, while the relaxation time determines how rapidly on average a fluctuation will dissipate back to the mean (i.e. the time scale of fluctuation). The stationary probability distribution of an OU process is a Gaussian or normal distribution with mean μ and variance $c\tau/2$. The OU process thus allows us to impose a fixed degree of heterogeneity (the shape and size of the stationary distribution) and observe the effect of varying the degree of epigenetic memory simply by modulating the values of c and τ as illustrated in Figure 4.14.

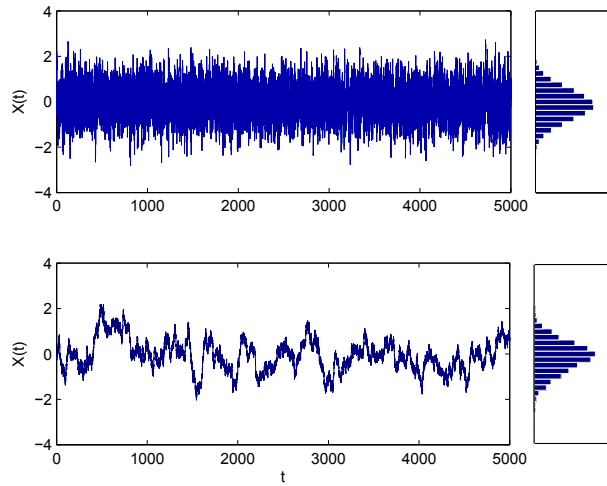


Figure 4.14: The Ornstein-Uhlenbeck process. Two realizations of the OU process representing low memory (fast relaxation, above) $\tau = 1$ and high memory (slow relaxation, below) $\tau = 100$, with the same stationary distribution. In both cases, $c\tau = 1$.

To reproduce the long-tailed protein distributions often seen experimentally and to eliminate the possibility of negative quantities, we model protein concentration by setting $\mu = 0$ and exponentiating $x(t)$ to give a geometric OU process:

$$y(t) = e^{x(t)-c\tau/4}. \quad (4.17)$$

The geometric OU process has a log-normal stationary distribution (which appears normal when plotted on a logarithmic scale), with variance $e^{c\tau/2}$. It has an approximate autocorrelation time of τ [32]. The constant factor of $e^{-c\tau/4}$ is included to normalize the concentration to have a dimensionless mean of 1.

Cell growth is not modeled using a volume-based threshold, but rather an abstract measure of reproductive capacity $\kappa(t)$ that depends on the level of protein expression and determines when a cell divides or dies. Starting at a base level of $\kappa = 1$, reproductive capacity evolves according to

$$\frac{d\kappa(t)}{dt} = w(y(t)) \kappa(t), \quad (4.18)$$

where $w(y)$ is the expression-dependent fitness or reproductive rate function, which is a sigmoidal Hill-type function of the form

$$w(y) = \frac{w_{\max} + w_{\min}(\frac{y}{K_w})^n}{1 + (\frac{y}{K_w})^n}, \quad (4.19)$$

where w_{\min} and w_{\max} are the minimum and maximum reproductive rates, K_w is the Hill constant, and n the Hill coefficient. The reproductive rate tends to w_{\max} when expression is low and falls to w_{\min} when expression is sufficiently high as a result of the metabolic stress caused by the protein. The steepness and midpoint of the curve of the fitness function $w(y)$ can be changed by modifying the Hill parameters. When $\kappa(t)$ reaches a threshold value of 2, the cell divides. However, $\kappa(t)$ may decrease due to stress if w_{\min} is negative, and if a cell's capacity falls below a threshold of 0.5, the cell is flagged as dead or nonviable. In the simulation experiments presented, division events are perfectly symmetric: the daughter cells have a reproductive capacity reset to 1 and both inherit the parental protein concentration (no partitioning error or asymmetry). The time unit of the model is set to be equal to the generation time (t_D)—the time it takes a cell's reproductive capacity to double—in the absence of stress (i.e., $t_D = \ln(2)/w_{\max}$).

The model was implemented using three local simulation channels: one for reproductive capacity, one for the time evolution of protein concentration (simulated using a numerically exact method [110]), and one time-driven channel to detect the crossing of division or death thresholds and respond accordingly. A global simulation channel was also included to turn on or off a global boolean variable **stress**, which corresponds to the addition or removal of FOA to the system. Finally, another global simulation channel was used to record data at regular intervals. The initial and maximum ensemble size used in the simulations was 10,000.

4.4.3 Results and discussion

Simulations were first conducted to demonstrate the flow of the population distribution in the response to stress. Beginning with two different populations in the absence of stress expressing $URA3^{GFP}$ at steady state, stress is induced after $t = 0$ and the distribution of viable cells is tracked over time. Figure 4.15 shows the effect of different degrees of expression memory. In the first population, the expression relaxation time is short: $\tau = 0.1$ or 10% of the stress-free cell generation time. In the second case $\tau = 15$, so cells have higher expression memory. The value of the diffusion constant c is adjusted so that the stress-free distributions have the same shape. The reproductive rate curves in the simulations shown (green dashed curves) have Hill constant $K_w = 0.1$ with a steep threshold $n = 10$.

Figure 4.15A shows that in the low-memory population, the number of viable cells diminishes over time and the population goes extinct by around 40 generations. On the other hand, in the high-memory population (Figure 4.15B), the expression distribution shifts to the left over time, producing a bimodal transient before settling to a new steady state. As a result, the population persists in the face of chronic stress. This occurs because cells in with lower $URA3^{GFP}$ expression levels tend to remain fit for a long enough period to reproduce. In the low-memory case, cells are rarely able to recover their reproductive capacity due to rapid gene expression fluctuations and eventually die.

Note that the profile of population drift is sensitive to the steepness of the reproductive rate function (i.e., the Hill coefficient or “cooperativity” n) and its the position of its half-saturation value (i.e., the Hill constant K_w). In Figure 4.16A and B, the half-saturation point of the fitness curve is set at expression values of 0.05 and 0.5, respectively, with $\tau = 10$ and $n = 10$. In 4.16A, a small subpopulation maintains viability after 40 generations, while when the stress is less severe (4.16B) the population shift is minor. Figure 4.16C and D show simulations with a steep $n = 10$ and soft $n = 2$ threshold,

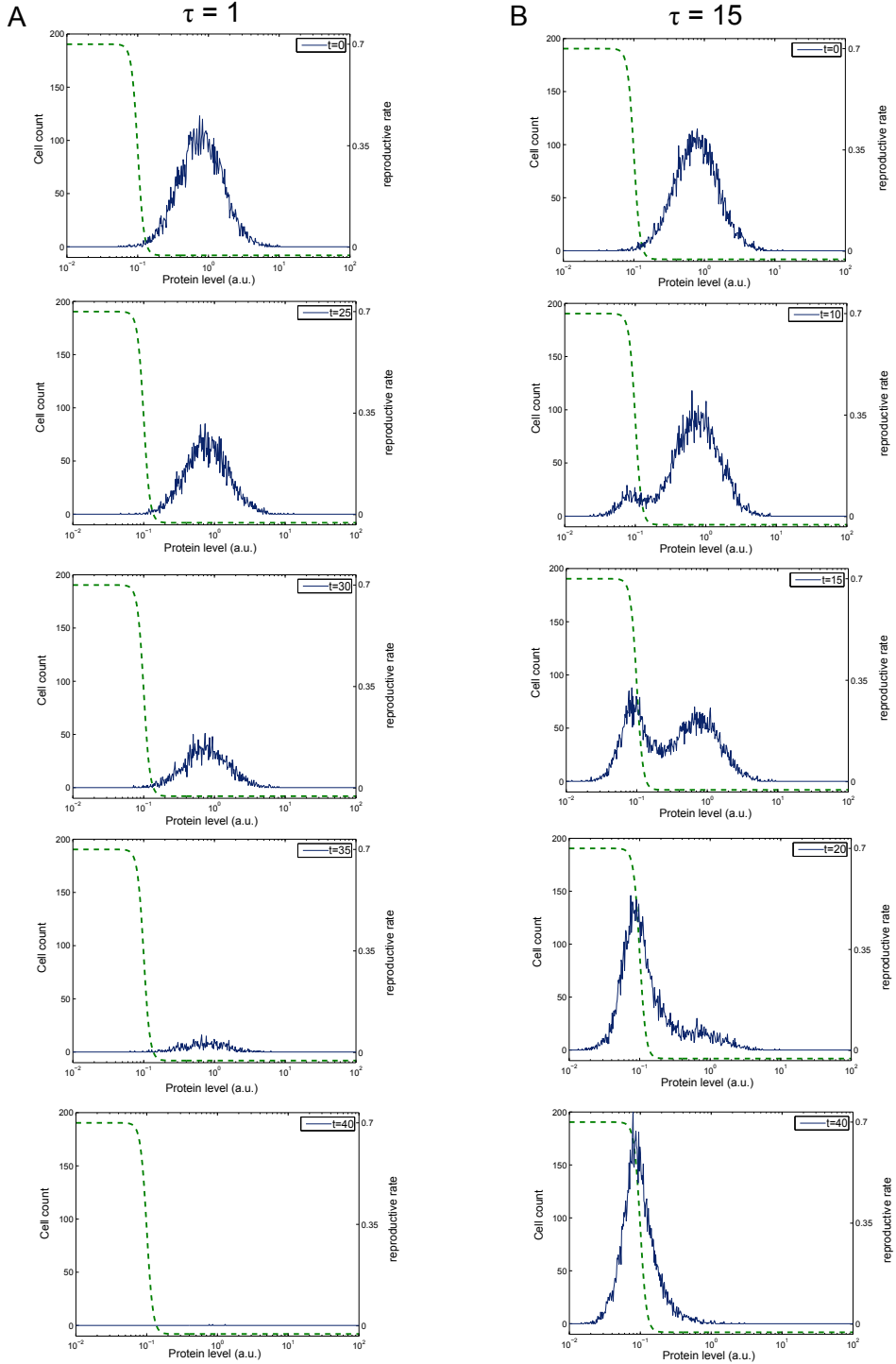


Figure 4.15: Slower relaxation of fluctuations causes adaptive drift of the population expression distribution under stress and confers resistance. Starting at steady-state in the absence of stress, stress is introduced at $t = 0$ and the distribution of viable cells is followed over time. The parameters of the reproductive rate function are $n = 10$ and $K_w = 0.1$. (A) Memory is on the order of a single generation time $\tau = 1$. (B) Memory is significantly longer than a generation $\tau = 15$.

respectively, with $\tau = 10$ and $K_w = 0.1$. As the threshold is made softer, the extent of drift appears and the intermediate bimodal distribution tend to diminish and give rise to a broader stationary distribution under stress. The lower panels show the effect of removing the stress at $t = 40$. Importantly, expression distributions always migrate back to the original steady-state distribution once stress is removed, as was observed experimentally [109]. The migration occurs with no bimodal transition.

Figure 4.17 shows a plot of the drift in the mean level of Ura3p^{GFP} following stress introduction and after its subsequent removal for different degrees of expression memory. The curves show the average and standard deviations of 10 runs for each set of parameters. The greater the relaxation time, the greater the extent of drift in mean expression. Note that the return of the mean to the pre-stress value appears to follow an exponential relaxation whose relaxation rate is roughly the memory parameter τ . This suggests that the monotonic relaxation of the expression peak in the absence of stress could be used experimentally as an empirical measure of the degree of epigenetic memory. A more direct measure of memory has been employed in live cell microscopy experiments of *YFP*-tagged proteins at different chromosomal loci of human cells [111]. There, the time it takes for a cell lineage to reach the different states found in a snapshot of a cell population was measured via the “mixing time” or the time at which the auto-correlation decays to half its initial value. It would be interesting to see how well lineage- and population-based experimental measurements of epigenetic memory agree.

Compare the simulation results with the experimental data of Zhuravel *et al.* shown in Figure 4.13, in which memory was not measured and could not be directly controlled, but instead the level of expression was varied. In the cases of cells induced at low and intermediate levels prior to stress introduction, the distribution settled to a similar final position under stress. In the case of cells induced to high pre-stress levels, the population died out, likely because expression levels cannot manage to drift to safer levels before toxicity sets in (in fact, the small visible subpopulation on the left is reminiscent

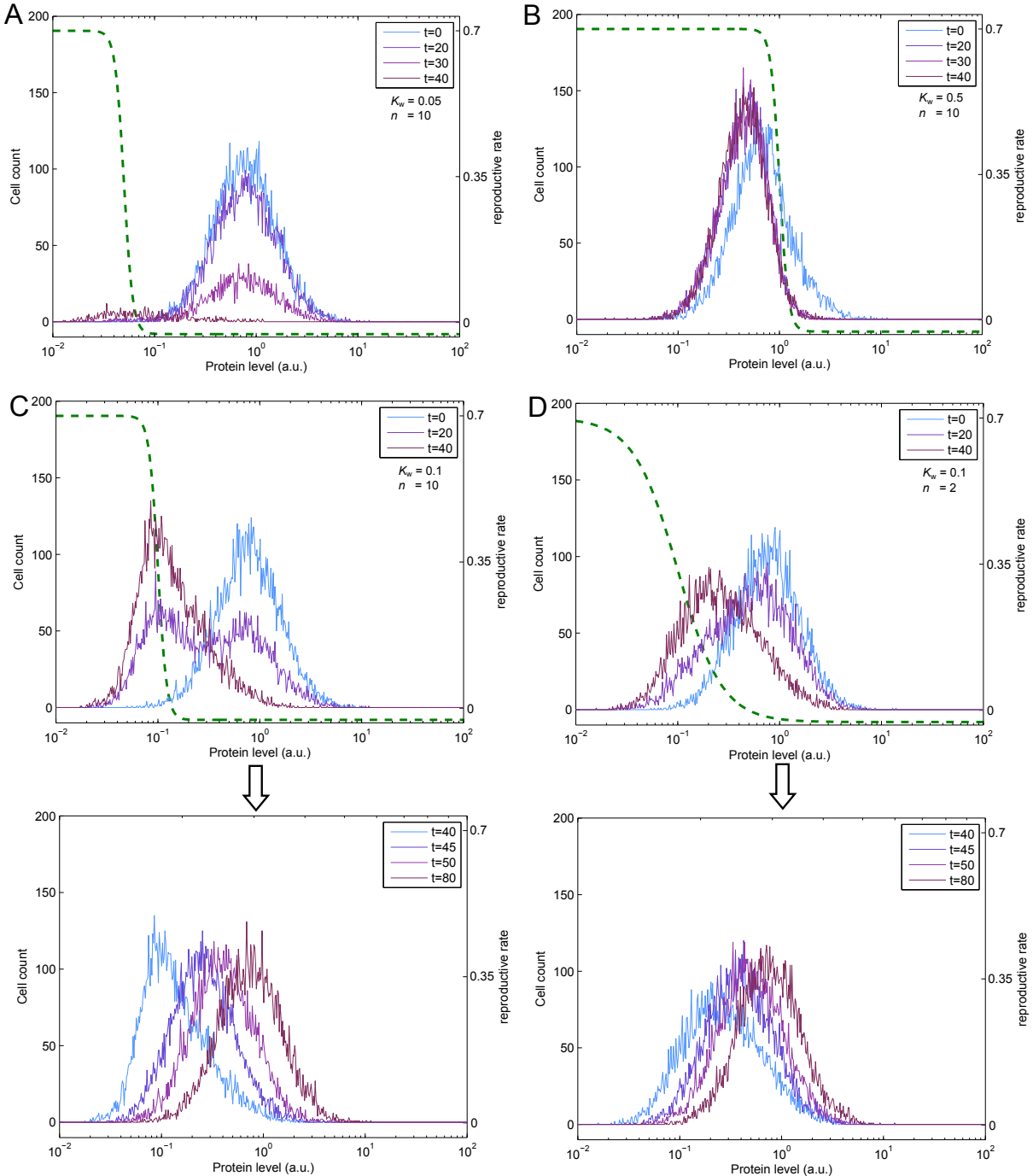


Figure 4.16: Varying the position and steepness of the reproductive rate function (green). (A,B) The Hill constant K_w is set at 0.05 and 0.5, respectively. (C,D) The Hill coefficient n is 10 and 2, respectively. The migration of the distributions back to their initial position following removal of stress is given in the panels below.

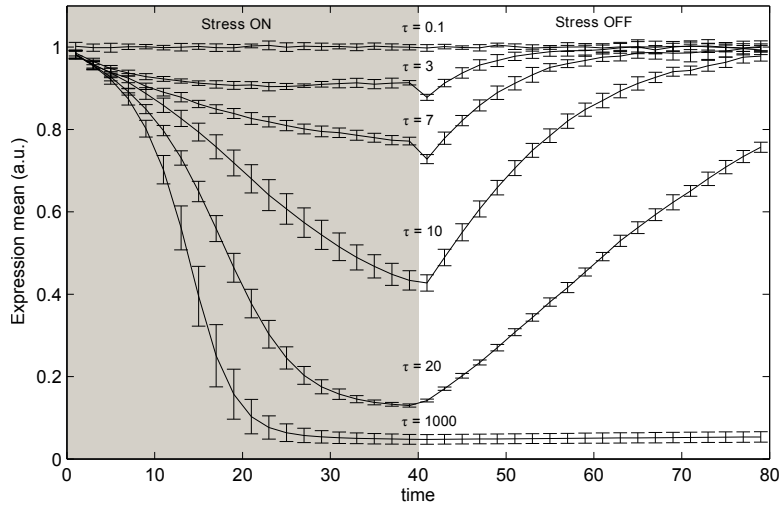


Figure 4.17: Reversible adaptive drift of mean $URA3^{GFP}$ expression for different values of τ . Curves give the average over 10 simulation runs with error bars measuring standard deviation. In all cases, $n = 2$ and $K_w = 0.1$. The rate of return to the initial level following FOA removal is related to the degree of memory τ .

of Figure 4.16A). The simulation study here suggests that slow fluctuation in protein expression may indeed be the primary factor responsible for the population dynamics observed.

Chapter 5

Conclusion

A general simulation framework has been presented that facilitates the development and execution of individual-based population dynamics simulations of biological cells. This is done by using modular and reusable objects called simulation channels which encapsulate separate state-updating algorithms. Given a complete set of simulation channels and an initial population state, a simulation run is conducted using one of two scheduling protocols (the meta-algorithms) that make use of user-specified channel interdependencies. These protocols ensure the correct execution sequence of simulation events and are designed to minimize or eliminate redundant rescheduling of channels. They also ensure the correct random substitution of newborn cells after a maximum number of cell entities is obtained. With this constant-number method, simulations can be run for arbitrarily long times, allowing the sample population to reach a state of balanced growth or steady-state composition. Furthermore, the framework permits the recording of multivariate snapshots of the ensemble of cell entities at scheduled times, or the recording of single-cell histories, allowing the construction of cell lineage trees. A series of modeling studies were presented to validate the framework implementation and to provide realistic use cases.

Simulation channels can be a very useful tool for model development; however, a

few limitations and drawbacks exist. For instance, one side-effect of defining models in terms of simulation channels is that this places the semantics of the biological model and its simulation on the same level, so that the model cannot be easily abstracted away from the simulation algorithms [84]. While there are disadvantages to this kind of formalism, it can also be an insightful way to decompose and analyze a dynamic system with complicated structure and to track down bugs. However, the primary limitation of the framework stems from the insulation of simulation channels from one another. In the current design, simulation channels—even those contained in the same engine—do not share information directly with one another. They can only coordinate their execution through the pre-defined rescheduling dependency graph or by passing information to one another indirectly by reading and modifying the state data of a common entity. This leads to the perhaps undesirable consequence of sometimes using cell entity or global state data as flags or variables for simulation algorithm logic rather than being properties that lie purely in the domain of the conceptual biological model.

This limitation complicates the simulation of cell-cell interactions and certain global events. In the current design, it is technically prohibited for a global simulation channel to modify cell entities directly, and the same goes for local channels and global data. The reason this should be enforced is that if cell entities could be modified by a global simulation channel, the manager would not be able to tell whether any cell entities were modified, and therefore decide, which, if any, local channels need to be rescheduled after a global event. Conversely, if a local simulation channel were permitted to modify global state variables, it would not be clear following local channel execution if any global simulation channels need to be rescheduled. To get around this, scheduling dependencies between global and local channels could be introduced into the framework, but the resulting relationships would become very complicated and place an undue burden on the model developer.

Under these restrictions, attempts at introducing direct cell-cell communication in a

model end up being contrived, involving the sending of information from global channels to local channels indirectly by modifying global state variables and vice versa by modifying local state variables. To resolve this difficulty and avoid the need for local-global dependencies, it would therefore be desirable to introduce some mechanism by which an isolated simulation channel may be invoked or rescheduled from within another simulation channel, rather than relate channels only by pre-defined dependence relationships. This way one could create, for example, a global simulation channel whose `execute` method selects some subset of cells and sends “directives” to execute some of their local simulation channels in order to change those cells; following execution of those local channels, the corresponding local engines would then be able to invoke the required rescheduling dependencies immediately. Such a mechanism would also allow local channels of one cell entity to trigger local channels of another cell entity.

These notification signals or directives would have to be relayed by the simulation manager, to whom all engines are visible, and it should only be permitted to occur when the system is synchronized in model time. In sum, a possible extension of the current framework would involve incorporating a means for the manager to relay messages from simulation channels to reschedule or perhaps to directly fire other simulation channels, as illustrated in Figure 5.1. However, if channels can fire one another without advancing the simulation clock, one must be careful not to accidentally introduce cyclic paths of channel invocations, as this will create deadlock.

While the framework meta-algorithm automatically initiates resampling substitution as soon as the number of cells exceeds N_{\max} , the current design only handles substitution upon addition (i.e., when new cells are born). The resampling counterpart for the case of cell death would be to remove a dead cell from the simulation and replace it with a copy of a randomly chosen cell entity. So far, cell death has been treated as a phenotype: a “dead” cell is kept as part of the sample population of interest, and can be replaced by new cells, but the cell entity is inactivated so that its engine ceases to simulate it

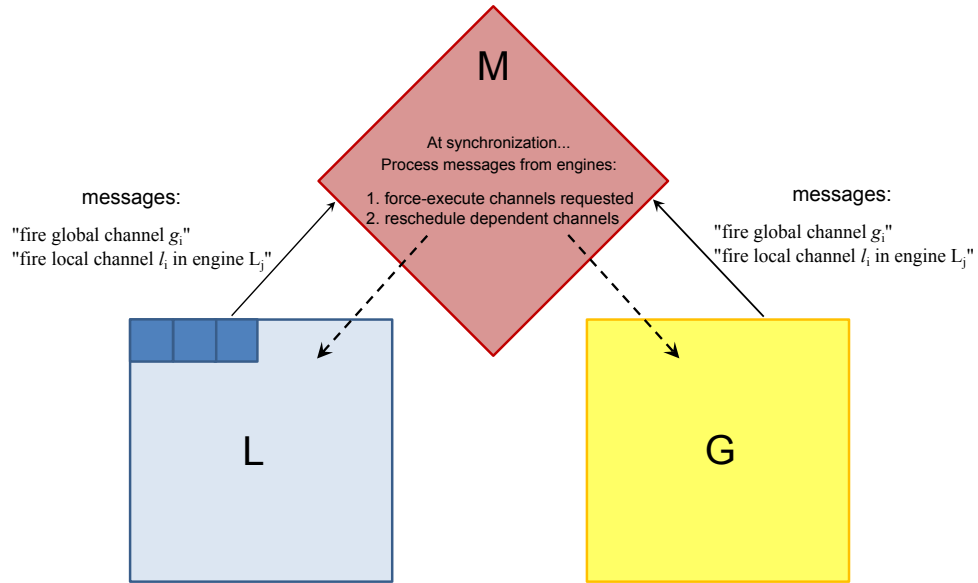


Figure 5.1: Possible extension of the framework allowing dynamic dependencies between simulation channels, even those in different simulation engines.

(see Appendix A). It is often the case that non-viable cells are part of the “population of interest” that the simulation is approximating, so this is usually the desired result. However, in some cases one might want to remove certain cells from the sample population because they are no longer of interest or because they are being physically destroyed (e.g., by necrosis or lysis due to osmotic stress). In those cases, the framework should provide the option to include resampling substitution upon removal. This would fit easily into the First-Engine Method version of the simulation meta-algorithm, but we run into difficulty again with the Asynchronous Method. Since correct substitution requires that the whole population be synchronized at the precise time the cell is removed, substitution cannot be triggered by local simulation channels during the asynchronous intervals between time barriers. Substitution could instead be performed at the next available time barrier, but unlike the case of substitution for newborns, there is no way to guarantee the consistency of substitutions of removed cells with those produced by the conservative First-Engine Method version of the meta-algorithm.

Another property of the constant-number method that was omitted is the fact that

the size or number concentration of the “true” or “total” population can be estimated and tracked as the simulation proceeds. This is based on the interpretation that each cell in the constant-number sample population is some sort of representational average of $1/N_{\max}$ of the cells in the total population [112]. In that case, each time a new cell is born in the sample population, the total population counter N_{total} is incremented by a proportional amount $N_{\max}/N_{\text{total}}$, and similarly decremented when a cell is removed. Such a population counter could easily be built into the framework. This is valuable because estimating macroscopic variables like total cell number, average cell mass, or external concentrations of signalling molecules directly from the sample population allows one to simulate indirect cell-cell communication through the environment. For example, one could simulate density-dependent growth by tying single-cell growth rates of individual cells to the estimated total population size N_{total} .

The CPS framework is designed around the idea of the constant-number ensemble as a representative sample of the population of interest. But in what situations is this method of replacing random individuals valid or meaningful? The constant-number method creates an ensemble that is structured by the proliferation and death rates of cells, not by spatial considerations or other special properties attached to cells—unless these have an affect on growth. In sample populations that are too small, some side-effects of this are that it is possible for the slowest-proliferating cell types to be completely suppressed due to constant replacement by newborns or for a population to experience random changes in composition similar to the phenomena of genetic drift and fixation in population genetics. Such small-number effects are important to keep in mind. If instead of capturing the composition of all cells, one were more interested, for example, in their spatial organization, one might want to produce a different kind of ensemble that tracks cells confined to a spatial area or volume. That would require some different approach to adding or removing cells from the sample, since cells may now enter or leave the space (e.g., a spatial lattice with cell-absorbing boundaries or cell reservoirs). It would be interesting

to explore how other entity-management approaches such as this could be combined with the basic engine-channel architecture described in this thesis.

Finally, although the Asynchronous Method was initially pursued for its parallelism, clearly models involving a constantly changing environment, consumption of resources, or cell-cell communication would, in general, require very frequent synchronizations of the simulation ensemble and preclude any runtime speed-up from parallelization. In any case, as with all types of experiments, most simulation experiments need to be reproduced or run multiple times; hence, it is probably ultimately more valuable to be able to perform multiple simulation runs in parallel rather than to parallelize the running of a particular realization. Future design work will therefore focus mainly on extending the framework to better accommodate coupling of local and global simulation events, to accommodate cell removal and substitution of removed cells, and to provide a built-in population counter. Furthermore, an efficient version of the current framework design is currently being implemented in the language C++.

References

- [1] Steven J. Altschuler and Lani F. Wu. Cellular Heterogeneity: Do Differences Make a Difference? *Cell*, 141(4):559–563, May 2010.
- [2] J. E. Ferrell Jr. The Biochemical Basis of an All-or-None Cell Fate Switch in *Xenopus* Oocytes. *Science*, 280(5365):895–898, May 1998.
- [3] H Rubin. The significance of biological heterogeneity. *Cancer metastasis reviews*, 9(1):1–20, July 1990.
- [4] Hannah H Chang, Martin Hemberg, Mauricio Barahona, Donald E Ingber, and Sui Huang. Transcriptome-wide noise controls lineage choice in mammalian progenitor cells. *Nature*, 453(7194):544–7, 2008.
- [5] A. Raj and A. Van Oudenaarden. Nature, Nurture, or Chance: Stochastic Gene Expression and Its Consequences. *Cell*, 135(2):216–226, 2008.
- [6] D B Kell, H M Ryder, a S Kaprelyants, and H V Westerhoff. Quantifying heterogeneity: flow cytometry of bacterial cultures. *Antonie van Leeuwenhoek*, 60(3–4):145–58, 1991.
- [7] Carla J Davidson and Michael G Surette. Individuality in bacteria. *Annual review of genetics*, 42:253–68, 2008.

- [8] A A Cohen, N Geva-Zatorsky, E Eden, M Frenkel-Morgenstern, I Issaeva, A Sigal, R Milo, C Cohen-Saidon, Y Liron, Z Kam, L Cohen, T Danon, N Perzov, and U Alon. Dynamic proteomics of individual cancer cells in response to a drug. *Science (New York, N.Y.)*, 322(5907):1511–6, December 2008.
- [9] Edo Kussell and Stanislas Leibler. Phenotypic diversity, population growth, and information in fluctuating environments. *Science (New York, N.Y.)*, 309(5743):2075–8, 2005.
- [10] Jan-Willem Veening, Wiep Klaas Smits, and Oscar P Kuipers. Bistability, epigenetics, and bet-hedging in bacteria. *Annual review of microbiology*, 62:193–210, 2008.
- [11] Dawn Fraser and Mads Kaern. A chance at survival: gene expression noise and phenotypic diversification strategies. *Molecular microbiology*, 71(6):1333–40, 2009.
- [12] A.L. Givan. *Flow cytometry: first principles*. Wiley-Liss, 2001.
- [13] James C W Locke and Michael B Elowitz. Using movies to analyse gene circuit dynamics in single cells. *Nature reviews. Microbiology*, 7(5):383–92, 2009.
- [14] Diane Longo and Jeff Hasty. Dynamics of single-cell gene expression. *Molecular systems biology*, 2:64, 2006.
- [15] Ido Golding, Johan Paulsson, Scott M Zawilski, and Edward C Cox. Real-time kinetics of gene activity in individual bacteria. *Cell*, 123(6):1025–36, 2005.
- [16] Long Cai, Nir Friedman, and X Sunney Xie. Stochastic protein expression in individual cells at the single molecule level. *Nature*, 440(7082):358–62, March 2006.
- [17] Ji Yu, Jie Xiao, Xiaojia Ren, Kaiqin Lao, and X Sunney Xie. Probing gene expression in live cells, one protein molecule at a time. *Science (New York, N.Y.)*, 311(5767):1600–3, 2006.

- [18] J Tyson, Katherine C Chen, and Bela Novak. Sniffers, buzzers, toggles and blinkers: dynamics of regulatory and signaling pathways in the cell. *Current Opinion in Cell Biology*, 15(2):221–231, April 2003.
- [19] Uri Alon. Network motifs: theory and experimental approaches. *Nature reviews. Genetics*, 8(6):450–61, 2007.
- [20] John J Tyson and Béla Novák. Functional motifs in biochemical reaction networks. *Annual review of physical chemistry*, 61:219–40, March 2010.
- [21] Naama Barkai and Ben-Zion Shilo. Variability and robustness in biomolecular systems. *Molecular cell*, 28(5):755–60, 2007.
- [22] Ernesto Andrianantoandro, Subhayu Basu, David K Karig, and Ron Weiss. Synthetic biology: new engineering rules for an emerging discipline. *Molecular systems biology*, 2:2006.0028, 2006.
- [23] Priscilla E M Purnick and Ron Weiss. The second wave of synthetic biology: from modules to systems. *Nature reviews. Molecular cell biology*, 10(6):410–22, June 2009.
- [24] Shankar Mukherji and Alexander van Oudenaarden. Synthetic biology: understanding biological design from synthetic circuits. *Nature reviews. Genetics*, 10(12):859–71, 2009.
- [25] C.H. Waddington. *The strategy of the genes: A discussion of some aspects of theoretical biology. With an appendix by H. Kacser.* London: George Allen & Unwin, Ltd., 1957.
- [26] Gábor Balázsi, Alexander van Oudenaarden, and James J Collins. Cellular decision making and biological noise: from microbes to mammals. *Cell*, 144(6):910–25, March 2011.

- [27] Avigdor Eldar and Michael B. Elowitz. Functional roles for noise in genetic circuits. *Nature*, 467(7312):167–173, September 2010.
- [28] Mads Kaern, Timothy C Elston, William J Blake, and James J Collins. Stochasticity in gene expression: from theories to phenotypes. *Nature reviews. Genetics*, 6(6):451–64, 2005.
- [29] Arjun Raj, Charles S Peskin, Daniel Tranchina, Diana Y Vargas, and Sanjay Tyagi. Stochastic mRNA synthesis in mammalian cells. *PLoS biology*, 4(10):e309, 2006.
- [30] Johan Paulsson. Summing up the noise in gene networks. *Nature*, 427(6973):415–8, January 2004.
- [31] Juan M Pedraza and Alexander van Oudenaarden. Noise propagation in gene networks. *Science (New York, N.Y.)*, 307(5717):1965–9, 2005.
- [32] Vahid Shahrezaei and Peter S Swain. The stochastic nature of biochemical networks. *Current opinion in biotechnology*, 19(4):369–74, August 2008.
- [33] Michael B Elowitz, Arnold J Levine, Eric D Siggia, and Peter S Swain. Stochastic gene expression in a single cell. *Science (New York, N.Y.)*, 297(5584):1183–6, 2002.
- [34] P S Swain, M B Elowitz, and E D Siggia. Intrinsic and extrinsic contributions to stochasticity in gene expression. *Proc. Natl. Acad. Sci. USA*, 99:12795–12800, 2002.
- [35] Gürol M Süel, Rajan P Kulkarni, Jonathan Dworkin, Jordi Garcia-Ojalvo, and Michael B Elowitz. Tunability and noise dependence in differentiation dynamics. *Science (New York, N.Y.)*, 315(5819):1716–9, March 2007.
- [36] Hédia Maamar, Arjun Raj, and David Dubnau. Noise in gene expression determines cell fate in *Bacillus subtilis*. *Science (New York, N.Y.)*, 317(5837):526–9, 2007.

- [37] Murat Acar, Attila Becskei, and Alexander van Oudenaarden. Enhancement of cellular memory by reducing stochastic transitions. *Nature*, 435(7039):228–32, May 2005.
- [38] Mathias F Wernet, Esteban O Mazzoni, Arzu Celik, Dianne M Duncan, Ian Duncan, and Claude Desplan. Stochastic spineless expression creates the retinal mosaic for colour vision. *Nature*, 440(7081):174–80, March 2006.
- [39] Edward R Sumner and Simon V Avery. Phenotypic heterogeneity: differential stress resistance among individual cells of the yeast *Saccharomyces cerevisiae*. *Microbiology (Reading, England)*, 148(Pt 2):345–51, February 2002.
- [40] Dann Huh and Johan Paulsson. Non-genetic heterogeneity from stochastic partitioning at cell division. *Nature genetics*, 43(2):95–100, February 2011.
- [41] Pao-Shu Wu, Boris Egger, and Andrea H Brand. Asymmetric stem cell division: lessons from *Drosophila*. *Seminars in cell & developmental biology*, 19(3):283–93, June 2008.
- [42] Ralph a Neumüller and Juergen a Knoblich. Dividing cellular asymmetry: asymmetric cell division and its implications for stem cells and cancer. *Genes & development*, 23(23):2675–99, December 2009.
- [43] Eric J Stewart, Richard Madden, Gregory Paul, and François Taddei. Aging and death in an organism that reproduces by morphologically symmetric division. *PLoS biology*, 3(2):e45, March 2005.
- [44] Nathalie Q Balaban, Jack Merrin, Remy Chait, Lukasz Kowalik, and Stanislas Leibler. Bacterial persistence as a phenotypic switch. *Science (New York, N.Y.)*, 305(5690):1622–5, September 2004.

- [45] S M Jazwinski. Aging and senescence of the budding yeast *Saccharomyces cerevisiae*. *Molecular microbiology*, 4(3):337–43, March 1990.
- [46] K C Chen, a Csikasz-Nagy, B Gyorffy, J Val, B Novak, and J J Tyson. Kinetic analysis of a molecular model of the budding yeast cell cycle. *Molecular biology of the cell*, 11(1):369–91, January 2000.
- [47] Mukund Thattai and Alexander van Oudenaarden. Stochastic gene expression in fluctuating environments. *Genetics*, 167(1):523–30, May 2004.
- [48] Edo Kussell, Roy Kishony, Nathalie Q Balaban, and Stanislas Leibler. Bacterial persistence: a model of survival in changing environments. *Genetics*, 169(4):1807–14, 2005.
- [49] David Gilbert, Hendrik Fuss, Xu Gu, Richard Orton, Steve Robinson, Vladislav Vyschemirsky, Mary Jo Kurth, C Stephen Downes, and Werner Dubitzky. Computational methodologies for modelling, analysis and simulation of signalling networks. *Briefings in bioinformatics*, 7(4):339–53, December 2006.
- [50] B.B. Aldridge, J.M. Burke, D.A. Lauffenburger, and P.K. Sorger. Physicochemical modelling of cell signalling pathways. *Nature cell biology*, 8(11):1195–1203, 2006.
- [51] Herbert M Sauro. Network dynamics. *Methods in molecular biology (Clifton, N.J.)*, 541:269, 2009.
- [52] Natal a W van Riel. Dynamic modelling and analysis of biochemical networks: mechanism-based models and model-based experiments. *Briefings in bioinformatics*, 7(4):364–74, December 2006.
- [53] E.D. Conrad and J.J. Tyson. Modeling molecular interaction networks with non-linear ordinary differential equations. In Zoltan Szallasi, Jorg Stelling, and Vipul

- Periwal, editors, *Systems Modelling in Cellular Biology: From Concept to Nuts and Bolts*. MIT Press, Cambridge, MA, 2006.
- [54] D.T. Gillespie. A general method for numerically simulating the stochastic time evolution of coupled chemical reactions. *Journal of computational physics*, 22(4):403–434, 1976.
- [55] N.G. Van Kampen. *Stochastic processes in physics and chemistry*. North-Holland personal library. North-Holland, 1992.
- [56] Daniel T Gillespie. Stochastic simulation of chemical kinetics. *Annual review of physical chemistry*, 58:35–55, 2007.
- [57] Daniel T. Gillespie. Exact stochastic simulation of coupled chemical reactions. *The Journal of Physical Chemistry*, 81(25):2340–2361, 1977.
- [58] Michael A. Gibson and Jehoshua Bruck. Efficient Exact Stochastic Simulation of Chemical Systems with Many Species and Many Channels. *The Journal of Physical Chemistry A*, 104(9):1876–1889, March 2000.
- [59] Yang Cao, Linda R Petzold, Muruhan Rathinam, and Daniel T Gillespie. The numerical stability of leaping methods for stochastic simulation of chemically reacting systems. *The Journal of chemical physics*, 121(24):12169–78, December 2004.
- [60] James M McCollum, Gregory D Peterson, Chris D Cox, Michael L Simpson, and Nagiza F Samatova. The sorting direct method for stochastic simulation of biochemical systems with varying reaction execution behavior. *Computational biology and chemistry*, 30(1):39–49, February 2006.
- [61] Alexander Slepoy, Aidan P Thompson, and Steven J Plimpton. A constant-time kinetic Monte Carlo algorithm for simulation of large biochemical reaction networks. *The Journal of chemical physics*, 128(20):205101, May 2008.

- [62] Marc R Roussel and Rui Zhu. Validation of an algorithm for delay stochastic simulation of transcription and translation in prokaryotic gene expression. *Physical biology*, 3(4):274–84, November 2006.
- [63] J Elf and M Ehrenberg. Spontaneous separation of bi-stable biochemical systems into spatial domains of opposite phases. *Cell*, 1(2), 2004.
- [64] Caroline Lemerle, Barbara Di Ventura, and Luis Serrano. Space as the final frontier in stochastic simulations of biological systems. *FEBS letters*, 579(8):1789–94, March 2005.
- [65] D.T. Gillespie. Approximate accelerated stochastic simulation of chemically reacting systems. *The Journal of Chemical Physics*, 115(4):1716, 2001.
- [66] Jürgen Pahle. Biochemical simulations: stochastic, approximate stochastic and hybrid approaches. *Briefings in bioinformatics*, 10(1):53–64, January 2009.
- [67] Mads Kaern, William J Blake, and J J Collins. The engineering of gene regulatory networks. *Annual review of biomedical engineering*, 5:179–206, 2003.
- [68] J. Paulsson and M. Ehrenberg. Noise in a minimal regulatory network: plasmid copy number control. *Quarterly reviews of biophysics*, 34(01):1–59, 2001.
- [69] J J Tyson and O Diekmann. Sloppy size control of the cell division cycle. *Journal of theoretical biology*, 118(4):405–26, February 1986.
- [70] Attila Csikász-Nagy. Computational systems biology of the cell cycle. *Briefings in bioinformatics*, 10(4):424–34, July 2009.
- [71] Stefan Klumpp, Zhongge Zhang, and Terence Hwa. Growth rate-dependent global effects on gene expression in bacteria. *Cell*, 139(7):1366–75, 2009.
- [72] Matthew Scott and Terence Hwa. Bacterial growth laws and their applications. *Current opinion in biotechnology*, 22(4):559–565, May 2011.

- [73] D. Ramkrishna. *Population Balances: Theory and Applications to Particulate Systems in Engineering*. Elsevier Science, 2000.
- [74] H. Von Foerster. Some remarks on changing populations. In F. Stohlman Jr., editor, *The kinetics of cellular proliferation*, pages 382–407. Grune and Stratton, New York, 1959.
- [75] A. G. Fredrickson and H. M. Tsuchiya. Continuous propagation of microorganisms. *AIChE Journal*, 9(4):459–468, July 1963.
- [76] A.G. Fredrickson, D. Ramkrishna, and H.M. Tsuchiya. Statistics and dynamics of prokaryotic cell populations. *Mathematical Biosciences*, 1(3):327–374, September 1967.
- [77] E Haseltine, D Patience, and J Rawlings. On the stochastic simulation of particulate systems. *Chemical Engineering Science*, 60(10):2627–2641, May 2005.
- [78] John J Tyson. Mini Review: Size Control of Cell Division. *Journal of theoretical biology*, pages 381–391, 1987.
- [79] Nikos V Mantzaris. Stochastic and deterministic simulations of heterogeneous cell population dynamics. *Journal of theoretical biology*, 241(3):690–706, August 2006.
- [80] Michael A. Henson. Dynamic modeling of microbial cell populations. *Current Opinion in Biotechnology*, 14(5):460–467, October 2003.
- [81] M. Smith and T. Matsoukas. Constant-number Monte Carlo simulation of population balances. *Chemical Engineering Science*, 53(9):1777–1786, 1998.
- [82] N.V. Mantzaris. From single-cell genetic architecture to cell population dynamics: quantitatively decomposing the effects of different population heterogeneity sources for a genetic network with positive feedback architecture. *Biophysical journal*, 92(12):4271–4288, 2007.

- [83] D.A. Charlebois, Jukka Intosalmi, Dawn Fraser, and M. Kaern. An Algorithm for the Stochastic Simulation of Gene Expression and Heterogeneous Population Dynamics. *Commun. Comput. Phys.*, 9(2011):89–112, 2011.
- [84] Kouichi Takahashi, Katsuyuki Yugi, Kenta Hashimoto, Yohei Yamada, Christopher J F Pickett, and Masaru Tomita. Challenges in Cell Simulation : A Software Engineering Approach. *IEEE Intelligent Systems*, 2002.
- [85] R.W. Lafore. *Object-oriented programming in C++*. Kaleidoscope Series. Sams, 2002.
- [86] M.A. Weisfeld. *The object-oriented thought process*. Developer's library. Sams Pub., 2004.
- [87] R.M. Fujimoto. *Parallel and distributed simulation systems*. Wiley series on parallel and distributed computing. Wiley, 2000.
- [88] Howard Salis and Yiannis Kaznessis. Accurate hybrid stochastic simulation of a system of coupled chemical or biochemical reactions. *The Journal of chemical physics*, 122(5):54103, 2005.
- [89] Johan Paulsson. Models of stochastic gene expression. *Physics of Life Reviews*, 2(2):157–175, June 2005.
- [90] Paul J Choi, Sunney Xie, and Eugene I Shakhnovich. Stochastic switching in gene networks can occur by a single-molecule event or many molecular steps. *Journal of molecular biology*, 396(1):230–44, February 2010.
- [91] E M Ozbudak, M Thattai, I Kurtser, A D Grossman, and A Van Oudenaarden. Regulation of noise in the expression of a single gene. *Nat. Genet.*, 31:69–73, 2002.

- [92] Vahid Shahrezaei and Peter S Swain. Analytical distributions for stochastic gene expression. *Proceedings of the National Academy of Sciences of the United States of America*, 105(45):17256–61, November 2008.
- [93] T Lu, D Wolfson, and L Tsimring. Cellular growth and division in the Gillespie algorithm. *Syst. Biol.*, 1(1):121–128, 2004.
- [94] E. Renshaw. Birth, Death and Migration Processes. *Biometrika*, 59(1):49, April 1972.
- [95] Eric Renshaw. A survey of stepping-stone models in population dynamics. *Advances in applied probability*, 18(3):581–627, September 1986.
- [96] J W Shay and W E Wright. Hayflick, his limit, and cellular ageing. *Nature reviews. Molecular cell biology*, 1(1):72–6, October 2000.
- [97] Kiersten A Henderson and Daniel E Gottschling. A mother’s sacrifice: what is she keeping for herself? *Current opinion in cell biology*, 20(6):723–8, December 2008.
- [98] Renata Zadrag-Tecza, Magdalena Kwolek-Mirek, Grzegorz Bartosz, and Tomasz Bilinski. Cell volume as a factor limiting the replicative lifespan of the yeast *Saccharomyces cerevisiae*. *Biogerontology*, 10(4):481–8, August 2009.
- [99] Renata Zadrag, Magdalena Kwolek-Mirek, Grzegorz Bartosz, and Tomasz Bilinski. Relationship between the replicative age and cell volume in *Saccharomyces cerevisiae*. *Acta biochimica Polonica*, 53(4):747–51, January 2006.
- [100] Jingye Yang, Huzefa Dungarwala, Hui Hua, Arkadi Manukyan, Lesley Abraham, Wesley Lane, Holly Mead, Jill Wright, and Brandt L Schneider. Cell size and growth rate are major determinants of replicative lifespan. *Cell cycle (Georgetown, Tex.)*, 10(1):144–55, January 2011.

- [101] B K Kennedy, N R Austriaco, and L Guarente. Daughter cells of *Saccharomyces cerevisiae* from old mothers display a reduced life span. *The Journal of cell biology*, 127(6 Pt 2):1985–93, December 1994.
- [102] Luis López-Maury, Samuel Marguerat, and Jürg Bähler. Tuning gene expression to changing environments: from rapid responses to evolutionary adaptation. *Nature reviews. Genetics*, 9(8):583–93, 2008.
- [103] A. Bar-Even, J Paulsson, N Maheshri, M Carmi, E. O’Shea, Y Pilpel, and N Barkai. Noise in protein expression scales with natural protein abundance. *Nature genetics*, 38(6):636–643, 2006.
- [104] J R Newman, S Ghaemmaghami, J Ihmels, D K Breslow, M Noble, J L Derisi, and J S Weissman. Single-cell proteomic analysis of *S. cerevisiae* reveals the architecture of biological noise. *Nature*, 441:840–846, 2006.
- [105] William J Blake, Gábor Balázsi, Michael a Kohanski, Farren J Isaacs, Kevin F Murphy, Yina Kuang, Charles R Cantor, David R Walt, and James J Collins. Phenotypic consequences of promoter-mediated transcriptional noise. *Molecular cell*, 24(6):853–65, 2006.
- [106] Amy Brock, Hannah Chang, and Sui Huang. Non-genetic heterogeneity—a mutation-independent driving force for the somatic evolution of tumours. *Nature reviews. Genetics*, 10(5):336–42, May 2009.
- [107] A. Raj and A. van Oudenaarden. Nature, nurture, or chance: stochastic gene expression and its consequences, 2008.
- [108] Edda Klipp. Timing matters. *FEBS letters*, 583(24):4013–8, December 2009.

- [109] Daniil Zhuravel, Dawn Fraser, Simon St-Pierre, Lioudmila Tepliakova, Wyoming L. Pang, Jeff Hasty, and Mads Kærn. Phenotypic impact of regulatory noise in cellular stress-response pathways. *Systems and Synthetic Biology*, April 2010.
- [110] Daniel T. Gillespie. Exact numerical simulation of the Ornstein-Uhlenbeck process and its integral. *Physical review. E, Statistical physics, plasmas, fluids, and related interdisciplinary topics*, 54(2):2084–2091, August 1996.
- [111] Alex Sigal, Ron Milo, Ariel Cohen, Naama Geva-Zatorsky, Yael Klein, Yuval Liron, Nitzan Rosenfeld, Tamar Danon, Natalie Perzov, and Uri Alon. Variability and memory of protein levels in human cells. *Nature*, 444(7119):643–6, 2006.
- [112] Y Lin, K Lee, and T Matsoukas. Solution of the population balance equation using constant-number Monte Carlo. *Chem. Eng. Sci.*, 57:2241–2252, 2002.
- [113] Dave Foti. Inside MATLAB Objects in R2008a. *Matlab Digest*, pages 1–6, September 2008.
- [114] S.M. Ross. *Introduction to probability models*. Introduction to Probability Models. Academic Press, 2007.

Appendix A

Simulator implementation

A complete implementation of the simulation framework was developed in MATLAB. MATLAB is a popular programming language and numerical computing environment used in science and engineering fields. Aside from domain-specific toolboxes (e.g., for signal processing, optimization, control systems, etc.), its primary strength is in matrix manipulation and interactive plotting. To improve support for the development of algorithms and applications, since version 7.6 it offers a modern object-oriented class system. Because the language is designed for technical users, it is more terse than lower-level languages and users do not deal with many administrative tasks like specifying data types or memory management. It is also an interpreted language that allows interactive programming through a console. These features make it easier for a less experienced user to implement their own simulation channel classes, and allow them to perform simulation runs and analyze the data in the same environment. For these same reasons and others, however, it is generally much less efficient than a statically typed and compiled language like C (although processor-optimized libraries are used for heavy matrix and vector computations). However, in spite of these limitations, MATLAB provided a decent development and debugging environment for a fully functional prototype and proof-of-concept of the simulation framework. The source code is available at <http://www.sysbiolab.uottawa.ca>.

A.1 Classes

The relationships between the classes that make up an object-oriented design can be described using the Unified Modeling Language (UML). The UML diagram of the MATLAB simulator classes is shown in Figure A.1. Each box describes a class, with the upper panel listing class properties with their types and the lower panel listing class methods and their signatures. Inheritance (*is-a*) and aggregation (*has-a* or *consists-of*) rela-

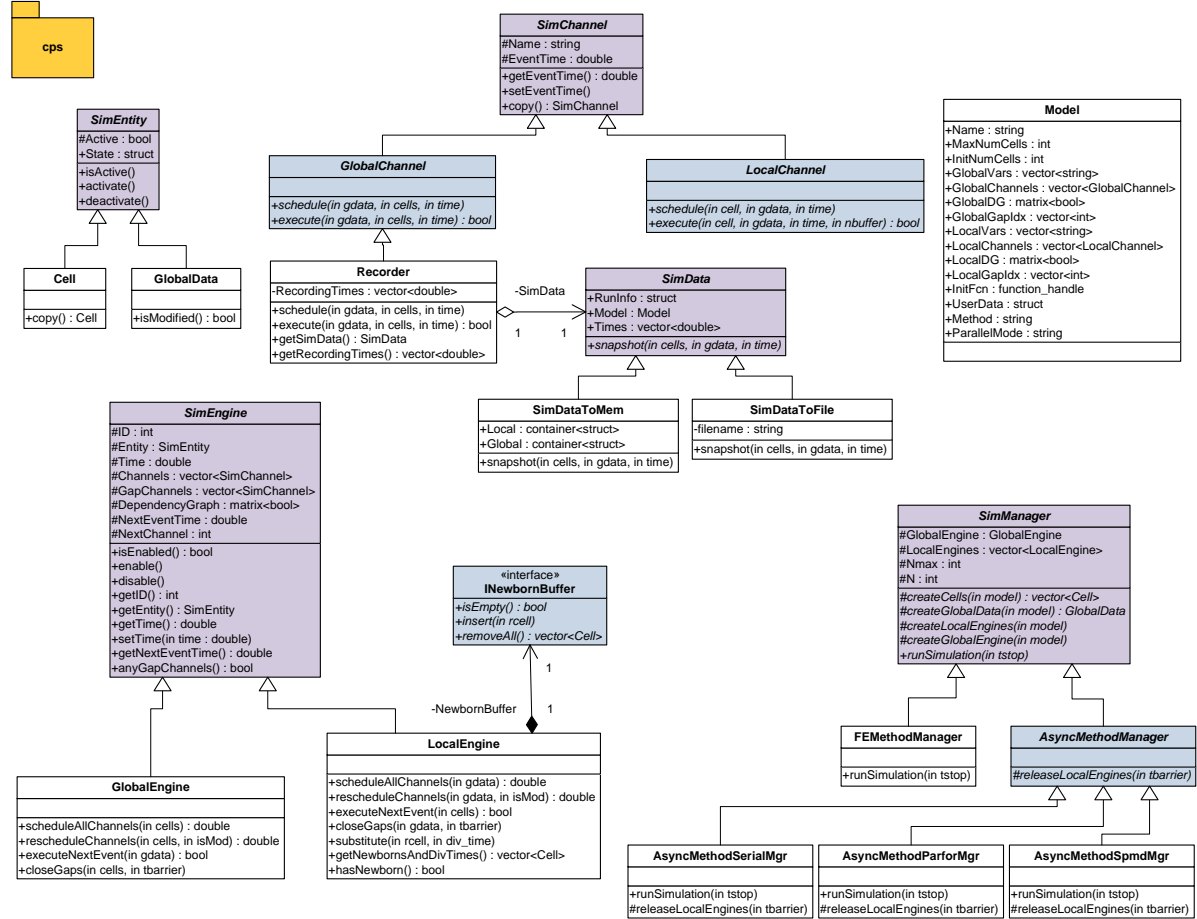


Figure A.1: UML diagram of main CPS framework classes in the MATLAB implementation. Root base classes are shaded purple and other abstract classes are shaded blue. Datatypes are indicated using C/C++-style notation.

tionships are described with arrows having triangular and diamond-shaped arrowheads, respectively. Member access rights are denoted + for public, - for private, or # for protected. Abstract classes have italicized headings and methods without implementations are also italicized. These methods must be implemented by all derived classes. All the framework classes are stored in a package called `cps`. Note that all the objects described follow “pass-by-reference” semantics, meaning that if an object is passed into a function and changes are made to the object within the function body, those modifications are realized in the variable used by the caller when the function returns. That is because the variable names used inside the function and in the caller are just different aliases for the same underlying data. These are referred to as “handle” objects in MATLAB terminology. They behave like pointers or reference variables of other languages, which differs from the usual semantics of variables in MATLAB.

In Figure A.1, the base classes `SimChannel`, `SimEntity`, `SimEngine`, `SimManager` and `SimData` are shaded purple for visual clarity and other important classes are shaded blue. The two classes designed for extension by users are the abstract classes `GlobalChannel`

and `LocalChannel` which allow the definition of specific global and local simulation channels, respectively. A user may also extend the abstract `SimData` class to define a custom way to record simulation data, or simply use one of the two concrete built-in classes, `SimDataToMem` or `SimDataToFile`, which record all state data. Within the framework, there is a separate simulation manager class for each meta-algorithm implementation: one for the First-Engine Method and ones for each of the serial and parallel implementations of the Asynchronous Method. Each of these classes implements the methods declared in the base class `SimManager` and may also define new ones. Note that the implementations of `GlobalEngine` and `LocalEngine` could be substituted for other ones which perform, for instance, the search for the earliest event time internally in a different way while fulfilling the same contract (namely, finding the earliest event time) externally. Also note that the `SimEntity` base class provides a method to “deactivate” an entity. This can be done when a cell entity is to be flagged as non-viable, and causes the engine to cease to schedule and execute its simulation channels, but the entity will still be available for substitution. Deactivating the global data entity, on the other hand, causes the simulation to terminate immediately instead of continuing until the specified stop time. Finally, the `Model` class is simply a utility class to check the input arguments to the main simulation function (methods not shown).

Noteworthy is the way in which newborn cell entities are stored. There are many ways by which this could be implemented. The approach chosen here was to provide a container to the user with a limited set of operations (the `INewbornBuffer` interface) to send the newborn cells back to the engine. Local engines hold the reference to the newborn buffer and pass it as the final parameter to the `execute` method of local simulation channels. When one wants to simulate cell division, one creates a copy (called `new_cell` in the example in Figure 3.7) of the main cell entity. The new cell entity produced is the newborn to be stored, so one “inserts” it into the buffer (this just attaches a reference that the engine can use to obtain access to the object); otherwise, its reference will be lost when `execute` returns (and MATLAB will destroy the object). In principle, more than one newborn cell can be stored in a single channel execution. Following channel execution, the local engine checks whether the buffer is occupied. If so, it will timestamp the birth event. At synchronization, the simulation manager retrieves all stored newborns by collecting them from the local engines along with their time stamps and the ID of the engine of origin.

A.2 Meta-algorithm implementations and performance

MATLAB’s Parallel Toolbox uses multiple processes to do its job: the main MATLAB process (usually the one the user interacts with) is called the *client* lab, whereas separate “headless” instances of MATLAB called *worker* labs are dedicated to each available processor on a computer or network. Because the labs are separate processes, they cannot share memory (processes are insulated from each other by the operating system). While arrays can be sliced and distributed among worker labs, in order to share data it must be sent between client and worker or exchanged between workers by message passing. The

Asynchronous Method managers support three different modes of execution, one in a fully sequential manner which does not make use of the parallel toolbox (*serial mode*, in which everything takes place on the client lab), and two parallel modes which make use of different language constructs from the toolbox. These are called *parfor mode*, in which the meta-algorithm uses MATLAB's parfor loop construct for releasing the local engines; and *spmd mode*, in which the meta-algorithm is implemented using a construct called single-program-multiple-data (spmd) blocks. Spmd blocks can use a special data type to create, gather, and reference variables on the worker labs directly. In spmd mode, such blocks need to be incorporated into a global simulation channel if it needs to access a cell entity object, because the cell entities always reside on worker labs. In parfor mode, on the other hand, one never includes parallel logic in simulation channel code, but parfor execution may involve a higher communication overhead.

Note that the time complexity of the simulation meta-algorithms depend strongly on the way the searches for earliest event times are implemented, as well as model-specific details such as the number of engines N versus the number of channels in each engine M . The current First-Engine Method implementation holds an array of the engine next event times and uses the built-in `min` function to find the smallest element. This approach has linear or $O(N)$ time complexity, where N is the number of engines. As a result, the First-Engine implementation tends to run more slowly than the serial Asynchronous Method implementation on the same model because the latter only performs $O(M)$ searches and M is usually much smaller than N . However, for large N or M , using a data structure such as a binary heap to create an indexed priority queue (as prescribed in the Next-Reaction variant of the SSA) would lead to overall more efficient $O(1)$ complexity for obtaining the smallest element and logarithmic complexity for sorting the event times each time one is updated. Such data structures are not supported natively in MATLAB.

Also, note that a protocol must be specified for handling *simultaneous events*. First, if two simulation channels in the same engine are scheduled to occur at the same time, the order in which the channels were provided to the program determines the priority order for firing. Second, if a global channel and a local channel are scheduled to fire at the same time, the local channel gets executed first. Lastly, because the simulation events executed by different local simulation engines do not influence one another, it does not matter in what order they are executed, so no protocol needs to be enforced. In the Asynchronous Method, they may be executed concurrently, while in the First-Engine method the order would be determined by the kind of data structure being used internally to sort the list of next event times of the engines.

Unfortunately, in developing their new class system, The MathWorks decided on a deterministic method for automatic memory management of objects that persist beyond the scope of function calls (i.e., handle objects) [113]. The details are undocumented, but involves doing bookkeeping in the background whenever functions or methods return. It also creates very long latencies when passing arrays of handle objects between labs. This, among other factors, ultimately proved to be unacceptably costly in terms of scale-up performance. Because these performance bottlenecks were not representative of the true run-time complexity of the framework algorithms, no run-time performance

benchmarks were performed using the MATLAB implementation. However, a C++ implementation, currently in final stages of development, demonstrates drastically more efficient and very practical run-times (e.g., 1-2min for each the 10,000-cell simulations in Section 4.4 running serially vs \sim 2h30min in MATLAB running in parallel on an 8-core Linux desktop!).

Appendix B

The birth-migration process

It will be shown here that the bistable switching model described in Section 4.2 is equivalent to a birth-migration continuous-time Markov chain, and expressions for the first moments of the variables of interest will be derived.

In the bistable switching model, each individual in one state can switch to the opposing state. The occurrence of a switching event in non-overlapping time intervals is independent (the process is memoryless), and the probability of an event or “arrival” in an infinitesimal interval is

$$\Pr\{\text{switch event in } (t, t + dt)\} = k_i dt \quad (\text{B.1})$$

This is also called a (homogeneous) Poisson process with rate k_i .

Recall that in addition to switching, each individual is also subject to a birth process. This can be formulated as the simultaneous occurrence of three independent events: the removal of one individual from the i -subpopulation (rate λ_i) and the addition of two new individuals with state chosen according to probability σ_i . For instance, supposing an OFF-cell gives birth, there are three mutually exclusive possible outcomes:

1. Both cells are born in the OFF-state (a *cis* birth)
2. One cell is born in each state (a *split* birth)
3. Both cells are born in the ON-state (a *trans* birth)

By independence, this translates into the following probabilistic rate equations

$$\Pr\{\text{cis birth in } (t, t + dt)\} = \sigma_i^2 \lambda_i, \quad (\text{B.2})$$

$$\Pr\{\text{split birth in } (t, t + dt)\} = \sigma_i(1 - \sigma_i)\lambda_i, \quad (\text{B.3})$$

$$\Pr\{\text{trans birth in } (t, t + dt)\} = (1 - \sigma_i)^2 \lambda_i, \quad (\text{B.4})$$

which are all memoryless and have constant rates; hence, they are all homogeneous Poisson processes.

It is a fact that the inter-arrival times of a Poisson process are exponentially distributed. That is, for a Poisson process with rate μ , the waiting time T to the next arrival obeys

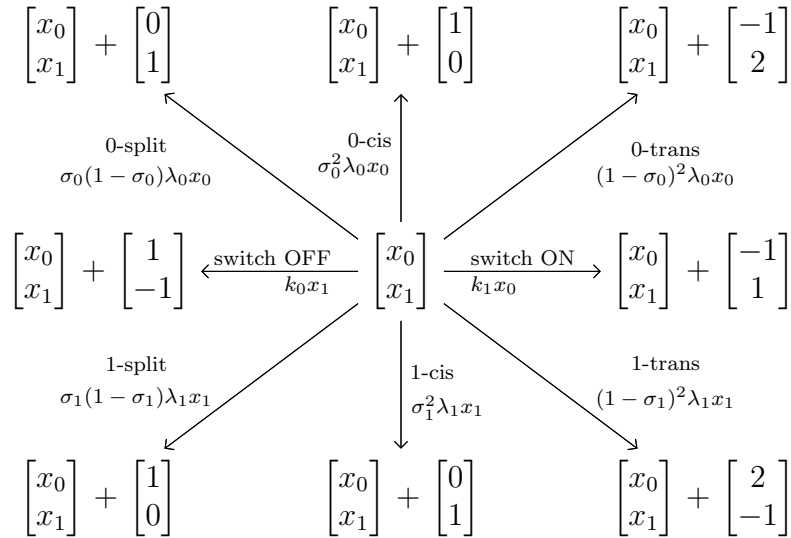
$$\Pr\{T = \tau\}d\tau = -\mu e^{-\mu\tau}d\tau. \quad (\text{B.5})$$

We will make use of the following property of the exponential distribution:

Lemma 1. Suppose that Y_1, Y_2, \dots, Y_n are independent exponential random variables with Y_i having rate μ_i , $i = 1, \dots, n$. Then the first order statistic $\min(Y_1, \dots, Y_n)$ is also exponentially distributed with rate $\sum_{i=1}^n \mu_i$.

For a proof of this result, see [114], p.291.

Let the random variables $X_0(t)$ and $X_1(t)$ represent the number of cells in the OFF and ON states, respectively. Then Lemma 1 tells us that given the system is in state $X_0 = x_0$ and $X_1 = x_1$ at time t , if we superimpose together all the $0 \rightarrow 1$ switching processes for all cells in the OFF-state, the occurrence of the first of the $0 \rightarrow 1$ switching events (i.e., the shortest waiting time) is also exponentially distributed, with rate $x_0 k_1$. Similarly the first $1 \rightarrow 0$ switching event would obey rate $x_1 k_0$, the first *cis* birth event among ON-cells would obey rate $x_1 \sigma_1^2 \lambda_1$, and so on. These events represent the *transitions* of the subpopulation counts (x_0, x_1) between states. This can be illustrated using a state transition diagram for the subpopulation counts:



The resulting system is a BM process. Because all the transitions are Markovian (have exponentially distributed waiting times in isolation), the system is a continuous-time Markov chain, like a chemical reaction model. Its probability distribution therefore obeys a master equation. We will use here the notation used for chemical master equations

$$\frac{\partial P(\mathbf{x}, t)}{\partial t} = \sum_{j=1}^8 [a_j(\mathbf{x} - \boldsymbol{\nu}_j)P(\mathbf{x} - \boldsymbol{\nu}_j, t) - a_j(\mathbf{x})P(\mathbf{x}, t)], \quad (\text{B.6})$$

which sums over all 8 transitions both into and out of the state $\mathbf{x} = [x_0, x_1]^T$, with “propensities” or transition rates $a_j(\mathbf{x})$, and “stoichiometries” $\boldsymbol{\nu}_j$ as shown in the diagram, $j = 1, \dots, 8$. Multiplying equation B.6 through by \mathbf{x} and summing over all \mathbf{x} gives

$$\frac{d\langle \mathbf{X}(t) \rangle}{dt} = \sum_{j=1}^8 \boldsymbol{\nu}_j \langle a_j(\mathbf{X}(t)) \rangle. \quad (\text{B.7})$$

In general, for nonlinear systems one cannot infer much about average behaviour, but fortunately, all the transition rates in the BM process are linear in the variables x_0 and x_1 , giving

$$\frac{d\langle \mathbf{X}(t) \rangle}{dt} = \sum_{j=1}^8 \boldsymbol{\nu}_j a_j(\langle \mathbf{X}(t) \rangle), \quad (\text{B.8})$$

which is a closed ODE solution for the first moment $\langle \mathbf{X}(t) \rangle$. Accordingly, the result for this system is equation 4.10.

However, we are not directly interested in the absolute subpopulation counts, but rather their relative sizes. Let $F_i(t) = X_i(t)/X_{\text{total}}(t)$, where $X_{\text{total}} = X_0 + X_1$, then

$$\langle F_i \rangle = \left\langle \frac{X_i(t)}{X_0(t) + X_1(t)} \right\rangle, \quad i = 0, 1, \quad (\text{B.9})$$

and also

$$\langle F_0(t) \rangle + \langle F_1(t) \rangle = 1. \quad (\text{B.10})$$

Note that if X_{total} is sufficiently large that fluctuations are small, then fluctuations in $1/X_{\text{total}}$ are vanishingly small. This means that

$$\text{Cov} \left(X_i, \frac{1}{X_{\text{total}}} \right) \rightarrow 0, \quad i = 0, 1, \quad (\text{B.11})$$

allowing the angle bracket in equation B.9 to be broken up

$$\langle F_i \rangle \approx \frac{\langle X_i \rangle}{\langle X_0 + X_1 \rangle} = \frac{\langle X_i \rangle}{\langle X_0 \rangle + \langle X_1 \rangle}, \quad i = 0, 1. \quad (\text{B.12})$$

With equation B.12, a closed-form expression can be obtained for the first moments from equations 4.10 using the quotient rule of differentiation

$$\langle F_0(t) \rangle = 1 - \langle F_1(t) \rangle,$$

$$\begin{aligned} \frac{d\langle F_1(t) \rangle}{dt} &= (\lambda_0 - \lambda_1) \langle F_1(t) \rangle^2 + [\lambda_0(2\sigma_0 - 3) + \lambda_1(2\sigma_1 - 1) - k_0 - k_1] \langle F_1(t) \rangle \\ &\quad + k_1 - 2\lambda_0(\sigma_0 - 1), \end{aligned}$$

which are exactly equations 4.12 and 4.13. They can be solved by numerical integration.

Alternatively, note that equation 4.13 is of a special form

$$\frac{df}{dt} = Af^2 + Bf + C, \quad (\text{B.13})$$

called a Riccati differential equation, which has an analytical solution.